Molecular Transport in Emulsions: From Permeation to Controlled Delivery using Microfluidics

Dissertation

for the award of the degree

'Doctor rerum naturalium'

of the Georg-August-Universität Göttingen

within the doctoral program

Göttingen Graduate School for Neurosciences, Biophysics and Molecular Biosciences (GGNB)

of the Georg-August University School of Sciences (GAUSS)

submitted by

Philipp Gruner

from Frankenberg

Göttingen 2014

Thesis committee:

Prof. Dr. Jean-Christophe Baret
[1]Centre de Recherche Paul Pascal (CNRS)
University of Bordeaux
[2]Max Planck Research Group 'Droplets, Membranes and Interfaces'
Max Planck Institute for Dynamics and Self-Organization, Göttingen

Prof. Dr. Sarah Köster
Institute for X-Ray Physics
Georg-August-Universität Göttingen

Prof. Dr. Stephan Herminghaus
Department of Dynamics of Complex Fluids
Max Planck Institute for Dynamics and Self-Organization, Göttingen

Members of the examination board:

Reviewer: Prof. Dr. Jean-Christophe Baret
[1]Centre de Recherche Paul Pascal (CNRS)
University of Bordeaux
[2]Max Planck Research Group 'Droplets, Membranes and Interfaces'
Max Planck Institute for Dynamics and Self-Organization, Göttingen

Second Reviewer: Prof. Dr. Jörg Enderlein
Third Institute of Physics
Georg-August-Universität Göttingen

Further members of the examination board:

Prof. Dr. Sarah Köster
Institute for X-Ray Physics
Georg-August-Universität Göttingen

Prof. Dr. Stephan Herminghaus
Department of Dynamics of Complex Fluids
Max Planck Institute for Dynamics and Self-Organization, Göttingen

Dr. Manfred Konrad
Department of Enzyme Biochemistry
Max Planck Institute for Biophysical Chemistry, Göttingen

Dr. Thomas Burg
Department for Biological Micro- and Nanotechnology
Max Planck Institute for Biophysical Chemistry, Göttingen

Date of oral examination: 06. October 2014

Contents

1 | New challenges for emulsion science

"Oil and water do not mix" - this maxim is based on experiences of our every-day life. It reflects the fact that hydrocarbon liquids and water differ in their chemical polarity, ultimately resulting in weak interactions and low solubilities in each other. However, immiscible liquids can transiently coexist in a mixture in the form of an emulsion, where one liquid is dispersed, typically in the form of small droplets, into the other.

Many products of our daily life are based on these disperse systems [1]. We encounter emulsions often as food, for example when enjoying a glass of milk or an ice cream. Furthermore, as a suitable platform for the efficient delivery of poorly water-soluble compounds, they are of great importance in pharmaceuticals. Also, many cosmetic products are based on their ability to deliver a wide variety of ingredients quickly and conveniently to skin and hair. Finally, emulsions are of importance for many industrial applications, such as polymer production and road surfacing.

As varied and interesting as the use of emulsions today is, the potential future applications are at least as fascinating. In recent times, the enormous potential of emulsion droplets as miniaturized reaction vessels has been exploited [2,3]. Interestingly, the idea of using droplets as microreactors has already been brought up in the middle of the 20^{th} century [4]. However, the concept had its breakthrough only with the recent advances in droplet-based microfluidic technology [5–8]. The technique allows the production and precise manipulation of calibrated emulsion droplets at high rates up to several kHz, unleashing an enormous potential for high-throughput screening applications [9–14]. Based on that platform, applications such as single cell [15], DNA [16] or drug screening [17] have already been demonstrated.

These emulsions are unconventional in the sense that each droplet typically has an individual composition at every time step, depending on the initial loading of compounds and on the biochemical processes taking place in the droplet. As a re-

sult, new types of aging mechanisms are expected in these emulsions. In addition to classical aging processes, such as flocculation, coalescence, gravitational separation, and Ostwald ripening, molecular transport driven by differences in chemical potential of encapsulated molecules are driving the system towards its equilibrium. Such transport processes lead to cross-talk between droplet microreactors [18–22]. As a consequence, the concept of using emulsion droplets as individual self-contained systems does not necessarily hold, ultimately resulting in a breakdown of the compartmentalization approach. Hence, for the establishment of emulsion droplets as a platform for biotechnological high-throughput applications, the understanding of mass transfer in these emulsions is essential. Furthermore, the control of transport processes between droplets can open new ways to temporally program the composition of droplet microreactors.

Microfluidic tools play an increasing role in the study of soft matter, as they provide great control over system geometry and material conditions. Hence, physicochemical processes are investigated in microfluidic systems with enormous precision [23]. Therefore, droplet-based microfluidic technology is not only a powerful tool for high-throughput screening applications, but also offers new opportunities for emulsion science [25]. In figure 1.1 emulsions obtained by inhomogeneous shearing and by flow focusing in a microfluidic environment are shown. Emulsification in microfluidics allows to form droplets with precisely defined size and composition, making it a very useful instrument for the quantitative investigation of the physicochemical properties of emulsions.

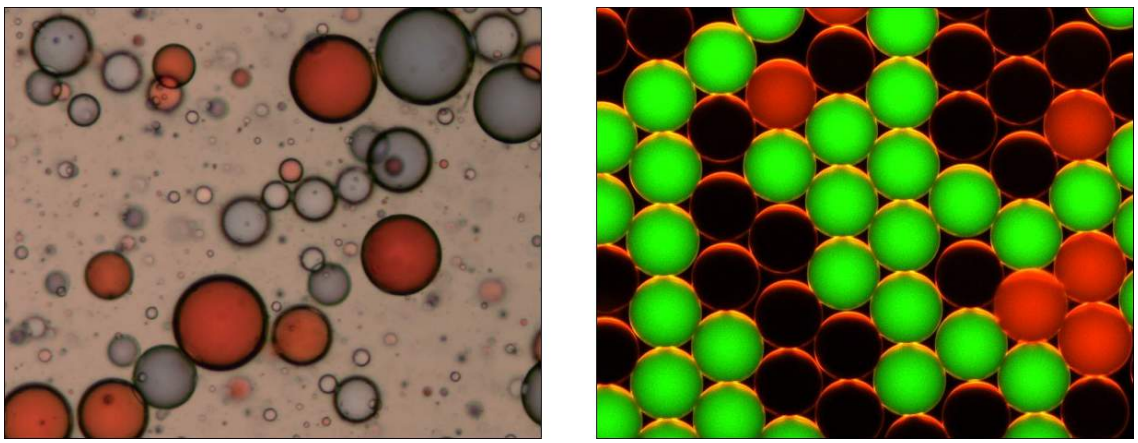

Figure 1.1: Water-in-oil emulsions created by inhomogeneous shearing (left, figure taken from [25]) and by homogeneous shearing in a microfluidic environment (right).

In this work, microfluidic tools are developed and applied to gain quantitative insights into mass transport processes between emulsion droplets. Fundamental information, which is inherently difficult to access with classical methods of bulk analysis, become experimentally accessible following this approach. In addition, based on these insights, novel concepts that allow a dynamic control of droplet composition are introduced. Generally, the focus is on emulsions comprised of aqueous droplets dispersed in fluorinated oils. Such systems are considered to be the most promising platforms for droplet-based biotechnological applications of emulsions [26]. Hence, the presented results directly impact the advancement of such systems and potentially widen their field of application.

This work contains seven chapters. In the following chapter, basic concepts of emulsions and droplet-based microfluidics are introduced. In chapter 3, an investigation of the collective dynamics of molecular transport in a macroscopic emulsion is presented. A complementary study of 'minimal emulsions' is introduced in chapter 4. In chapter 5, studies of the osmotically driven transport of water and the transfer of inorganic ions between emulsion droplets are presented. Subsequently, in chapter 6 the influence of fluorosurfactants on the retention of solutes in emulsion droplets is investigated. Finally, chapter 7 summarizes the main aspects of this work.

This work was performed as part of SFB 755.

2 | Theoretical background

In this chapter, fundamental principles of emulsions and basic mechanisms of mass transport within these are discussed. Furthermore, microfluidics is introduced as a powerful tool for emulsion science. Moreover, the special characteristics of organofluorine compounds are discussed providing a foundation for the understanding of mass transport in emulsions comprising a fluorous phase. Finally, the state of the art is highlighted by discussing the most recent microfluidic studies of mass transport in emulsion.

Contents

2.1 | Emulsions: Basic concepts

Emulsions are dispersions made out of two or more immiscible fluids. The fluid being dispersed is called the dispersed phase while the surrounding fluid is termed continuous phase. Emulsions are classically obtained by shearing the immiscible liquids resulting in the fragmentation of one phase into the other [27]. This is realized by for example shaking or stirring the fluids.

Different types of emulsions can be formed. For example, water and oil can form water-in-oil emulsions (figure 2.1a) consisting of water droplets dispersed in a continuous oil phase as well as oil-in-water emulsions (figure 2.1b) composed of oil droplets surrounded by water. Furthermore, multiple emulsions can be formed, where the droplets of the dispersed phase contain smaller droplets themselves (figure 2.1c). Such systems are typically obtained by a two step emulsification process, where a primary emulsion is again dispersed in an external phase.

From a thermodynamic perspective, emulsions are out of equilibrium systems. Over time they evolve towards a state where both phases are separated by an interface of minimal energy. The time-scale for this process is linked to ageing mechanisms such as Ostwald ripening and coalescence. Ostwald ripening occurs by diffusion of the dispersed phase through the continuous phase resulting in an increase in the average droplet diameter and a decrease in the number of droplets. Coalescence is the process by which adjacent droplets fuse.

To increase the lifetime, emulsions are kinetically stabilised in a metastable state by the use of surfactant molecules. Surfactant is the contraction of 'surface active agent' [28] reflecting the fact that these amphiphilic molecules tend to enrich at

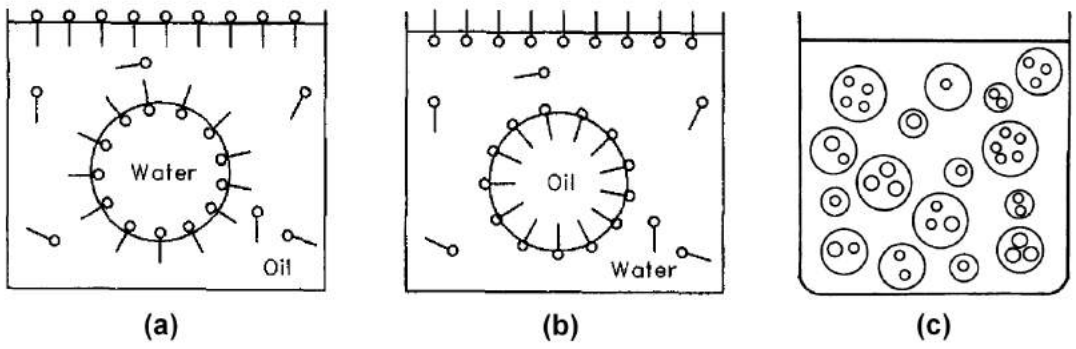

Figure 2.1: Schematic representation of different types of emulsions. (a) Water-in-oil emulsion. (b) Oil-in-water emulsion. (c) Multiple emulsion. Images taken from [1].

the interface of immiscible fluids. In the presence of surfactants, the coalescence of droplets is inhibited. Two possible mechanisms have been proposed to explain this phenomenon. One considers the steric repulsion between the surfactant molecules adsorbed at the drop interface. The second is based on the hindrance of film drainage during the approach of droplets. While droplets are approaching, a flow-induced heterogeneous distribution of surfactant molecules at the droplet interfaces emerges, resulting in a force counteracting the film drainage [29]. In summary, the addition of surfactant molecules to emulsions generally results in an increase of the height of the energy barrier between the local energy minima of the system and the equilibrium state. This typically leads to a significant increase in the lifetime of emulsions. For this reason surfactants are an essential part of most emulsification systems.

2.2 | Microfluidics

Microfluidics is a multidisciplinary research field equally attracting scientists from areas such as physics, engineering, chemistry or biotechnology. George Whitesides defined microfluidics as "the science and technology of systems that process or manipulate small (10^{-9} to 10^{-18} litres) amounts of fluids, using channels with dimensions of tens to hundreds of micrometres" [30]. Because of the relatively small dimensions, fluid flows in microfluidic environments are typically characterized by low Reynolds numbers resulting in laminar flow. Consequently, mixing between parallel fluid streams occurs generally via diffusion (figure 2.2).

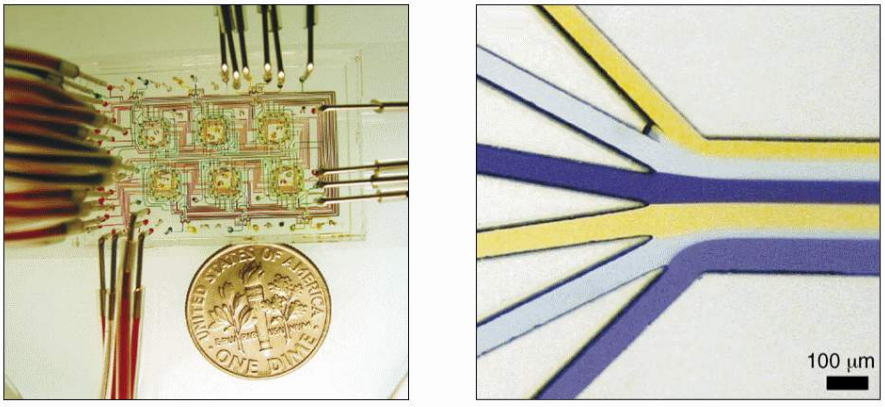

Figure 2.2: Images of microfluidic devices and channels. (a) Example of a microfluidic device used to grow and study bacteria. Image taken from [32]. (b) Dye solutions flowing through a microfluidic channel demonstrating laminar flow. Image taken from [33]

The technology offers fundamentally new opportunities to spatially and temporally control concentrations of molecules. Furthermore, experiments in a microfluidic environment require only small sample and reagent volumes and at the same time enable fast and accurate detection. However, only with the advances in micro-fabrication, allowing the convenient and inexpensive fabrication of microfluidic devices via soft lithography in polydimethylsiloxane (PDMS) [31], the technology became easily accessible and subsequently spread to many research laboratories up to industrial applications (Fluidigm Corporation, RainDance Technologies).

2.2.1 | Droplet-based microfluidics

Droplet-based microfluidics emerged at the very beginning of the 21^{st} century as a subdomain of microfluidics [5]. It employs immiscible phases that are flown through microchannels such that homogeneous shearing of the liquids results in the formation of emulsions with discrete monodisperse droplets. The most widely used channel geometries for microfluidic droplet production are the T-junction and the flow-focussing geometry (figure 2.3). At a T-junction, the breakup of a stream of a first fluid is induced by shearing with a cross flow of a second fluid [5]. In a flow-focusing geometry, one fluid is sheared off from two sides by a second fluid [34]. In this geometry the two fluids are often flown through an orifice. In both cases highly monodisperse droplets are formed due to the homogeneous shearing. The flow rates can be easily adjusted by syringe or pressure driven pumps to obtain droplet production frequencies ranging from a few to more than 10 kHz [35]. This approach allows to form droplets with volumes down to the femtolitre range [36]. Alternatively, step

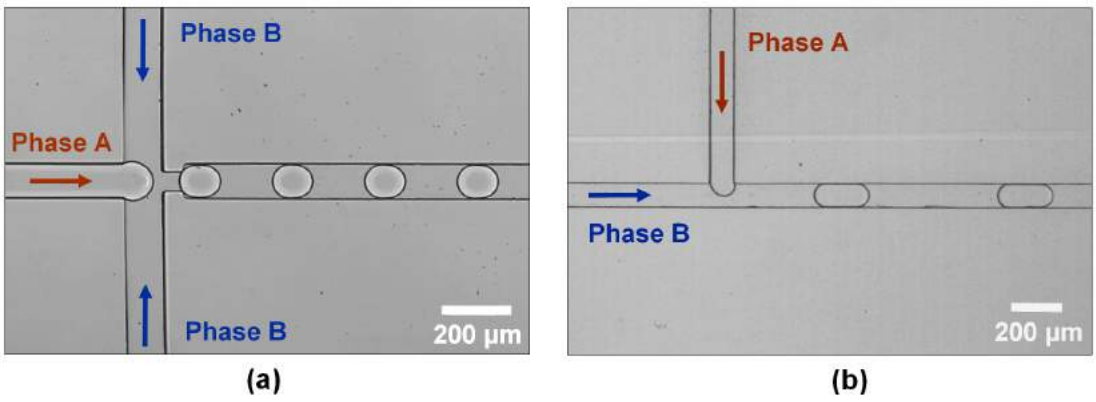

Figure 2.3: Different geometries for droplet production in microfluidics. (a) Droplet production in a flow focussing geometry. (b) Droplet generation at a T-junction.

emulsification can be applied. Here the droplet production relies on an a step change in the height of a microchannel [37].

Besides generating droplets, several techniques have been developed to reliably manipulate droplets in microfluidic devices. Many methods have been presented that allow to sort, split, trap or fuse droplets. For example acoustic waves [38], single-layer membrane valves [39], local heating by focused laser [40] or electrowetting [41] have been exploited to manipulate droplets. However, probably the most popular method for the manipulation of droplets in microfluidics is to apply electric fields. This is based on the incorporation of electrodes, which are fabricated by injecting molten solder into microfluidic channels resulting in precisely aligned electrodes [42, 43]. Electric fields can be applied for example to sort droplets according to their optical properties [6, 44] or to inject reagents [7] (figure 2.4).

The injection of fluids is based on flowing droplets through a microchannel with a small orifice containing a pressurized reagent. As the droplets are stabilized by surfactants, no injection of fluid is observed normally. Only in the presence of an electric field, destabilizing the surfactant layers [8], injection of the fluid to the passing droplets is achieved.

Droplet sorting is based on dielectrophoresis, exploiting the circumstance that immiscible phases mostly have different dielectric constants. The principle is based on the dispersed phase having a higher polarizability than the continuous phase. In

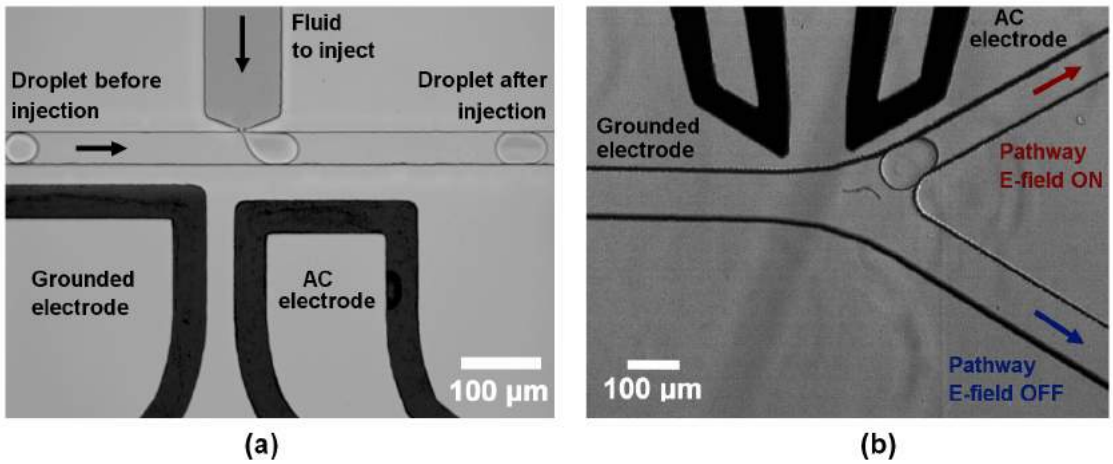

Figure 2.4: Images of picoinjection and droplet sorting. (a) Injection of fluids from a channel containing a pressurized fluid to bypassing droplets is obtained in the presence of an electric field destabilizing the surfactant layers. (b) Droplets passing the sorting junction are deflected towards the upper, narrower channel in the presence on an AC electric field. In the absence of an electric field, droplets follow the path of lower hydrodynamic resistance into the wider microfluidic channel.

such case, the presence of an electric field results in an attractive force pulling the droplets towards the electrodes. Applying this principle allows the efficient sorting of droplets with distinct properties from a monodisperse emulsion [15, 24].

2.2.2 | Directing droplets in surface energy landscapes

For both, addressing fundamental questions in emulsion science as well as for biotechnological applications, it is of great interest to hold droplets stationary. Immobilizing, arranging and spacing droplets in a predefined way, allows to significantly reduce the degree of freedom of an emulsion system. Such a level of control is only accessible applying microfludic tools. Several approaches to hold droplets stationary have been presented such as localized laser heating [46] or micromechanical obstacles [45, 47–49]. However, these methods either require a constant energy input or rely on physical boundaries between the droplets. In both cases the applicability of such methods for addressing physicochemical phenomena in emulsion is restricted.

Recently, it was shown that droplets can be trapped and guided along gradients of surface energy [50–52]. The principle is based on the fact that the deformation of a droplet from a spherical shape into another, for example a pancake-like shape, leads to an increase of interfacial area A resulting in an increase in surface energy E_γ, proportional to the interfacial tension γ:

$$E_\gamma = \gamma A \tag{2.1}$$

Hence, a decrease in surface energy is obtained when a droplet, constraint in a microchannel enters regions of lower confinement. For instance, droplets can be immobilized in the presence of circular regions of increased channel height called anchor (figure 2.5). Similarly, grooves can act as rails for guiding droplets [50]. Dangla *et al.* [52] have shown that the anchoring force F_γ exerted to a squeezed droplet in the presence of a circular well with a diameter w can be described as:

$$F_\gamma \propto \frac{|\Delta E_\gamma|}{w} \approx \gamma \frac{\pi}{2} h \left\{ \frac{b}{2} - \frac{4}{3b} \left[1 - \left(1 - \frac{b^2}{4} \right)^{3/2} \right] \right\} \tag{2.2}$$

with h as the height of the microfluidic channel and b as the quotient of w and h.

Whether or not a droplet remains anchored depends on the ratio of the anchoring force and the hydrodynamic drag force F_d, exerted to an immobilized droplet in an

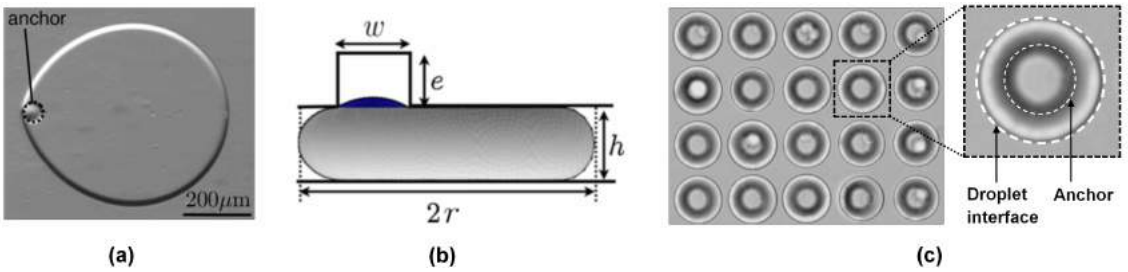

Figure 2.5: Sketch and images of droplets immobilized in wells of the surface energy. (a) Top view of a droplet held stationary against an external flow in the presence of an anchor (picture taken from [52]). (b) Schematic side view of a droplet with radius R squeezed in a microchannel of height h, in the presence of an anchor with diameter d and depth e (picture taken from [52]). (c) Droplets arrayed in a surface energy landscape designed for square packing.

external flow field. This force is proportional to the viscosity η and the flow velocity U of the continuous phase [52]:

$$F_d \propto \frac{\eta\, U r^2}{h} \tag{2.3}$$

with r as the droplet radius. As a consequence, if the flow rate exceeds a critical value, an immobilized droplet will be released from an anchor.

In practical droplet-based microfluidic applications, trains of droplets are produced. In the presence of anchors, droplets will tend to collide with each other. Depending on the flow velocity, droplets can be entering a 'buffering' or a 'parking' mode [50]. In 'parking' mode, an anchored droplet will remain immobilized even if other droplets collide with it. In the buffering mode, anchored droplets are pushed off the well in surface energy and the incoming droplets take their place. This characteristics can be exploited to create arrays of droplets. Moreover, selective manipulation of droplets can be achieved with localized laser heating [51].

2.3 | Basic aspects of mass transport in emulsions

Mass transfer between emulsion droplets occurs as a result of phase partitioning due to a finite solubility of the dispersed phase respectively its solutes in the continuous phase [63, 64] or alternatively through bilayers of surfactant molecules [65], possibly forming when droplets are closely packed.

In the following sections, various mechanisms resulting in mass transfer in emulsion will be discussed. First, the mass transport of the dispersed phase as a result of

heterogeneities in the distribution of droplet sizes, known as Ostwald ripening is discussed. Subsequently, mass transfer of the dispersed phase driven by heterogeneities in the chemical composition of droplets is described (osmotically driven transport). Afterwards, the transport of solutes between droplets is discussed. Finally, the transport of molecules occurring through bilayers of surfactant is thematized.

2.3.1 | Ostwald ripening

The chemical potential of molecules of the dispersed phase is dependent on the size of the droplets, respectively their radius [53, 54]:

$$\mu(r) = \mu_\infty + \frac{2\gamma V_m}{r} \tag{2.4}$$

with $\mu(r)$ as the chemical potential of molecules in an emulsion droplet of radius r, μ_∞ as the chemical potential in bulk, V_m as their molar volume and γ as the interfacial tension. The additional pressure within a droplet is also known as Laplace pressure ($2\gamma/r$). The dependence of the solubility S of an emulsion droplet on its size can be described by the Kelvin equation [55, 56]:

$$S(r) = S_\infty \exp \frac{2\gamma V_m}{rRT} \tag{2.5}$$

with S_∞ as the bulk solubility of the dispersed in the continuous phase, R as the ideal gas constant and T as the absolute temperature.

Hence, polydisperse emulsion systems are characterized by heterogeneities in chemical potential, respectively solubility. The equilibration process of these differences is called Ostwald ripening. Diffusion of dispersed phase molecules phase through the continuous phase results in a net mass transport from smaller to larger droplets. Hence, small droplets shrink on the expense of larger droplets that grow in size, ultimately resulting in an temporal increase of the average droplet size and a reduction of the interfacial area of the emulsion.

2.3.2 | Osmotically driven transport

Mass transport of the dispersed phase may also be induced by heterogeneities in chemical potential resulting from different droplet compositions. In this context, the concept of osmotic pressure is discussed.

Empirically it was found that a pressure difference between two fluid reservoirs divided by a semi-permeable membrane with uneven solute concentrations exists [57]. In 1887, Van't Hoff described this pressure difference, also named osmotic pressure Π, to be dependent on the concentration difference Δc of nonpermeable solutes across a membrane [58]:

$$\Pi = RT\Delta c \tag{2.6}$$

This equation holds for dilute solutions [57]. Interestingly, it has been demonstrated that the osmotic pressure is independent on the nature of the solute molecules in the limit of infinitely diluted solutions [59]. Instead, it is only dependent on the ratio of solvent and osmotically active solute molecules. The molecular mechanism causing osmosis remains unclear [60, 61]. However, from a thermodynamic point of view, osmosis is well understood.

According to equation 2.6, an osmotic pressure exists between two droplets with different solute concentrations. This difference can be explained considering the dependence of the chemical potential on the activity a of a species i in a mixture [62]:

$$\mu_i = \mu_{i,0} + RT \ln (a_i) \tag{2.7}$$

where $\mu_{i,0}$ is a constant standard chemical potential at any given temperature and pressure. Correspondingly, a difference in chemical potential arises from differences in activity:

$$\mu_{i,1} - \mu_{i,2} = RT \ln \frac{a_{i,1}}{a_{i,2}} \tag{2.8}$$

Furthermore, assuming the system to be isothermal, the variation of chemical potential with the pressure p can be related with the partial molal volume $\bar{V}_i$:

$$\left(\frac{\partial \mu_i}{\partial p}\right)_T = \bar{V}_i \tag{2.9}$$

Consequently, the difference in activity results in a pressure difference:

$$\Delta p = \frac{RT}{\bar{V}_i} \ln \frac{a_{i,1}}{a_{i,2}} \tag{2.10}$$

The activity of a species can be expressed as the product of its mole fraction x_i and the activity coefficient Γ_i, accounting for deviations from ideal behaviour:

$$a_i = \Gamma_i x_i \tag{2.11}$$

The mole fraction of the solvent decreases with increasing solute concentration. Hence, its activity and therefore its chemical potential, decreases with increasing solute concentration. For ideal solutions, respectively in first approximation for very diluted solutions, the activity coefficient Γ_i can be assumed to be independent on the mole fraction x_i. In such case, the activity of the solvent is inversely proportional to the solute concentration. With this assumption equation 2.10 is simplified to van't Hoff's law of osmotic pressure (eq. 2.6) [62].

2.3.3 | Solute transport

According to the considerations in the previous section, the net transport of solutes between emulsion droplets is a consequence of heterogeneities in chemical potential of solutes among the droplets.

A finite solubility of solutes in the continuous phase generally results in the leakage of compounds from emulsion droplets. The release rate was described to be dependent on the partition coefficient of the solutes between the dispersed and the continuous phase [63,64]. However, in several studies it has been suggested that additionally the interfacial properties of the emulsion influence the rate of release [66–71]. Typically, changes in the compositional properties of the system were considered to affect the permeability of the interface and would influence the rate of release of molecules from emulsion droplets for that reason. However, it should be noted that a change of the composition variables might also alter the partition coefficient of the solutes. In addition, a decrease in the rate of release was observed when replacing hydrogenated with fluorinated components as the continuous phase [67, 71, 72]. This effect was attributed to changes in the interfacial tension, the size of the surfactant molecules and a higher cohesive energy between the fluorinated surfactant molecules [70]. However, the partitioning coefficient of most organic molecules in the investigated water-in-oil emulsions would be significantly altered when replacing hydrogenated with fluorinated components [73, 74].

Interestingly, the before frequently stated finding that an interface acts as an

effective barrier to the diffusion of molecules was withdrawn by some authors recently [75]. This understanding was based on a model revealing that the diffusion of a reagent across the continuous phase is the rate-limiting step, suggesting that no significant energy barrier for molecules crossing an interface exists [76]. In such case, the transport of molecules between emulsion droplets is limited by the diffusive flux J in the continuous phase predicted by Fick's law:

$$J = -D\frac{\partial c}{\partial x} \tag{2.12}$$

where $\frac{\partial c}{\partial x}$ is the concentration gradient and D is the diffusion coefficient of the solute in the continuous phase. The temporal equilibration of the concentration difference $\frac{\partial c}{\partial t}$ can accordingly be described with Fick's second law of diffusion:

$$\frac{\partial c}{\partial t} = D\frac{\partial^2 c}{\partial^2 x} \tag{2.13}$$

Assuming that no significant energy barrier for solutes crossing the interface exists, the concentration of solutes close to the interface can be derived from the concentration in the dispersed phase by taking the partition coefficient K between the continuous phase and the dispersed phase into account.

$$J = -K\,D\,\frac{\partial c}{\partial x} \tag{2.14}$$

Where K is defined as the quotient of the equilibrium solute concentrations in the continuous $c_{eq,cont}$ and the dispersed phase $c_{eq,disp}$:

$$K = \frac{c_{eq,cont}}{c_{eq,disp}} \tag{2.15}$$

As a consequence the timescale of equilibration of concentration differences between two fluid reservoirs is proportional to the diffusion coefficient of solutes in the continuous phase D, the partition coefficent K and inversely proportional to their distance d. As a time-independent parameter reflecting the timescale of equilibration the permeability P is introduced:

$$P = \frac{KD}{d} \tag{2.16}$$

Equation 2.16 is also known as Overton's rule, frequently used to described the rate of transport through biological membranes [79, 80].

However, in literature other models claim that the rate limiting step of solute transfer between droplets is the transport across the droplet boundary [77]. Such deviations may arise from the fact that the characteristics of the concerned emulsion systems are not identical in all cases. To clarify such fundamental questions, a precise method to experimentally determine the rate limiting step of mass transport between emulsion droplets is needed. However, a method decoupling potential rate limiting steps from each other has not yet been presented. In this work, a reliable method allowing to experimentally determine the rate limiting step of mass transport between emulsion droplets will be presented.

Additional aspects concerning the release and transport of solutes from emulsion droplets have not been clarified yet. For example the effect of the nature of the solute on the rate of release remains unclear [75]. Generally, great variations are found for the rate of release depending on the molecular properties [72]. While the specific effect of for example molecular weight and interfacial activity remain unclear, there is clear evidence about rate of release being affected by the solubility of the solute in the continuous phase. For example it has been shown that the release of an organic molecule was significantly altered by changing the pH of the dispersed phase. This effect was attributed to a modification of the partitioning coefficient [78]. Hence, inducing solubility changes results in a modified rate of release respectively exchange rate [22].

2.3.4 | Transport through bilayers of surfactant

Alternatively to the transport processes based on phase partitioning, molecular exchange between droplets might also arise from transport through bilayers of surfactant possibly forming between emulsion droplets [65]. Such bilayers form upon the interaction of surfactant monolayers adsorbed at the interface of emulsion droplets [81, 82]. After formation of a bilayer, the droplets become strongly adhesive without coalescing, as a result of the molecular interactions between the surfactant molecules [81]. In figure 2.6, images of adhesive droplets upon bilayer formation are shown.

Whether or not bilayers of surfactants form in a given emulsion system is dependent on several parameters. For example, the solubility of the surfactant molecules in the continuous phase plays an important role. It was shown that changing the composition of the continuous phase significantly alters the adhesion energy between

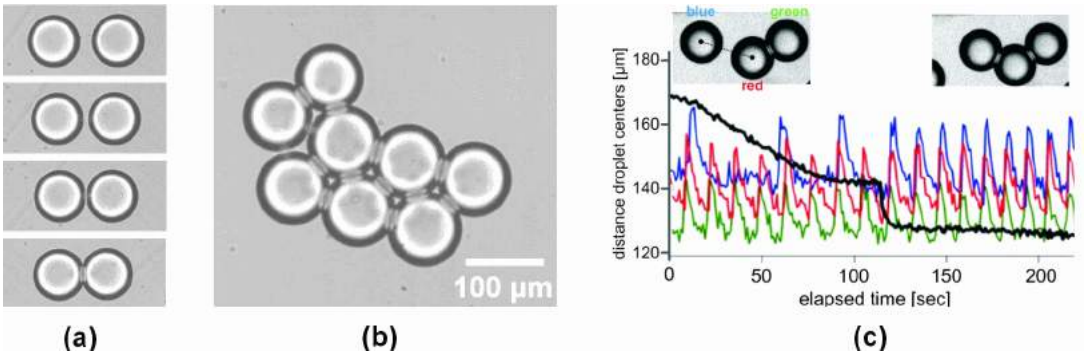

Figure 2.6: Images of bilayer formation between aqueous droplets dispersed in squalane. Monoolein is used as surfactant. (a) Image sequence of two droplets approaching and subsequently forming a bilayer (sequence frame rate: 0.5 frames per second). (b) Assembly of strongly adhesive droplets obtained after bilayer formation. (c) Bilayer formation and phase coupling of chemical oscillators (figure taken from [83]).

the droplets. In fact, the energy of adhesion is essentially zero in good solvents [81] resulting in the absence of bilayers. Hence, the adhesion energy between monolayers of surfactant molecules is significantly increased by decreasing the solubility of the surfactants in the continuous phase [65].

For mass transport across bilayers two distinct mechanisms have been suggested. One is based on the partitioning into and diffusion through the bilayer [84], the other one is based on transient pores in the bilayer occurring due to thermal fluctuations [85]. It has been suggested that the transient pore mechanism is dominant for inorganic ions while the partitioning and diffusion mechanism is more relevant for neutral molecules [86].

In more recent studies, it has been shown that the permeability of the bilayer is linked to its adhesion energy. It was found that an increase in adhesion energy results in a lower membrane fluidity and ultimately in a lower permeability [65]. Remarkably, it was also found that molecular transport through a bilayer membranes can result in the phase coupling of chemical oscillators opening the way for multi-functional, self-assembling emulsion-based systems [83].

2.4 | Emulsions with a fluorous phase

2.4.1 | Organofluorine chemistry

Usually organic compounds containing fluorine are considered to be hydrocarbon derivatives. However, highly fluorinated molecules are typically called organofluorine compounds. Most organofluorine molecules can be classified either as fluorocarbon or as perfluorinated compounds. While fluorocarbons exclusively contain carbon and fluorine, perfluorinated compounds are characterized be the replacement of all carbon-hydrogen bonds with carbon-fluorine bonds. Therefore fluorocarbons, in contrast to perfluorinated compounds, do not contain atoms such as nitrogen or oxygen. However, it should be noted that this terminology is not necessarily strictly followed [87].

For the understanding of some of the properties of organofluorine compounds, a discussion of the fundamental unit of these compounds, the carbon-fluorine bond, is required. The C-F-bond is highly polarized due to the high electronegativity of the fluorine. Despite that fact, fluorine is not characterized by a very good hydrogen bond donor ability. This can be reasoned by the fact that the lone pairs of the fluorine, due to the high electronegativity of the atom, do not significantly interact with hydrogen-bonding acceptors [88]. Further, the low polarizability of the fluorine atom, respectively the C-F-bond, results in relatively weak London dispersion forces between the molecules, which are scaling with the square of polarizability [87]. In fact, perfluorocarbon compounds were reported as "extremely nonpolar" [89] respectively the least polar existing fluids [90]. For example Teflon has a relative permittivity of only 2.1 [91].

As a consequence of the generally very weak interactions of fluorinated compounds with other molecules, most organic compounds are practically insoluble in fluorous fluids [73, 74]. This is also reflected by the fact that fluorinated compounds are not only immiscible with water but also with most organic solvents.

Moreover, the weak intermolecular forces result in a relatively high compressibility of the fluids, which reflects the availability of interstitial space [87]. For that reason, respiratory gases such as oxygen and carbon dioxide are generally highly soluble in fluorous fluids. In fact, the solubility of oxygen in fluorocarbons is about three to ten times higher than in the parent hydrocarbons [94]. This characteristics makes them highly valuable for the use as blood substitutes or breathing liquids [95–97].

Furthermore, using perfluorinated compounds as a continuous phase, cells can be cultured in aqueous emulsion droplets [50, 92, 93].

In summary, perfluorination of organic compounds generally results in significantly altered chemical and physical properties. As a result of their weak intermolecular interactions, they generally possess an outstanding gas-dissolving capacity and are simultaneously hydro- and lipophobic.

For droplet-based screening applications these properties are highly valuable. The low solubility of organic molecules in fluorous fluids results in restricted cross-talk between emulsion droplets [20] while the high solubility of respiratory gases is a key for cell survival in droplets [98–101]. Furthermore, while conventional hydrocarbon compounds may swell the microfluidic core material PDMS, leading to device delamination or channel deformation, fluorinated compounds are highly compatible with PDMS [102]. Water-in-fluorinated-oil emulsions are therefore considered to be the most promising systems for the miniaturization of biochemical assays in emulsion droplets [26].

2.4.2 | Phase partitioning into fluorous fluids

Due to the very low polarizability, fluorinated compounds are generally of extremely nonpolar character. Therefore, only molecules with a similar character or in other words, molecules that are fluorophilic enough, are efficiently phase partitioned from a more protic solvent. In fact nonfluorous solutes, with the exception of small gases, are in general virtually insoluble in fluorous solvents [103]. Thus these liquids can be valuable for the selective extraction of molecules covalently modified with fluorous tags [104–110].

Furthermore, it has been shown that specific noncovalent interactions can result in an increased solubility of organic molecules in fluorous liquids [90]. The increased solubility is the result of noncovalent associations of perfluororinated molecules and organic molecules based on hydrogen bonding or ion pairing. Attention has for example been drawn to fluorous carboxylic acids. They were shown to act as molecular receptor for organic molecules significantly increasing their solubility in fluorous liquids. One of the first reports came from Palomo *et al.* [111]. The authors found a dramatic solubility increase in fluorous solvents for fluorinated urea in the presence of fluorinated carboxylic acids (Fig. 2.7).

In the absence of any other functional groups, carboxylic acids were shown to exist as hydrogen bonded dimers in fluorous fluids [113]. However, it has been demonstrated that hydrogen bonds with the lone pair of nitrogen are more stable than the hydrogen bonds present in cyclic carboxylic acid dimers [114, 115]. As a consequence, most nitrogen H-bond acceptors are more successful at competing for the carboxylic acid H-bonds than the carboxylic acids themselves [112]. This in turn results in the effective extraction of organic molecules comprising Lewis base characteristics as shown for pyridines [103, 112]. In fact, the presence of equimolar amounts of fluorinated carboxylic acids in the fluorous phase leads to an almost complete extraction (up to 99%) of pyridine derivatives from chlorofrom into the fluorous phase [112]. Furthermore, it was demonstrated that the extraction of aniline in similar conditions is much less efficient (5%). This was explained by the fact that pyridyl nitrogen acts as a better hydrogen bond donor than primary amines. Moreover, it was argued that the highly selective and effective extraction is based on the fact that the substrate-receptor interactions are reinforced in fluorous liquids, as they are considered to be ultimate noncompetitive solvents [103].

In summary, noncovalent interactions significantly improve the extraction of organic molecules into a fluorous phase. The efficiency is strongly dependent on the compatibility of substrate and receptor. Particularly fluorous carboxylic acids have been studied that were shown to form strong hydrogen bonds with nitrogen containing Lewis Bases.

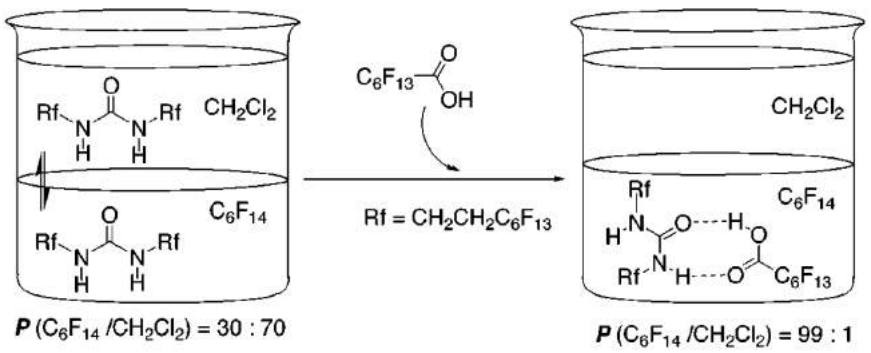

Figure 2.7: Sketch of solubility enhancement of fluorinated urea in a fluorous solvent, in the presence of fluorinated carboxylic acids. Solubility increase was observed for N,N-di(polyfluoroalkyl)ureas due to hydrogen binding with perfluoroalkanoic acid scavengers. Image taken from reference [111].

2.5 | Mass transport in microfluidic environments

One of the first microfluidic studies about mass transfer in two-phase systems was presented by Burns *et al.* [116]. The authors have shown that in droplet-based microfluidic systems the mass transfer rates between the continuous and the dispersed phase can be up to several orders of magnitude faster than in non-miniaturized systems. Similar studies were presented by Mary *et al.* [117] (figure 2.8a) and Xu *et al.* [118]. The enhancement in the interfacial mass transfer was reasoned by internal convective circulation resulting from shear forces [116, 119, 120].

Courtois *et al.* [19] were among the first to study the retention of organic molecules in emulsion droplets in microfluidic environments. The investigated emulsions were comprised of aqueous droplets dispersed in mineral oil and stabilized by a silicon-based surfactant. Experimentally, droplets were produced and stored in a reservoir on a microfluidic chip (figure 2.8b). Qualitatively it was shown that the mass transfer of fluorophores between aqueous droplets dispersed in mineral oil was dependent on the nature of the compounds, the surfactant concentration and the number and composition of neighbouring droplets. Furthermore, it was stated that the release of fluorophores to the continuous phase "is a consequence of diffusion into the oil phase as well as formation of reverse micelles". However, the mechanism of mass transfer remains mostly unclear. Moreover, a method based on the addition of the protein bovine serum albumin was presented to decrease the leakage of compounds from aqueous emulsion droplets. The effect was considered to be based on the formation of a protein layer at the droplet interface acting as a kinetic barrier.

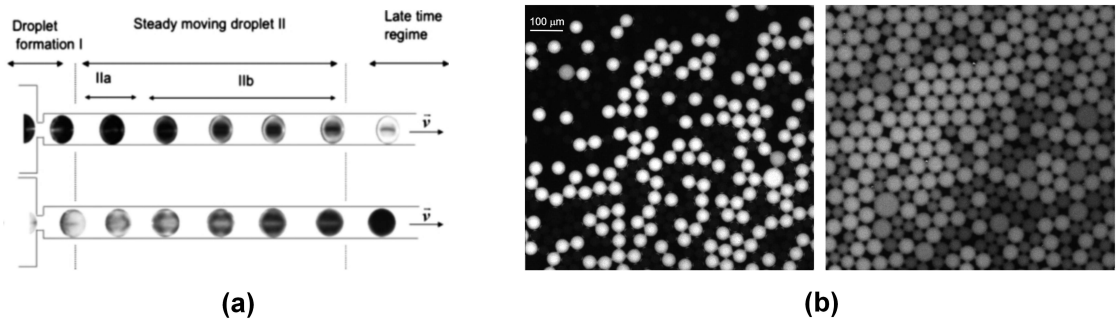

Figure 2.8: Microfluidic studies of mass transfer in two-phase systems. (a) Extraction and purification of compounds from/in emulsion droplets shown at different times. Image taken from [117]. (b) Fluorescence images of emulsion droplets incubated on a microfluidic chip, immediately after droplet formation (left) and after 6 hours of incubation (right). Image taken from [19].

Bai *et al.* [20] have developed a double droplet trap system to study mass transport between emulsion droplets. The authors suggested that the transport of small molecules is occurring "across the resultant surfactant bilayers formed between droplet pairs". This was justified with the observation that "the droplets were clearly deformed, strongly suggesting the formation of a surfactant bilayer". However, as their trapping strategy is relying on constant fluid flow through the experimental zone to keep the droplets in contact, such deformations might be the result of the hydrodynamic drag force acting on the droplets (figure 2.9a). In contrast, undoubtedly it was shown that the transport of the fluorophore fluorescein between neighbouring droplets is significantly faster when the continuous phase is based on hydrocarbon liquids (mineral oil, 1% Span80) than when its based on perfluorinated compounds (FC-77, 1% 'EA' surfactant) (figure 2.9b). It was reasoned that "the nature of the bilayer determines the transfer rate of molecules". In detail it was stated that "Span 80 has a high fluidity at the water/oil interface and shows high leakage of entrapped water-soluble dye molecules. In contrast, the RainDance surfactant leads to more stable droplets and provides a superior sealing of the interface [...].". However, the solubility of fluorescein in hydrocarbon and fluorocarbon liquids is expected to differ dramatically. Therefore it can not be excluded that these observations are a result of a transport mechanism based on phase partitioning rather than transport through surfactant bilayers.

Woronoff *et al.* [22] have shown in their experiments that the exchange rate of small molecules between droplets is dependent on their hydrophobicity. Their study was based on the measurement of the retention of several coumarin derivatives in

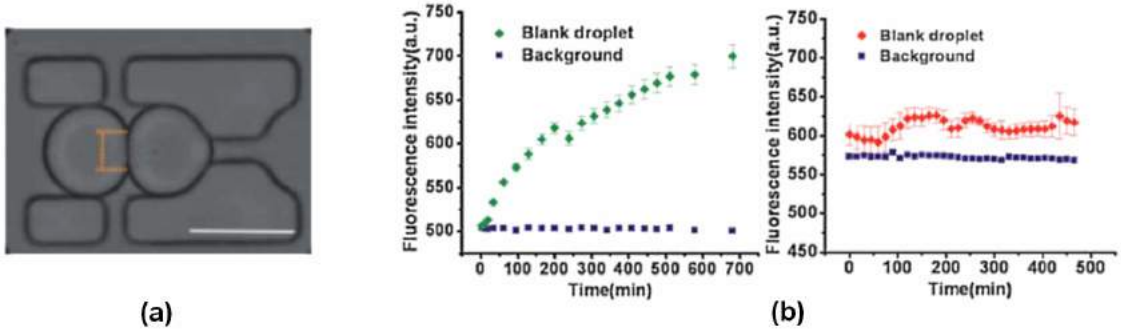

Figure 2.9: Images and results of a microfluidic double droplet trap system. (a) Two droplets trapped in microfluidic obstacles at an oil flow rate of 8000 μL h^{-1}. (b) Transfer of fluorescein between two trapped droplets for a hydrocarbon continuous phase (left) and a perfluorinated continuous phase (right). Images taken from [20].

water-in-fluorinated-oil emulsion droplets. A direct link between half-life of retention of the fluorophores in the emulsion droplets and the predicted partition coefficient of the dye was found.

Besides experimental studies giving insight into solute transport processes between monodisperse emulsion droplets, theoretical studies have been presented [76, 77]. Interestingly, the results of these studies are radically different. While Chen *et al.* report the rate limiting step of transport between emulsion droplets to be the transport of solutes across the droplet boundary, Dunstan *et al.* report it to be the solute diffusion through the continuous phase.

Chen *et al.* [77] used numerical methods to model the transport of fluorophores between water-in-hydrocarbon oil or alternatively in water-in-fluorinated oil emulsion droplets arranged in a two-dimensional hexagonal packing. The authors are using a model assuming an effective permeability of fluorophores across the droplet interface of 10^{-8} m s^{-1}, which is based on the permeability of rhodamine B across the cornea, measured in another study [121]. The authors found, for the examined case, that "the leakage process was rate-limited by the transport of the probe across the droplet boundary, rather than by diffusion through the continuous phase [...]".

Dunstan *et al.* [76] presented a study, which was as well investigating the transport of reagents between water-in-hydrocarbon oil emulsion droplets in two-dimensional hexagonal packing. Their model is based on the assumption that no significant energy barrier for molecules crossing the droplet interface exists. Accordingly they find that the rate limiting step of transport is the diffusion across the continuous phase.

In summary, albeit the recent progress using microfluidic tools, fundamental understanding about the mechanism of mass transport in emulsion is still lacking. In literature, the interpretation of experimental data as well as theoretical models, trying to access fundamental information about the mechanism of mass transport, are contradictory. Especially the discussion about the rate limiting step of transport and the role of the surfactant in mediating mass transfer in emulsion is controversial.

However, exploiting the full potential of microfluidic tools allows to create more sophisticated systems than the ones that have been presented. Controlling not only the composition and the size but also the spacing and packing of emulsion droplets allows to access these fundamental issues as shown in this work.

3 | Dynamics of molecular transport in emulsion

Philipp Gruner, Yousr Skhiri, Benoît Semin, Quentin Brousseau and Jean-Christophe Baret

In this chapter, microfluidic tools are applied to produce and analyse emulsions with hundreds of thousands of calibrated droplets. The transport of solutes between droplets is investigated by measuring the equilibration of fluorophore concentration differences. The key characteristics affecting the timescale and dynamics of fluorophore exchange are revealed and discussed in light of an analytical model based on a discrete diffusion equation. The results presented in this chapter have been published in Reference [122].

Contents

3.1 | Abstract

The dynamics of solute transport between two populations of randomly ordered monodisperse emulsion droplets, initially containing different solute concentrations, are investigated. The exchange rate is found to be dependent on the chemistry of the solute and proportional to the surfactant concentration in the continuous phase for the investigated water-in-fluorinated-oil emulsion. Furthermore it is demonstrated how the organisation of the droplets affects the exchange dynamics with the help of an analytical model. Additionally, it is shown that additives such as Bovine Serum Albumin (BSA) can significantly slow down the exchange process. This effect is relying on an increased solubility of the solutes in the aqueous droplets rather than on creating a barrier at the droplet interface as frequently described in literature.

3.2 | Introduction

The understanding of mass transport processes between emulsion droplets is crucial for the optimization of various emulsion-based products in areas such as food, cosmetics or pharmaceuticals. However, in the case of a mayonnaise, a cream or a pharmaceutical formulation, all droplets have the same composition and the ageing is mainly linked to mass transfer of the dispersed phase through the continuous phase or through bilayers possibly forming between the emulsion droplets.

With the recent applications of emulsion droplets for biotechnological applications, the paradigm for emulsion ageing has slightly shifted. Here each emulsion droplet has typically an individual composition at every time step depending on the initial loading of compounds and on the biochemical processes taking place inside the droplets [123, 124]. Hence, in these systems the exchange of solutes has to be considered as an additional ageing process, which leads to the equilibration of solute concentrations among the emulsion droplets and ultimately to a breakdown of the compartmentalization concept. As a consequence, it becomes important to understand such transport processes possibly enabling the control of molecular transfer between emulsion droplets [159]. However, understanding the transport of solutes in emulsions is not only essential for the optimization of microreactors for biochemical applications, but is also of great importance for other encapsulation systems which rely on controlled release such as drug delivery systems [125–129].

Several studies investigating the exchange of solutes between emulsion droplets

have already been performed without the help of microfluidic tools [130–132]. However, these studies do not capture the microscopic details of the mass transport process at the single droplet level. Using microfluidic tools does not only allow measurements at the single droplet level, but also provides a fine control of the droplet actuation and size as well as an access to short timescales ($\sim$ ms). Hence, it has become an appealing new tool to quantitatively study the physics and physical chemistry of interfaces and emulsions [133–138]. The transport of solutes between emulsion droplets was also investigated with the help of microfluidic tools [19–22]. However, the understanding of the mechanism of mass transport and the collective dynamics in populations of droplets is still lacking.

In this chapter, the dynamics of molecular exchange between hundreds of thousands of droplets containing different fluorophore concentrations is addressed. The relaxation of these concentration differences is measured experimentally and with the help of an analytical model the link between the microscopic exchange between two adjacent droplets and the collective dynamics at the scale of the entire emulsion is made. While the incubation of the emulsion takes place in a reservoir off chip, the droplets are produced and analysed in a microfluidic environment. The case of water-in-fluorinated-oil emulsions is studied, as they represent the most promising systems for biotechnological applications [26].

3.3 | Materials and methods

3.3.1 | Chemicals

Resorufin sodium salt and fluorescein sodium salt were purchased from Sigma-Aldrich. The solutions were prepared by dilution in Phosphate Buffer Saline (PBS) 1x, obtained by a 10 fold dilution in millipore water of a PBS solution (10x, Roth). Bovine Serum Albumin (BSA) was purchased from Acros Organics (Albumin bovine, fraction V).

3.3.2 | Surfactant

Aqueous droplets were produced in a hydrofluoroether (HFE-7500, 3M) and stabilised against coalescence by a block-copolymer surfactant (see Figure 3.1). The surfactant was prepared from the commercially available fluorous carboxylic acid Krytox 157-FSH (Dupont) and Jeffamine polyether diamines (ED 600, Huntsmann).

Surfactant solutions prepared from two different batches and referred in the following as KryJeffa$^{(1)}$ and KryJeffa$^{(2)}$ were used. The synthesis scheme was based on the synthesis described in Holtze *et al.* [139]. The surfactants used in this chapter are kindly provided by Dr. E. Mayot (Universite de Strasbourg).

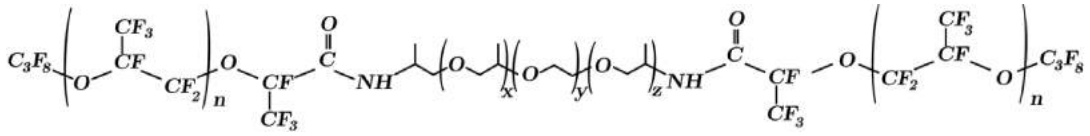

Figure 3.1: Structural formula of the used surfactant. It is a Krytox-Jeffamine block-copolymer ($x + z \approx 3.6$, $y \approx 9.0$, n =35-40).

.

3.3.3 | Surfactant characterizations

To characterize our system, the surface tension was measured for varying concentrations of surfactant using the pendant droplet method (DataPhysics OCA). Equilibria are reached after a time on the order of several minutes to several hours, depending on the surfactant concentration for droplets of volumes of $\sim$ 1 to 20 μL. Using Dynamics Light Scattering (Malvern Zetasizer), the scattered intensity of the surfactant solution was measured as a function of concentration. The automatized optimised mode for signal acquisition was used and the data were rescaled by the corresponding gain provided by the manufacturer. From the scattered intensity, a critical concentration for the formation of surfactant assemblies was conducted. The size of the scattering objects was obtained by the time-correlation of the scattered signal. Both methods suggest a critical surfactant concentration in HFE-7500 in the range of 0.02-0.04 wt% (Figure 3.2). The Dynamics Light Scattering (DLS) measurements also showed an increase of the scattering signal corresponding to an increase of the number of objects with the surfactant concentration (quasi-linear relationship) with a weak change in the size of the assemblies at higher concentrations (from a radius of 80 nm to 120 nm over 3 decades in concentration).

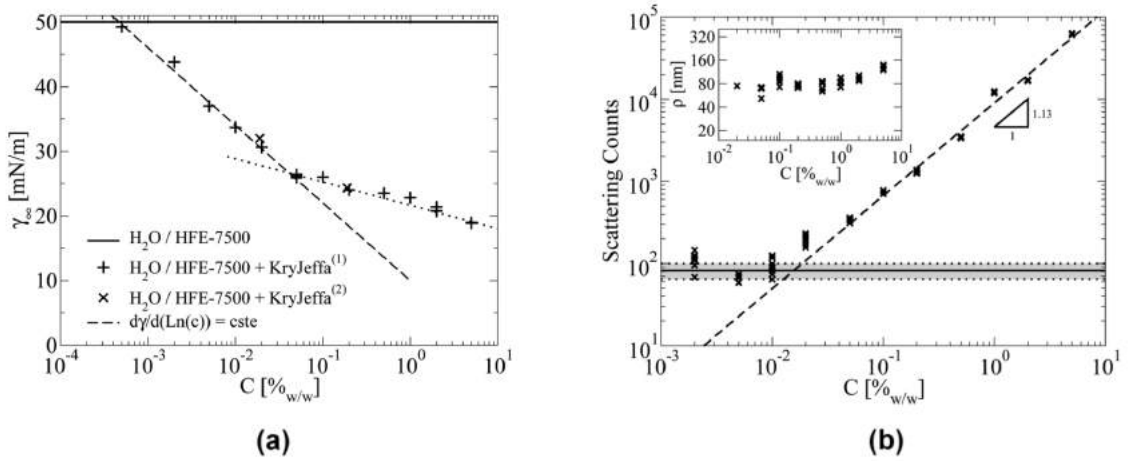

Figure 3.2: Surfactant characterization by surface tension and dynamic light scattering. (a) Equilibrium surface tension for the water/HFE7500 interface in the presence of the surfactant at different concentrations. The reproducibility of the synthesis was checked with two batches of surfactant (+ and ×). (b) Dynamic Light Scattering of HFE7500 containing various concentrations of surfactant. The background count rate of the pure oil is given by the horizontal full line. The grey area represents the standard deviation for 10 measurements. At low surfactant concentrations (below 0.02 wt%), the scattered count rate is in the oil background. Above 0.02 wt%, the count rate of the diffused light is quasi-linear (exponent 1.13). Inset: The radius ρ of surfactant assemblies measured by correlation of the scattering signal is slightly increasing from around $\rho = 80$ nm at 0.02 wt% to 120 nm at 5 wt%. In some runs at 0.02 wt% the background was too large to obtain a proper correlation. Combining both methods leads to a critical surfactant concentration in the range to 0.02 - 0.04 wt%. Measurements were conducted by Quentin Brousseau.

3.3.4 | Microfabrication

Microchannels of depth 60 μm were produced with standard soft-lithography techniques by replica molding of a SU-8 master in Polydimethylsiloxane [140]. The PDMS stamp was then bound to glass after oxygen plasma activation and hydrophobized using a commercial coating agent (Aquapel, PPG Industries). A collection vial was prepared using a 1 mL plastic syringe (BBraun) cut at both ends with a scalpel. Two cylindrical PDMS blocks cut from a crosslinked PDMS slab were prepared: in one PDMS cylinder, one hole was punched with a Harris Unicore biopsy punch (0.75 mm diameter) to allow a connection with a teflon tubing. Two holes were punched in the second cylinder. Both cylinders were then used to close both ends of the vial.

3.3.5 | Chip connection

All flow rates were controlled by Nemesys syringe pumps (Cetoni GmbH). The bottom of the collection vial was connected to the outlet of the droplet production device at one hole and to a syringe at the second one. The syringe was actuated by the syringe pumps (Control Pump) to either push or withdraw liquid. The top of the collection vial was connected back to the chip. Before each experiment the collection vial was filled with HFE-7500 containing surfactant in a concentration specific for each experiment.

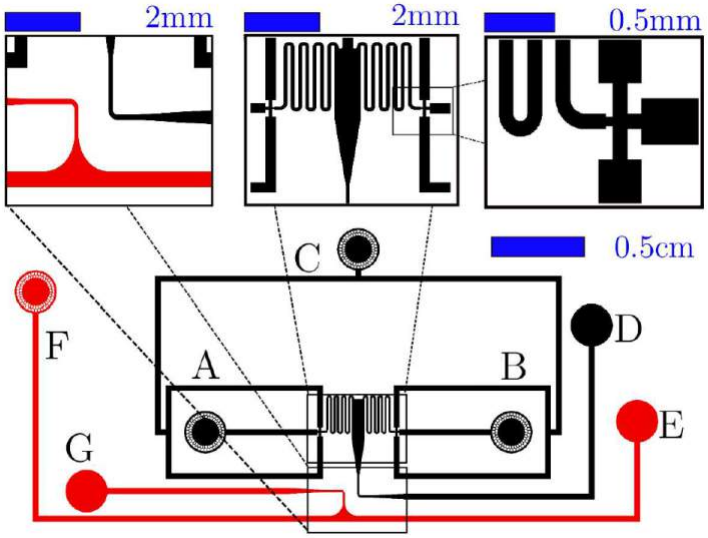

Figure 3.3: Sketch of the microfluidic device used for the production of calibrated emulsions with two populations of droplets containing two different fluorophore concentrations with zooms on the parts of interest. The microfluidic chip does have two separate parts. The production unit is shown in black and the reinjection unit is colored in red. In the production unit, the aqueous solutions are injected to inlets A and B. Inlet C is the inlet for the fluorous phase. The droplets flow towards outlet D. At the outlet D, the droplet are collected in the vial. After incubation in a vial, the droplets are reinjected into inlet E and flow towards outlet G. F is an additional inlet for the fluorous phase, required to sufficiently space droplets for a precise measurement of the fluorescence signals of individual droplets.

3.3.6 | Droplet production, collection and reinjection

Droplet-based microfluidic systems were used to produce a monodisperse emulsion. The droplets were containing specific concentrations of resorufin sodium salt in PBS (either 0 μM or 10 μM). Both droplet types were produced in parallel with the

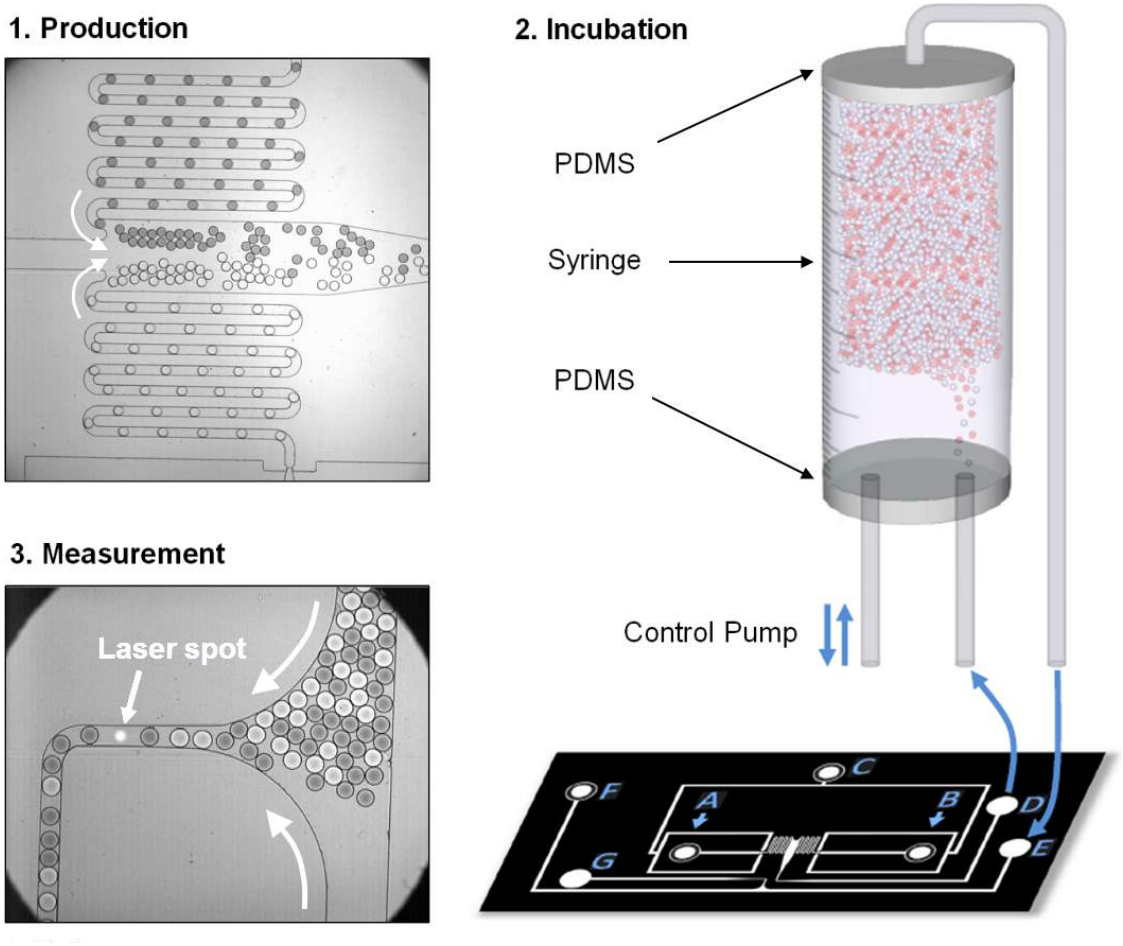

Figure 3.4: Overview of the experimental procedure. Two populations of droplets are produced on chip, incubated off chip and reinjected back into the microfluidic chip, where the fluorescent read-out takes place. The arrows indicate the fluid flows. The control pump is used to pump liquids into (reinjection mode) or out (filling mode) of the vial.

same size and frequency at two nozzles by flow focusing in a fluorinated oil (HFE-7500, 3M). The droplets additionally contained a specific concentration of fluorescein sodium salt used for long-term encoding of the droplet type (150 nM and 50 nM). The measurement of the fluorescein fluorescence provided a way to determine if droplets initially contained 0 μM or 10 μM resorufin, even after the resorufin concentrations among the droplets are equilibrated. The oil flow rate was set to 100 μL/min (except when BSA is used, the oil flow rate being increased to 200 μL/min) and each aqueous flow rate was set to 50 μL/min resulting in droplet volumes of 0.3 nL. The droplets were stabilised against coalescence by the surfactant at concentrations ranging from 0.1 wt% (limit of emulsion stability) to 5 wt%. With the chosen conditions no coalescence events were observed. As demonstrated in a previous study [137], preventing droplets from touching each other after generation increases

emulsion stability. Therefore the microfluidic device was designed with an incubation line of about 1 centimeter to increase droplet stability (see figure 3.3). During the stabilization time of the whole system, the Control Pump (CP) was set up to 'infuse' and the droplet flow through the collection vial towards the outlet. When the system was stabilised, CP was set to 'withdraw' with a flow rate tuned to stop the flow at the outlet of the collection vial and collect the emulsion in the vial (see figure 3.4). After typically 5 minutes, a volume of about 500 microlitres of emulsion was stored ($\sim 10^6$ droplets). Subsequently, the production of the droplets was stopped and CP was set to 'infuse' (typically at 1 μL/min). As a consequence, the droplets were flowing out of the collection vial back into the microfluidic chip towards the reinjection part where the fluorescence readout took place. The fluorescence signal of typically 10 - 100 droplets per second was measured. The delay time between the first droplet being produced and the first droplet being measured was typically 5 minutes.

3.3.7 | Fluorescence measurement

The fluorescence signal of each droplet was measured as it was flowing through the microfluidic channel using a laser-induced fluorescence setup equipped with a 473 nm and a 532 nm laser (DragonLaser) and photomultiplier tube (PMT, Hammamatsu)(Figure 3.5). The laser spot size was focused to be only a few microns in diameter and hence much smaller than both the droplets and the microfluidic channels, which have a width of 100 μm. The optical filters and dichroics were purchased from AHF, the mounts and optical accessories from Thorlabs. For each droplet, the maximum fluorescence intensity in the green (fluorescein signal) and the orange (resorufin signal) channel was recorded. The relative fluorescence unit RFU is here defined as the measured voltage U rescaled by the Gain G as: RFU $= U/G^{6.8}$. The exponent 6.8 depends on the type of PMT used. It has been experimentally verified to correspond to the data of the manufacturer. The droplet intensity as a function of time is recorded in real-time by using a FPGA board (cRIO, National Instruments) controlled by a home-made LabVIEW routine. The measurement of the maximum of the signal is optimized for fast processing with the FPGA board (up to several thousands of droplets per second processed in real time). It should be noted that it is sometimes sensitive to noise levels and laser instabilities leading to small variations in the measurements (of maximum 10 percent). However, the ratio of signals stays

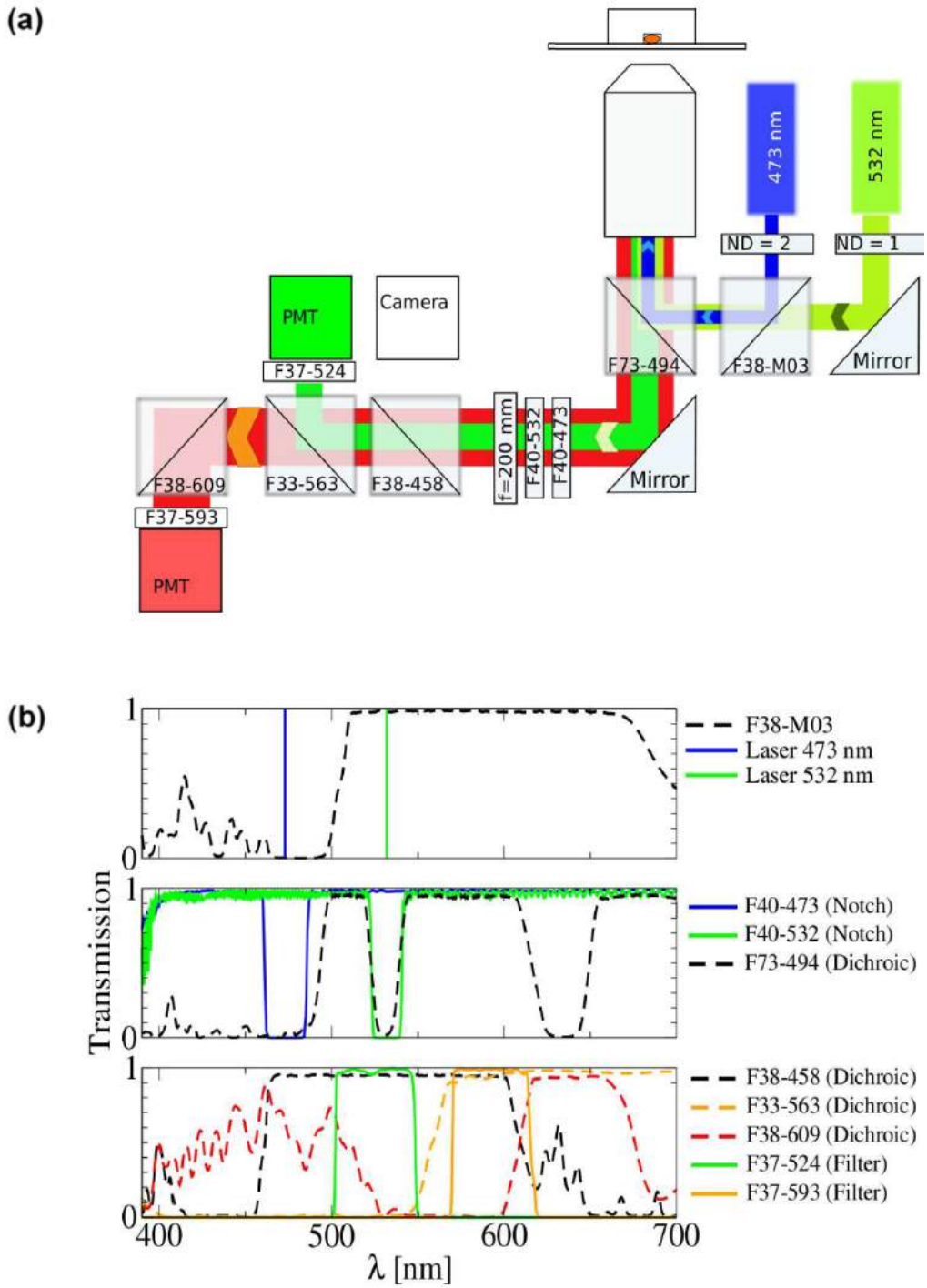

Figure 3.5: Optical setup used for the measurement of fluorophore concentrations in emulsion droplets. (a) Sketch of the laser-induced fluorescence setup for high-throughput single droplet measurement at two different wavelengths. Droplets flowing through laser spots focused into a microfluidic channel emit fluorescent signals according to their fluorophore concentrations. The signals are separated by dichroic mirrors and detected by PMTs. (b) Transmission spectra of the applied optical components.

constant. The single point measurement provides a tool to measure the dynamics of equilibration of the chemical potential of the fluorophores on the single droplet level.

3.3.8 | Data processing

Data were post-processed with home-made scripts using standard toolbox in MATLAB. First the green fluorescence was analysed to distinguish the two populations of droplets. These signals were constant at the time-scale of our experiments. The orange fluorescence of both populations was fitted by Gaussian distributions to obtain the means m_1 and m_2 of each droplet population. The fluorescence signals were found to be proportional to the fluorophore concentrations. Therefore the value $m_2 - m_1$ is proportional to the difference of fluorophore concentrations Δc between the two populations. By rescaling the data, we obtained a measurement of the concentration difference rescaled by the initial concentration difference Δc_0: $\Delta c/\Delta c_0 = (m_2 - m_1)/(m_2 - m_1)_0$. This parameter is equal to 1 at the beginning of the experiment and reaches 0 when the fluorophore concentrations are equilibrated. This approach provides means to compare experiments performed for different fluorophores and different initial ratios of fluorophore concentrations.

3.4 | Experimental results

In the presented study, resorufin sodium salt was chosen as a model fluorophore that is exchanged between aqueous droplets dispersed in fluorinated oils. The fluorophore was chosen for two reasons. First it is often used for biochemical assays frequently applied in the field of droplet-based microfluidics [141, 142]. Second, the timescale of equilibration for systems comprising heterogeneous concentrations of the fluorophore was reported to be on the order of a few hours in water-in-fluorinated-oil emulsions [18], perfectly suited to precisely access the dynamics of the exchange process. Additionally, it was reported that no detectable exchange of fluorescein was found in the concerned system [18]. These findings were verified in preliminary experiments (see Fig. 3.6). For these experiments, similar to the experimental procedure described by Courtois et al. [19], droplets containing two distinct concentrations of a fluorophore were incubated in a microfluidic chamber and the fluorescent signals of the two droplet populations were measured as a function of time.

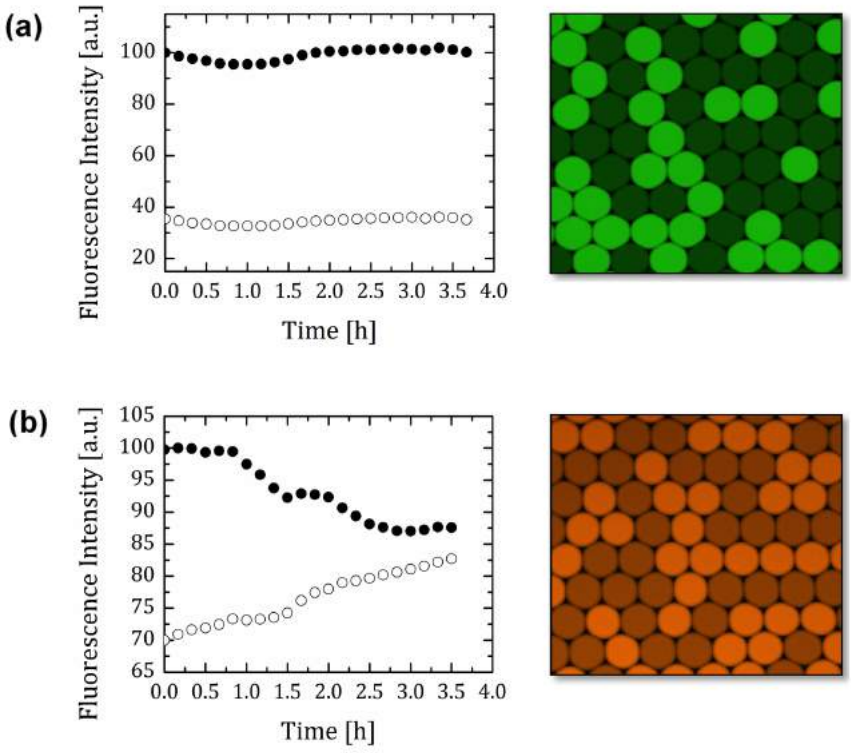

Figure 3.6: Qualitative results of fluorophore exchange. The surfactant concentration in the continuous phase (HFE7500) was 1 wt%. Aqueous droplets were containing PBS (1x) and initially a fluorophore concentration of 100 μM or 10 μM. (a) No detectable exchange of fluorescein sodium salt was observed on a timescale of 4 hours. (b) Equilibration of resorufin sodium salt concentrations between two droplet populations on a timescale of 4 hours.

As reported in literature [18] it was observed that the chemistry of the fluorophore influences the rate of exchange. This confirms previously published results [22] suggesting that the exchange rate of organic molecules increases with their hydrophobicity. In fact, in simple partitioning experiments it can be shown that resorufin sodium salt is more hydrophobic than fluorescein sodium salt. The partition-coefficient of organic molecules between an aqueous phase and octanol is generally accepted as a measure of how hydrophobic a chemical substance is [143]. In figure 3.7, such partitioning experiments are shown for various fluorophore molecules.

The partition coefficient is calculated by measuring the fluorophore concentration via fluorescence intensity in the aqueous phase with a microplate reader (Spectra Max Paradigm, Molecular Devices). Concretely, the partition-coefficient $\log P$ is calculated as the logarithm of the ratio of fluorophore concentrations in the octanol c_{oct} and in the aqueous phase c_{aq} in equilibrium: $\log P = \log \frac{c_{oct}}{c_{aq}}$. The exchange rate of the fluorophores was accessed qualitatively as quantitative measurements on

(a)

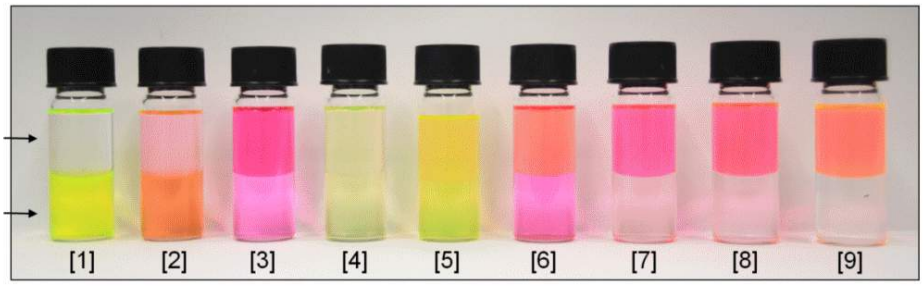

(b)

#	Name	log P	Exchange timescale
[1]	Fluorescein	- 1.5 ± 0.4	Days
[2]	Eosin Y	- 0.8 ± 0.3	Days
[3]	Rose Bengal	0.6 ± 0.2	Days
[4]	Rhodamine 110	- 0.1 ± 0.1	Hours
[5]	Rhodamine 123	0.1 ± 0.1	Hours
[6]	Resorufin	0.5 ± 0.2	Hours
[7]	Rhodamine 101	1.1 ± 0.1	Minutes
[8]	Rhodamine B	0.9 ± 0.1	Minutes
[9]	Rhodamine 6G	2.3 ± 0.2	Minutes

(c)

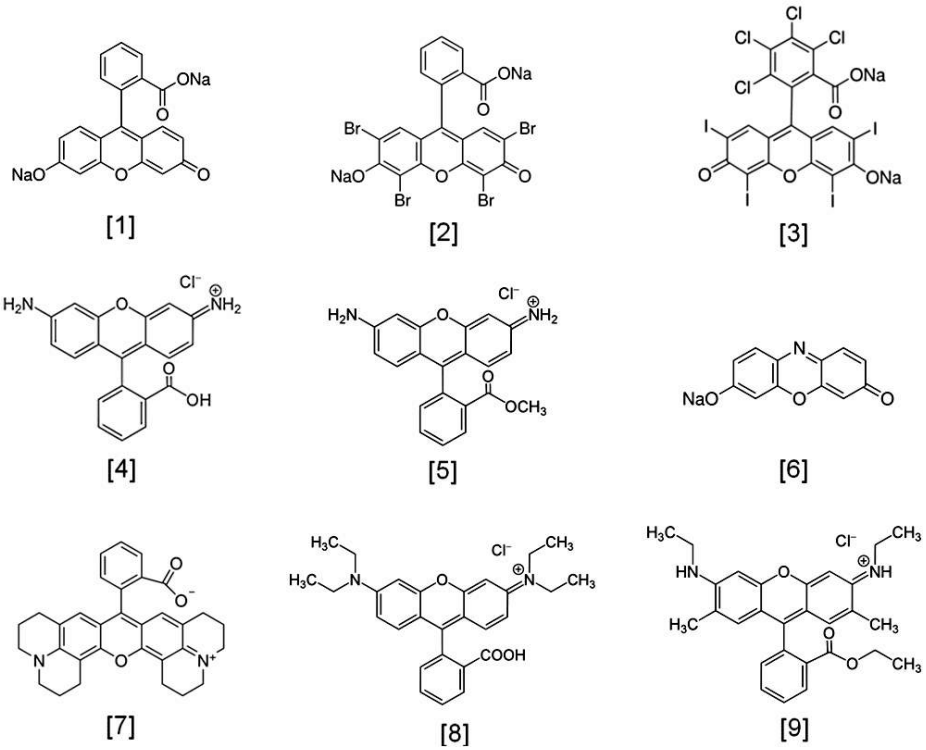

Figure 3.7: Impact of fluorophore chemistry on rate of exchange. (a) Determination of octanol-water-partition-coefficent $\log P$ for various fluorophores. Aqueous solutions containing initially a fluorophore concentration of 100 μM were exposed to octanol and incubated for 72 hours. (b) Qualtitative measurements of the exchange timescale, measured with the same procedure as described in the 'Materials and Methods' section and a surfactant concentration of 1 wt%. (c) Structural formula of the investigated fluorophores.

a much longer (several days) and or a much shorter timescale (few minutes) require a different approach for the incubation of droplets.

In agreement with the results obtained by Woronoff et al. [22] a clear trend, suggesting that the rate of exchange is increasing with the log P value (increasing hydrophobicity) of the fluorophore, is found. Higher $\log P$ values reflect an increased tendency of the molecule to be partitioned from the aqueous phase into another phase due to more favourable interactions with the alternative solvent. The observed dependency of the exchange rate on the hydrophobicity of the molecule is suggesting a mass transport mechanism based on phase partitioning.

However, it is important to note that other properties of the molecule might also affect the rate of exchange. For example, in the case of Rose Bengal a $\log P$ value on the order of resorufin sodium salt was measured, but the exchange rate is significantly smaller. It is therefore suspected that additionally specific non-covalent interactions between organic molecules and the fluorous surfactant molecules affect the rate of exchange. This topic is discussed in detail in chapter 5.

To quantitatively study the equilibration of fluorophore concentration differences in a macroscopic emulsion, an approach was developed allowing the precise measurement of fluorophore concentrations in single droplets as a function of time. Here, two populations of monodisperse droplets with a volume of about 0.3 nL are produced and mixed on a microfluidic chip. One population contains resorufin sodium salt (10 μM) while the other does not contain this fluorophore. However, both populations contain a specific, relatively low concentration of fluorescein sodium salt (150 μM and 50 μM), used to encode the droplet type. The equilibration of the fluorophore concentrations, are accessed by measuring the fluorescent signals of the droplets as they are flown through a laser spot. In figure 3.8a a typical time trace of the droplets flowing through the measurement point is shown. Figure 3.8b shows the typical time distributions of the droplet fluorescence over a few hours for a surfactant concentration of $C = 0.5$ wt%. From the raw data, the time distribution of the fluorescence signal were generated by binning typically 2000 droplets. In this manner color plots corresponding to the time evolution of the histogram can be generated (figure 3.8c).

The sum of the fluorescence signals of the two populations was constant throughout the measurements indicating that the fluorophore is preserved (no chemical modification nor bleaching). This also indicates that the fluorophore mainly remains in

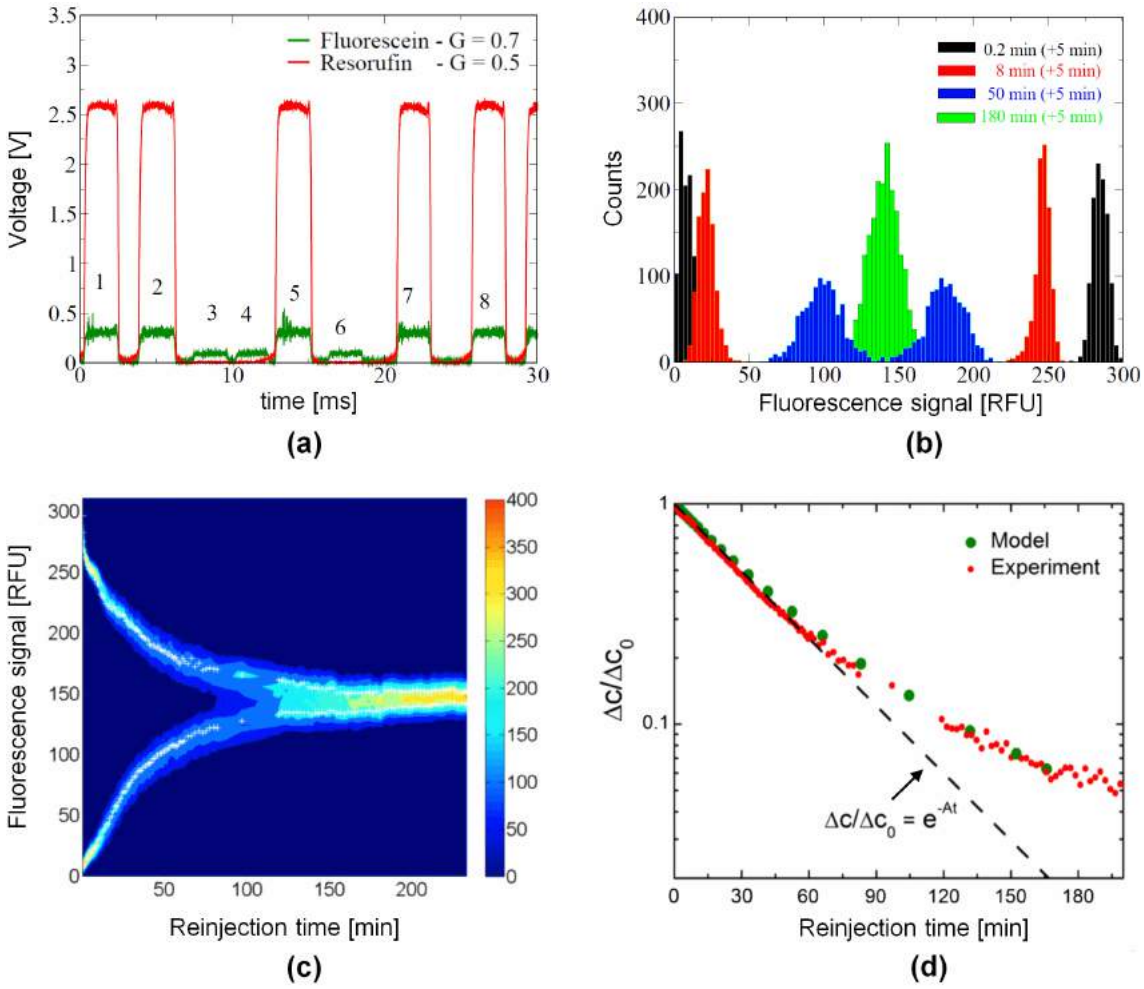

Figure 3.8: Fluorescence measurement and data analysis. (a) Signals measured on the PMTs after droplet production and mixing. Droplets containing 10 μM of resorufin (droplets 1, 2, 5, 7 and 8) are encoded with 150 nM of fluorescein sodium salt. The droplets initially containing no resorufin (3, 4 and 6) are encoded with 50 nM of fluorescein sodium salt. (b) Histogram of resorufin fluorescence at different reinjection times for $C = 0.5$ wt% of KryJeffa$^{(1)}$. The histograms are obtained from about 2000 droplets each. (c) Full time histogram (colorplot) of the resorufin fluorescence recorded over ~ 4 hours in HFE-7500 with $C = 0.5$ wt% of KryJeffa$^{(1)}$-surfactant. (d) Equilibration of the normalized concentration difference $\Delta c/\Delta c_0$ between the two droplet populations. The red dots correspond to the experimentally obtained values. The dashed line corresponds to a fit of the early time kinetics with an exponential function, with A as a fitting parameter. The relaxation dynamics are recovered by an analytical model indicated by the green dots. The model is introduced in section 'Modelling'.

the aqueous compartments. We further observed that the initial fluorophore concentration did not significantly impact the time-scale of the process which justifies the rescaling of the concentration difference by the initial concentration c_0. In addition, no change of droplet size was observed over the time-scale of the experiments. The transport of water between the droplets was prevented due to the fact that all

droplets contain PBS buffer, effectively fixing the chemical potential of the water molecules in both populations.

The relaxation of the fluorophore concentration differences among the droplets fits an exponential decay only in the early time kinetics (figure 3.8d). The exponential decay is not maintained at longer time-scale. This finding is explained taking the random distribution of micro-environments of the droplets into account. The connection between the relaxation dynamics and the micro-environments of the droplets is explained in detail in the 'Modelling' section.

Accessing the late kinetics of the process is not necessarily straight-forward as the fluorescence distributions of both populations overlap before equilibrium is reached. The ability to measure the mean fluorescence signal of each population in the late kinetics of the relaxation process relies on the encoding of the droplet populations with fluorescein sodium salt, whose exchange is negligible on the timescale of the experiment. The concentration difference in fluorescein sodium salt is therefore preserved throughout the experiment and allows to correlate each droplet to its respective population even when the resorufin sodium salt concentrations are equilibrated.

Experiments were performed for several surfactant concentrations above the critical surfactant assembly concentration, found by surface tension and light scattering measurements. Figure 3.9a shows the time variation of the concentration difference over several hours of incubation for various surfactant concentrations. Clearly, the rate of fluorophore exchange increases with the surfactant concentration. Interestingly, all the experimental data collapse on a single master curve (Figure 3.9b) using a single time-scale τ_e for each surfactant concentration. This is indicating that the mechanism for the fluorophore exchange is similar at all measured surfactant concentrations. The late kinetics follow a power-law with an exponent -3/2. This behaviour is recovered in the analytical model introduced in the section 'Modelling'.

The perhaps most important finding is that τ_e is inversely proportional to the surfactant concentration (Figure 3.10) over almost two orders of magnitude. Hence, in contrast to other systems where the exchange is linked to bilayer formation [65], the investigated emulsion system shows the importance of the surfactant molecules remaining in the continuous phase on the transport process. Here, the transport of the fluorophores is primarily mediated by surfactant molecules apparently mediating solubility in the fluorous phase.

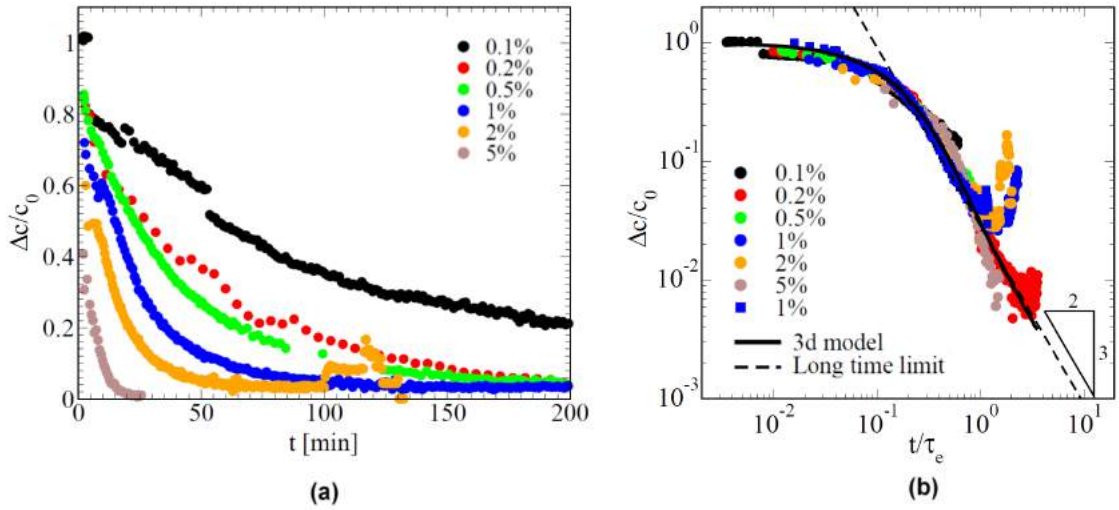

Figure 3.9: Kinetics of the relaxation of fluorophore concentration differences as a function of surfactant concentration. (a) Measurement of the normalized concentration difference $\Delta c/c_0$ of the two populations of droplets for increasing surfactant concentration. The kinetics are faster for larger surfactant concentrations. (b) Rescaling of the experimental data by the time-scale τ_e (given in figure 3.10) and comparison with an analytical model considering the relaxation in a 3-dimensional case with 6 neighbours (full line). At large time, the kinetics follows a power-law with an exponent -3/2 (dashed line). The increase observed at the end of certain runs are artefacts resulting from the reinjection of the last droplets from the vial.

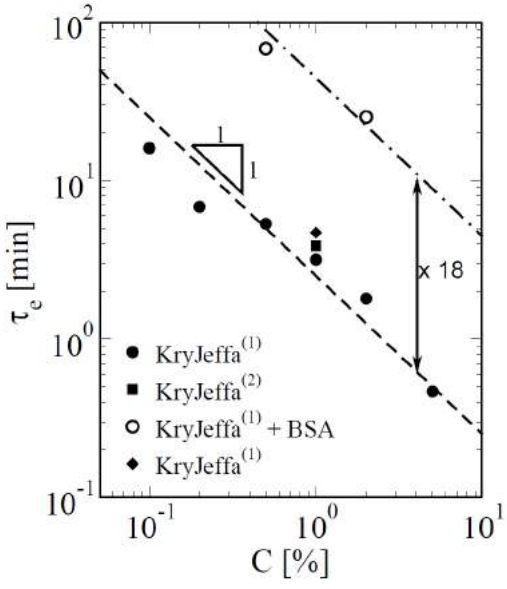

Figure 3.10: Time-scale τ_e of the exchange process as a function of surfactant concentration C. The data were obtained with with 10 μM initial resorufin concentration, except for the diamond, where for a 1 μM resorufin initial concentration was used. The open circles correspond to the rescaling in presence of Bovine Serum Albumin (the dashed line and the dotted-dashed line correspond to a linear relationship and the ratio of both is 18).

Ultimately, the obtained results suggest that assemblies of surfactant molecules act as nanoscopic environments for the solubilization of organic compounds in the fluorous phase [132].

As a method to significantly slow down the exchange of organic molecules between emulsion droplets it was suggested to add the protein bovine serum albumin (BSA) to the dispersed phase [19]. Indeed, this effect was also found in the investigated emulsion system. More precisely, by adding BSA to the aqueous phase at a concentration of 25 mg/mL, an 18 fold decrease of the exchange rate of resorufin was obtained. However, the exchange rate is still proportional to the surfactant concentration (Figure 3.11).

The decelerated exchange process in the presence of BSA was reasoned by the formation of a "strong film" [19] at the oil-water interface acting as a barrier to the transport of organic molecules across the droplet boundary. Interestingly, in such case one would not expect a dependency on the surfactant concentration in the presence of BSA as the fluorophore transfer across the droplet boundary would be the rate limiting step of transfer. To clarify the role of BSA in the exchange of organic molecules between emulsion droplets, the following experiment was performed: All droplets contained initially the same resorufin concentration but the BSA (25 mg/mL) was present in only one droplet population. Those droplets were encoded with 150 nM fluorescein. Droplets containing no BSA contain only 50 nM fluorescein encoding the presence respectively the absence of the protein. Within this system the variation of the resorufin fluorescence signal was measured as a function of time. Surprisingly, it is observed that the relaxation process leads to an *a priori* counter-intuitive result: the difference in fluorophore concentrations is increasing during incubation with a relatively short time-scale on the order of 50 minutes (figure 3.11a). At equilibrium, the fluorescence signals of the two droplet populations are different by a factor of 15 (figure 3.11b) and the most fluorescent droplets are the ones containing BSA. Hence, after equilibration of the chemical potential of the fluorophores, the concentration in the droplets containing BSA is about 15 fold larger than in droplets containing no BSA.

These experimental results clearly contradict the assumption that BSA slows down the exchange process by creating a viscoelastic layer at the droplet interface acting as a kinetic barrier. If the BSA would only act as a barrier to exchange, the chemical potential of the fluorophores in the droplets would be initially at equi-

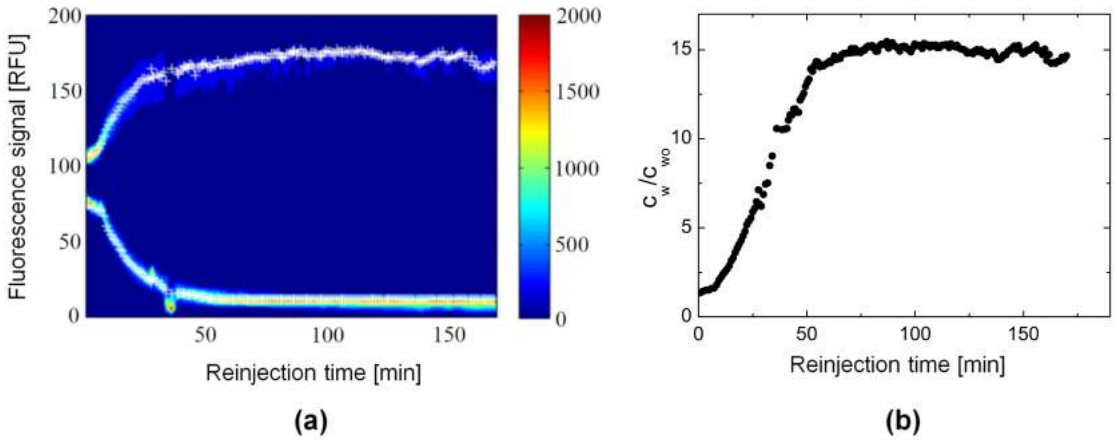

Figure 3.11: Modification of exchange kinetics in the presence of heterogeneous concentrations of bovine serum albumin. (a) Full time histogram (colorplot) of the resorufin fluorescence recorded over ~ 3 hours in HFE-7500 with $C = 2$ wt% of KryJeffa$^{(1)}$-surfactant when all droplet initially contain 5 μM resorufin sodium salt and additionally half of the droplets contain 25 mg/mL of BSA. (b) Ratio of resorufin fluorescence between the two droplet populations as a function of time. c_w is the fluorophore concentration in the droplet with BSA and c_{wo} without BSA. In equilibrium a 15 times higher concentration of resorufin sodium salt in droplets containing BSA compared to droplets not containing the protein is obtained.

librium. In such case the fluorescence signals in both populations should remain constant. Furthermore the time-scale of the equilibration process is similar to the time-scale of exchange previously measured for the corresponding surfactant concentration (2 wt%), which indicates that the mechanism of transport by the surfactant molecules is not affected by the presence of BSA. Finally, the obtained fluorescence ratio between the droplet populations in equilibrium matches quantitatively the decrease of the exchange rate upon addition of BSA. In conclusion, this experiment shows unambiguously that BSA acts on the partitioning behaviour of the fluorophores and therefore has the ability to slow down the exchange process rather than by creating energy barriers at the droplet interface. This topic is discussed in more detail in the section 'Discussion'.

3.5 | Modelling

A model to describe the fluorophore exchange process recovering the collective relaxation dynamics in emulsions was developed. An ensemble of droplets separated by a porous membrane of thickness L [144] is considered. Furthermore, for simplicity, droplets arranged on the nodes of a three dimensional square lattice are considered.

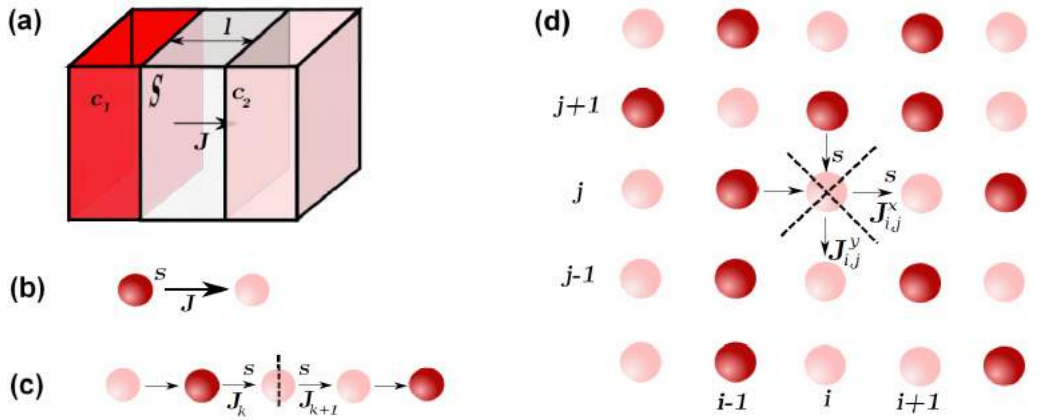

Figure 3.12: Schematic illustration of the model for molecular exchange between emulsion droplets. (a) For a porous membrane separating two compartments, the flux J depends on the concentration difference and geometry parameters (s, L). (b) For droplet pairs a similar description is used, where the flux is proportional to the concentration difference. In an ensemble of droplets, the exchange occurs with the nearest neighbours: (c) corresponds to a one-dimensional case, and (d) to the two-dimensional case on a square lattice.

The droplet on the node (k, l, m) contains molecules in a solvent at concentration $c_{k,l,m}$ and exchanges molecules with its 6 first neighbours only (4 neighbours in 2 dimensions, 2 neighbours in 1 dimension). The area of contact between the compartments is s (a fraction of the droplet surface area S) and the volume of the compartment is V (figure 3.12).

The difference in the chemical potential of the fluorophores between the two compartments is responsible for the diffusive flux J along each axis proportional to the concentration difference δc between neighbours as described for membranes or bilayers [65, 145, 146]:

$$J = -P\delta c \tag{3.1}$$

J is expressed in mol s^{-1} m^{-2}, the concentrations in mol m^{-3} and the permeability P has the dimension of a speed (m s^{-1}). In this case, the mass balance and Fick's law leads to a discrete version of the heat equation:

$$\frac{\partial c}{\partial \tilde{t}} = \underline{\Delta} c, \tag{3.2}$$

where $\underline{\Delta}$ is a discrete Laplacian and $\tilde{t} = t/\tau$ is the dimensionless time with $\tau = V/(Ps)$.

For periodic boundary conditions, the eigenvalues of the discrete Laplace operator are in three dimensions:

$$\lambda_{p,q,r} = -4 \times \left[\sin^2\left(\pi \frac{p}{N_x}\right) + \sin^2\left(\pi \frac{q}{N_y}\right) + \sin^2\left(\pi \frac{r}{N_z}\right) \right] \tag{3.3}$$

(for $0 \leq p, q, r < N - 1$) and the eigenvectors

$$V_{p,q,r}(k, l, m) = \omega_p^k \omega_q^l \omega_r^m \tag{3.4}$$

with

$$\omega_p = \exp(2i\pi p/N_x) \tag{3.5}$$

Due to the special form of the eigenvectors, the time evolution of the ensemble of N droplets is analytically expressed in the Fourier space as:

$$\mathcal{F}(c) = \mathcal{F}(c_i) \mathrm{e}^{\lambda_{p,q,r}\tilde{t}} \tag{3.6}$$

where c_i is the initial distribution and $\mathcal{F}$ denotes the Discrete Fourier Transform. Since equation (3.2) is linear, in the following the mean value of concentration are subtracted and normalized to 1 to represent concentrations between -1 and 1, defining the two subpopulations of droplets.

The smallest eigenvalue of the Laplace operator is -12 (in three dimensions) corresponding to the fastest decaying mode. In two dimensions the smallest eigenvalue is -8, in one dimension -4 and -2 for a single droplet pair. It corresponds in all dimensions to an eigenmode of a perfectly alternating array, where an empty droplet is surrounded solely by filled droplets and *vice versa*. In chapter 4 it will be shown that it is actually possible to construct an emulsion showing this eigenmode relaxation. An alternated three dimensional packing would equilibrate following an exponential decay with a time scale $\tau/12$. All other configurations decay more slowly.

The relaxation kinetics towards a uniform concentration depends on the excitation of the eigenmodes in the initial conditions. Experimentally, the mixing of droplets in the incubation vial leads to a random distribution of droplet positions. To investigate the effect of the disorder, equation 3.2 is solved for a completely random and uncorrelated initial condition. The scaling law is then recovered analytically. Since the value of the initial concentrations is 1 or -1 depending on the subpopulation, $\Delta c/c_0$ is proportional to the scalar product of c by c_i. Using Par-

seval's theorem, this scalar product can be computed in the Fourier space. In 3-d, one obtains:

$$\frac{\Delta c}{c_0} \propto \sum_{p,q,r} |\mathcal{F}(n_0)|^2 \mathrm{e}^{\lambda_{p,q,r}\tilde{t}} \tag{3.7}$$

Due to the completely random initial condition, all the modes are statistically excited with the same weight and $\Delta c/c_0 \propto \sum_{p,q,r} \mathrm{e}^{\lambda_{p,q,r}\tilde{t}}$. At long time, only the modes with the smaller eigenvalues remain, so that

$$\lambda_{p,q,r} \sim -4\pi^2((p/N_x)^2 + (q/N_y)^2 + (r/N_z)^2) \tag{3.8}$$

and the sum can be extended to $+\infty$. For large systems, we can use a continuum approximation, and

$$\frac{\Delta c}{c_0} \sim \int_0^{+\infty}\int_0^{+\infty}\int_0^{+\infty} \mathrm{e}^{-4[(\pi p/N_x)^2+(\pi q/N_y)^2+(\pi r/N_z)^2]\tilde{t}} \mathrm{d}p\mathrm{d}q\mathrm{d}r \tag{3.9}$$

which scales as $t^{-3/2}$ (for the 3-dimensional case). Figure 3.13 shows a summary of the model data in the three dimensional case and the corresponding asymptotic

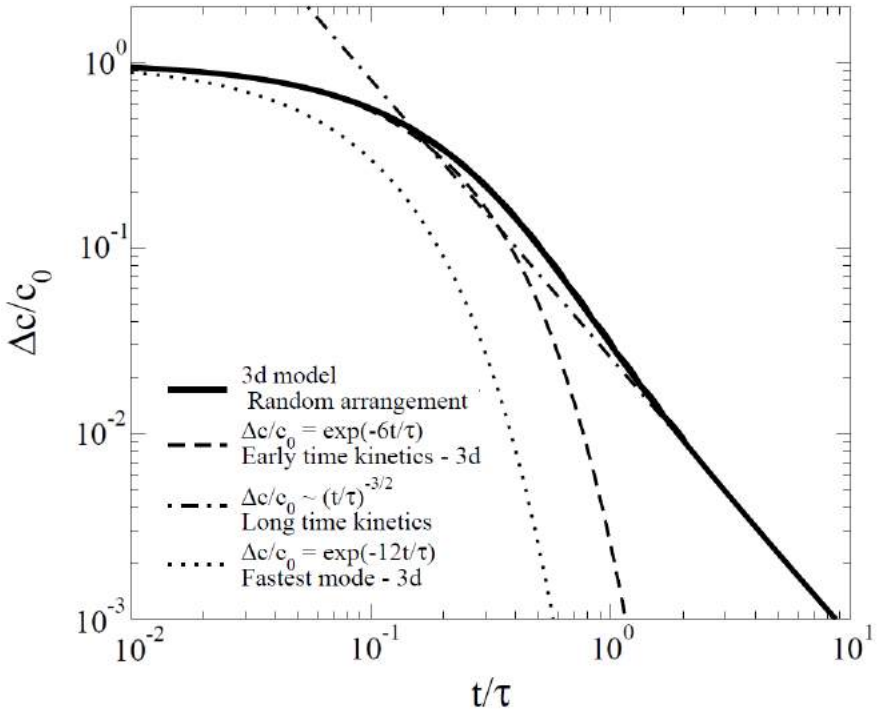

Figure 3.13: The model is solved for a three-dimensional packing on a square lattice. The results of the model in the three-dimensional case are shown. In agreement with the experimental findings, the early kinetics follow an exponential behaviour while the late kinetics follow a the power law with an exponent -3/2.

regimes. The model can also be solved for the 1-dimensional and the 2-dimensional cases and for any set of initial conditions using similar schemes. Similarly, it is recovered analytically that $\Delta c/c_0$ scales in 1-d like as $\tilde{t}^{-1/2}$, and in 2-d as $\tilde{t}^{-1}$. At short-times, an argument similar to the one at large time-scales leads to $\Delta c/c_0 \sim \sum_{p,q,r} \mathrm{e}^{\lambda_{p,q,r}\tilde{t}}$. Expanding the exponential close to 0 leads to $\Delta c/c_0 \sim 1 - \lambda\tilde{t}$, where λ is the average value of the eigenvalues, which is equal to -6 in three dimensions (-4 in two dimensions and -2 in one dimension). Therefore the early time kinetics in a random initial distribution is an exponential decay two times slower than the exponential decay of the fastest mode (the alternating case) of the corresponding dimension. In summary, the relaxation of the chemical potential at the emulsion level is a function of the initial distribution of the droplets in the packing. The maximum rate is obtained for an alternating packing and corresponds to the rate of exchange at the droplet pair level (corrected by the number of nearest neighbours). The early time kinetics of a random distribution is twice slower but has the same order of magnitude, while alternatively, the rate of exchange of an emulsion made of two layers would equilibrate with a much longer time-scale, that can be several orders of magnitude longer. These results are generic and do not rely on the exact description of the exchange mechanism at the droplet level.

3.6 | Discussion

The relaxation of heterogeneous fluorophore concentrations in water-in-fluorinated-oil-emulsions was investigated. It was shown that in the investigated system surfactant molecules play the key role for the transport of a model fluorophore, presumably by mediating solubility in the continuous phase. Additionally the role of additives such as BSA in slowing down the exchange process was clarified. Furthermore, with the help of an analytical model, it was presented how the organisation of the droplets affect the kinetics of equilibration. These key findings are discussed in the following.

3.6.1 | Rate limiting step of transport

It was measured how the time-scale of the relaxation of heterogeneous fluorophore concentrations is influenced by surfactant concentration, the chemistry of the transported molecules and the presence of additives such as BSA in the aqueous phase. The obtained results are in agreement with models of membrane permeability [25,

145,146]. When the rate-limiting step is the diffusion in the continuous phase respectively in a 'membrane' (case I of Zwolinksi *et al.* [145]), the membrane permeability can be expressed as $P = KD/L$ [145], K being the partition coefficient of the transported molecule between the continuous and the dispersed phase, D the diffusion coefficient of the transported species and L the membrane thickness. Here, the partition coefficient between the compartment and the membrane is an important parameter affecting the timescale of the transport process. Non-fluorinated organic molecules, such as resorufin, are typically highly insoluble in fluorinated oils. However, it is assumed that the used surfactant molecules, comprising an organic part, are mediating solubility in a fluorous phase. Hence an increase in surfactant concentrations results in an increased solubility of organic molecules in the continuous phase and consequently in a modified partitioning coefficient K, ultimately leading to an increased exchange rate as experimentally observed.

Furthermore, performing an experiment with BSA in half of the droplets provided means to indirectly address the role of the partition coefficient. Starting from droplets which all have an identical concentration of resorufin, but where half of the droplets contained 25 mg/mL of BSA, the concentration of resorufin in the two populations diverged until, at equilibrium, there was 15 fold higher concentration of resorufin in the droplets containing BSA than in those containing no BSA. Therefore adding BSA provides a means to modify the parameter K without modifying the fluorophore or the continuous phase. Exchange experiments performed with 25 mg/mL BSA in all droplets and with resorufin in only 50 % led to a decrease of the exchange rate by a factor of about 18, which matches quantitatively the corresponding decrease of K. The obtained experimental results are therefore consistent with a diffusion-limited permeability model.

This mechanism is also consistent with the results obtained with other fluorophores showing an increased exchange rate with increasing hydrophobicity: if the solubility in the aqueous phase increases, K decreases and hence the rate of exchange.

3.6.2 | Mechansim of molecular transport

While in other studies the permeability of a bilayer membrane has been linked to its fluidity [65], in the presented case, the surfactant molecules do not form bilayers. Instead, the surfactant in the fluorous phase plays the key role for the transport

process. In fact, the exchange rate was found to be proportional to the surfactant concentration, suggesting that the solubility in the continuous phase is increasing linearly with the surfactant concentration. Therefore the likely mechanism for transport is through the solubilisation of the fluorophore molecules into assemblies of surfactant molecules, which can act as relatively large ($\sim$ 100 nm diameter) carrier of organic molecules between aqueous droplets. That assemblies of surfactants and not single surfactant molecules are mediating the transport is also supported by the fact that above the critical surfactant assembly concentration, the free surfactant concentration is generally considered to be constant. Hence, no significant influence of the surfactant concentration on the rate of exchange would be expected in such case. The shape and size of the surfactant assemblies should be considered as an important parameter to control the transport of molecules between microreactors. In chapter 3, additional experiments are presented supporting these assumptions.

3.6.3 | The role of BSA in affecting the rate of molecular exchange

The decrease of solute exchange mediated by BSA has here been quantitatively measured with fluorinated oils as the continuous phase, but was previously reported for non fluorinated oils [19]. One of the initial explanation for the effect of BSA is the creation of a protein layer at the inner surface of the droplets which provides a barrier in a capsule-like manner as suggested earlier for mineral oils [19]. This layer would decrease the permeability of the medium between the droplets [147]. In this case, the rate-limiting step would be the diffusion through the BSA layer (case II or III of Zwolinksi et al. [145]). However with such picture one would not expect that (i) the surfactant concentration plays a role in the presence of BSA and that (ii) starting from equilibrated concentrations, the final state shows a concentration difference between droplets with and without BSA. The presented experiments therefore show unambiguously that BSA acts on the solubility of the fluorophore (a thermodynamic property) rather than on kinetic parameters such as energy barriers. The quantitative link between the equilibrium concentration ratio of resorufin in aqueous droplets with and without BSA and the exchange rate with BSA is consistent with a porous membranes model, where the permeability is controlled by the partition coefficient between the aqueous phase (the droplets) and the continuous phase (fluorinated oil containing surfactant). It is speculated that

the change in the partition coefficient of resorufin in the presence of BSA may be due to the remarkable capacity of serum albumins to bind a structurally diverse set of small molecules, including many drugs [148]. Such binding processes of resorufin, or other solutes, to BSA could potentially increase its solubility in the aqueous phase and hence lead to a decreased rate of exchange as experimentally observed.

3.6.4 | Geometrical considerations

For a given emulsification system, the time-scale $\tau = V/(Ps)$ controls the exchange, with a prefactor corresponding to the number of nearest neighbours. It is assumed that the surface area s is proportional to the droplet area scaling with the square of the droplet radius R^2. Therefore τ is expected to scale with the droplet size. Hence, a decrease of droplet size results in an increase of the molecular exchange rate. Other geometric parameters such as the droplet spacing distance or the dimensionality of the system are also expected to influence the rate of exchange. Further experiments investigating these scalings are presented in chapter 4, where the permeability P is clarified to be a function of geometrical parameters.

3.6.5 | Outlook

Microfluidic experiments provide means to study isolated assemblies of droplets receptively to generate a controlled packing in one, two or three dimensions. By measuring the exchange kinetics in different dimensions and varying the number of nearest neighbours, it will be possible to extract microscopic information on the membrane (for example what is the exact description of P and s). Microfluidic systems have a huge potential to address the remaining open questions by the possible on-chip control of packing geometries, droplet spacing or sizes for a deeper understanding of such transport phenomena. In chapter 4, as a next step, the effect of the packing geometry on the dynamics of the relaxation as well as the effect of specific droplet arrangements is studied.

Microfluidics provides a very powerful platform for the study of such transport problems by the possible control of droplet packing and lateral ordering of the droplets [50, 92, 149]. Finally, the mechanisms involved in this study are generic (a diffusive process) and could potentially be applied to a better control of collective effects in droplet population, for example, in active emulsions [83, 150, 151], to

control signalling in cell populations (chemotaxis, quorum sensing) entrapped in different ecological niche (here the droplets), or to design new systems for screening compounds by affinity. The ability to control the transport by additives selectively encapsulated in specific droplets in the emulsion would also open the door to applications for separation.

3.7 | Conclusion

In summary, microfluidics provides the tools to produce calibrated emulsions and to analyse hundreds of thousands of droplets at very high-throughput opening the way to quantitatively address physicochemical processes on the single droplet level in macroscopic emulsions.

Here, experimentally the equilibration of the chemical potential of organic molecules in an emulsion initially composed of two droplet-populations characterized by different fluorophore concentrations was measured. Interestingly, it was found that in the investigated system the transport of organic molecules is practically exclusively mediated by surfactant molecules. The exchange timescale is controlled by the surfactant concentration in the continuous phase and relates to a classical description of a porous membranes, where transport is occurring through partitioning of molecules between the dispersed and continuous phase. The obtained results suggest that organic molecules are transported with assemblies of surfactant molecules acting as nanoscopic environments for the solubilization in fluorinated oils and that the rate limiting step of transport is there diffusion through the continuous phase.

Furthermore it was shown that, due to the disorder in the initial condition, the macroscopic kinetics are not a simple exponential decay but a power-law and that the initial conditions have a major influence on the behaviour of the system. Additionally it was demonstrated how the initial distribution of droplets can affect the time-scale of the exchange process. The early time kinetics in a mixed emulsion are twice slower than the maximum rate, obtained for a perfectly organized alternating packing. Most of the important physics of the relaxation is contained in an analytical model: the equilibration process is a classical diffusion process through a Laplace equation from which emerge a dimension-dependent power-law.

Finally, the role of additives such as BSA in modulating the timescale of fluorophore transport was investigated. In contrast to reports in literature [19], here this effect is found to be relying on an increased solubility of the fluorophores in

the aqueous droplets rather than on creating a barrier at the droplet interface. Our findings have led other authors to suggested that "This hypothesis, usually adopted in the field, probably needs being revisited." [175].

By clarifying the role of BSA in affecting mass transport processes, new strategies, based on selective mass transport may be obtained by controlling the concentration of specific additives in the droplets to enrich a compound of interest. Such approach may be used for a versatile control of solute concentrations in emulsion droplets.

4 | Molecular transport in 'minimal emulsions'

Philipp Gruner and Jean-Christophe Baret

In Chapter 3, the dynamics of molecular transport between hundreds of thousands of randomly packed droplets were investigated. In this chapter the concept of 'minimal emulsions' is introduced. These emulsions are characterized by a small number of droplets precisely ordered and spaced. The investigation of these systems allows to precisely access fundamental information about the mechanism of mass transport in emulsions.

Contents

4.1 | Abstract

Emulsions are complex out of equilibrium multiphase systems. The complexity of these systems makes quantitative studies of dynamic physiochemical processes on a microscopic level difficult. To minimize the degree of complexity microfluidic tools are applied to produce and arrange calibrated emulsion droplets on a microarray. In this manner emulsions are simplified down to a level where the chemical composition and the microenvironment of each droplet is precisely controlled. The introduction of these 'minimal emulsions' provides new methods to access fundamental information about mass transport processes between emulsion droplets.

In this chapter the transport of fluorophores between two populations of droplets arranged in an alternating order on a one-dimensional array is investigated. Increasing the spacing distance between the droplets is slowing down the transport process as predicted by a diffusion-limited model describing the mass transfer by a purely diffusive transport through the continuous phase. The timescale of the process is inversely proportional with the surfactant concentration reflecting the fact that the solubility in the fluorinated oil is mediated by surfactant molecules. The methodology furthermore provides a measurement of the translational diffusion coefficient of the fluorophores in the continuous phase. We obtain a value of about 8×10^{-9} cm^2 s^{-1} suggesting that the fluorophore transport occurs via assemblies of surfactant molecules. Furthermore an approach to actively feed droplets with chemicals contained in neighboring droplets is suggested. This targeted delivery strategy is based on the use of additives and provides a simple solution to program the transport of compounds to droplet microreactors.

4.2 | Introduction

In chapter 3, the dynamics of molecular transport in emulsion were investigated. Although the application of microfluidic tools allowed the production of calibrated emulsion droplets and the precise temporal measurement of solute concentrations in single droplets, the rate-limiting step of transport could not be directly identified with this approach. In fact, experimentally accessing the rate-limiting step of mass transport in emulsion is not straight-forward. In literature recent theoretical models suggested that the rate determining step is either the transport of molecules across the droplet boundary [77] or alternatively the diffusion through the contin-

uous phase [76] for water-in-hydrocarbon-oil emulsions. Although, naturally this might depend on the specific emulsion system and mass transport process that is considered, there is no common agreement on whether a significant energy barrier for molecules crossing a surfactant-stabilized interface exists.

To experimentally access such fundamental information the microenvironments of the droplets must be precisely controlled to allow quantitative analysis. In this context the concept of 'minimal emulsions', made of an assembly of monodisperse droplets with defined order, composition and center-to-center distances, is introduced. In contrast to classical approaches where emulsions are created in a top-down manner by e.g. bulk or membrane emulsification, these minimal emulsions are constructed in a bottom-up way using microfluidic tools. Here the complexity of the emulsified system is reduced down to a level where the microenvironment of each droplet is precisely controlled: both composition and size of each droplet as well as the packing of the emulsion is fully controlled. By controlling all geometrical aspects, the complexity of the resulting emulsion is reduced to its minimum set of relevant parameters. Such a level of control is unreachable in bulk emulsification. By arranging trains of droplets with alternating distinct properties on a predefined array, the kinetics of equilibration are drastically simplified. Further by varying the distance between the droplets, fundamental information on the mechanisms of the mass transfer process, such as the rate-determining step of transport, are becoming experimentally accessible. The obtained information is applied to design effective strategies for the control of solute concentrations in emulsion droplets.

4.3 | Minimal emulsions

Emulsions are usually prepared by applying external forces to a mixture of oil and water to disperse one fluid into the other. When co-flown in a microfluidic environment, the homogeneous shearing of the liquids results in the production of highly monodisperse emulsion droplets. While following the microfluidic approach, the size of the droplets is precisely adjusted, other aspects affecting the timescale of physicochemical processes in emulsions, such as droplet spacing distance, system dimensionality or droplet order, are experimentally hardly controllable. Due to the lack of control on these parameters only a limited insight into the mechanism of mass transport processes can be achieved. Until now the rate determining step of molecular transport in water-in-oil emulsions has not been experimentally unambiguously

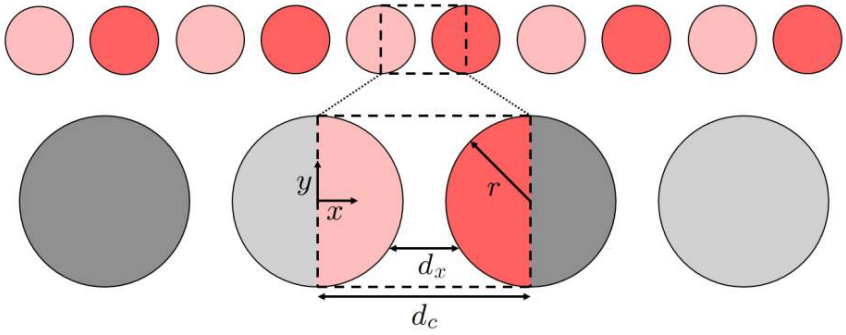

Figure 4.1: Schematic of the structure of a minimal emulsion. One dimensional row of droplets with alternating properties. The array can be expressed as the sum of identical microenvironments with the given geometrical characteristics: r as the droplet radius, d_c as the centre-to-centre distance between the droplets and d_x as the distance between the interfaces in the direction of x being a function of direction y.

identified. Often it is assumed that the transport of molecules across the phase boundary is rate limiting the mass transfer between the droplets. This viewpoint is supported by recent results from numerical simulations [77]. However, the experimental results presented in chapter 3 for a water-in-fluorinated-oil emulsion suggest that the diffusion of solutes through the continuous phase is the rate determining step of transport.

To clarify the mechanism of mass transfer, microfluidic tools were developed, allowing to arrange calibrated emulsion droplets on a microarray in a controlled manner. In contrast to earlier approaches, in these 'minimal emulsions' spacing distance and order of the droplets can be controlled. The simplest emulsion system for such a study is a one-dimensional array of droplets with alternating properties. Such a 'minimal emulsion' behaves as the superimposition of identical microenvironments (figure 4.1), or in other terms, the behaviour of a one-dimensional droplet array with alternating properties is an eigenmode of the discrete Laplace equation of diffusion.

Three basic operations are required for creating the presented type of emulsion: (I) Production of a train of monodisperse droplets with alternating properties, (II) On-demand direction of droplets towards an experimental zone, (III) Controlled immobilization of droplets. For an alternating droplet production a geometry with two opposing T-junctions was selected. When one of the aqueous fluids is advancing into the cross-section, the other stream is hindered resulting in a reliable production of droplets with alternating properties [152–154]. To implement a function for on-demand direction of droplets, hydrodynamic flow switching was applied. Here the fluid flow is split up into two microfluidic channels of different width. In the

absence of any additionally applied pressure, the droplets will be directed towards the wider microfluidic channel due to a lower hydrodynamic resistance [13]. However, by increasing the pressure level in the wider microfluidic channel, droplets can be directed towards the narrower channel. The alternating droplet order resulting from production remains unaffected in this case. For the immobilization of droplets in microfluidic environments several techniques have been suggested [45–49]. Recently it was shown that droplets can be trapped and guided along gradients of surface energy [50–52]. This principle is based on the fact that droplets created in microfluidic environments are typically squeezed and therefore holes fabricated into a microchannel can act as anchors while grooves can act as rails for guiding droplets due to the reduction in surface energy. Making use of this principle a surface energy landscape made of rails and traps, where droplets can buffer each other from one towards the next local minimum in surface energy, was designed. In combination the presented microfluidic tools allow a controlled immobilization of droplets with alternating properties and defined spacing and hence the creation of 'minimal emulsions'.

4.4 | Materials and methods

4.4.1 | Chemicals

Droplets partially containing resorufin sodium salt (Sigma Aldrich) and in some cases sodium chloride (Sigma Aldrich) were produced in fluorinated oil (HFE-7500, 3M) and stabilised against coalescence by a home made block-copolymer surfactant. The surfactant was prepared from Krytox (157-FSH, Dupont) and Jeffamine polyether diamines (ED 600, Huntsmann). The synthesis scheme was based on the synthesis described in Holtze et al. [139].

4.4.2 | Microfluidic device fabrication

Chips were made of Norland Optical Adhesive 81 (NOA81). Briefly, a positive SU-8 mold is made by 2-layer photolithography to fabricate a negative PDMS stamp by replica molding. A drop of NOA81 is deposited on the patterned PDMS substrate. For curing, the liquid film is covered with a blank PDMS substrate and exposed to UV light (4 minutes, Polylux PT, Dreve). For fluidic connection, holes are punched into the crosslinked NOA81 layer (Harris Uni-Core Punch, 0.75 mm). Subsequently,

the layer is sticked to a glass substrate, which was previously coated with a thin, spin coated layer of NOA81 glue (500 rpm) and then crosslinked improving the bonding of the patterned NOA structure to the substrate. Ports (Upchurch) are glued on top of the punched holes. A second layer of NOA81, made in the same way is put in contact with the first layer to provide overlying microfluidic chambers that can be filled with water during the experiment. The completed chip is exposed to UV light for 40 minutes. To treat the internal channel surface fluorophilic, Aquapel (PPG Industries) is flown through the microchannel.

4.4.3 | Hydrodynamic switch

Droplets are produced in an alternating order in a microfluidic cross section by coflowing two aqueous streams with a stream of fluorinated oil (HFE7500) containing surfactant (1 wt%, 2 wt% or 5 wt%) as shown in figure 4.2. The following delay line is designed to allow surfactant adsorption and to increase the hydrodynamic resistance. This increase in resistance is essential as pressure variations in other parts of the microfluidic chip would otherwise have a tremendous effect on droplet production. At the hydrodynamic switch, droplets can either flow through a wide or

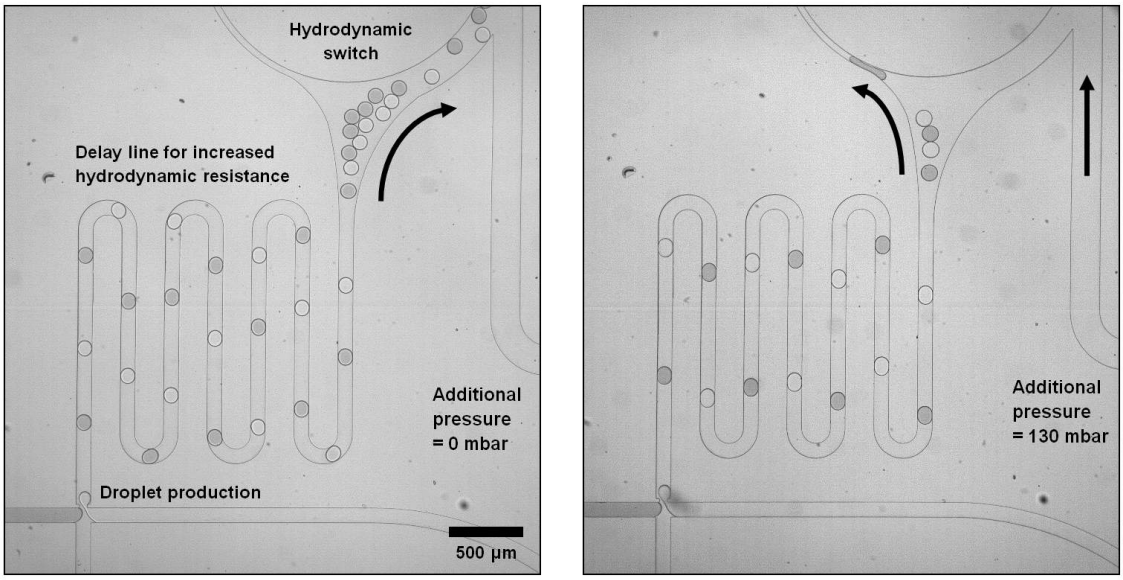

Figure 4.2: Working principle of the applied hydrodynamic switch. (Left) Droplets follow the path of lower hydrodynamic resistance towards the wider switch channel in the absence of any additionally applied pressure. (Right) Droplets pass through the narrow switch channel and are directed to the experimental zone as a result of an increased pressure in the wider microfluidic channel.

a narrow microfluidic channel. In the absence of any additionally applied pressure droplets follow the path of lower hydrodynamic resistance through the wider microfluidic channel. When a sufficiently high pressure is applied in the wider channel, droplets pass through the narrow channel and are directed to the experimental zone. The typical pressures levels applied for droplet production were 280 mbar for each aqueous phase and 260 mbar for the fluorinated oil phase. When the pressure level in the wider microfluidic channel is increased to above 110 mbar, all droplets pass through the narrow microfluidic channel.

4.4.4 | Device operation

A pressure driven pump (Fluigent, MFCS-8C) was used to control the fluid flows in the microfluidic device (figure 4.3). For droplet production, two aqueous solutions were co-flown with the fluorinated oil containing a distinct concentration of surfactant (1 wt%, 2 wt% or 5 wt%). A stable alternating droplet production is obtained when applying a pressure level of 280 mbar for each aqueous phases and a pressure of 260 mbar for the oil phase. For an on-demand delivery of droplets towards the experimental zone of the microfluidic chip, a hydrodynamic switch was applied. By controlling the pressure level in one arm of this switch, the delivery of droplets towards the experimental zone can be efficiently switched on and off. Until applying an additional pressure of up to 110 mbar all droplets are directed towards the wider

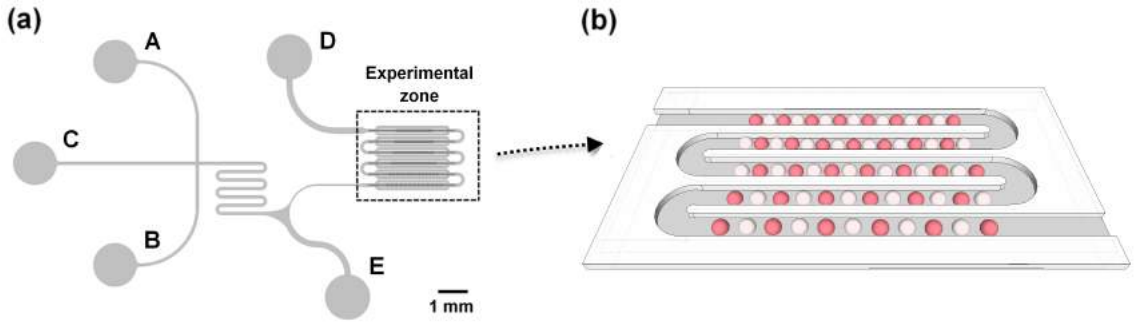

Figure 4.3: Sketch of the microfluidic device used to create 'minimal emulsions'. (a) Microfluidic chip design for the controlled immobilization of droplets with alternating properties in one-dimensional microarrays. A and B are inlets for the two aqueous streams, the fluorous phase is introduced at inlet C. E is used to control the pressure level at the hydrodynamic switch and can act as both inlet and outlet. Droplets flowing through the experimental zone are leaving the chip through outlet D. (b) Three-dimensional view on the experimental zone. Droplets are trapped in wells of surface energy. The spacing distance between the droplets varies for each row.

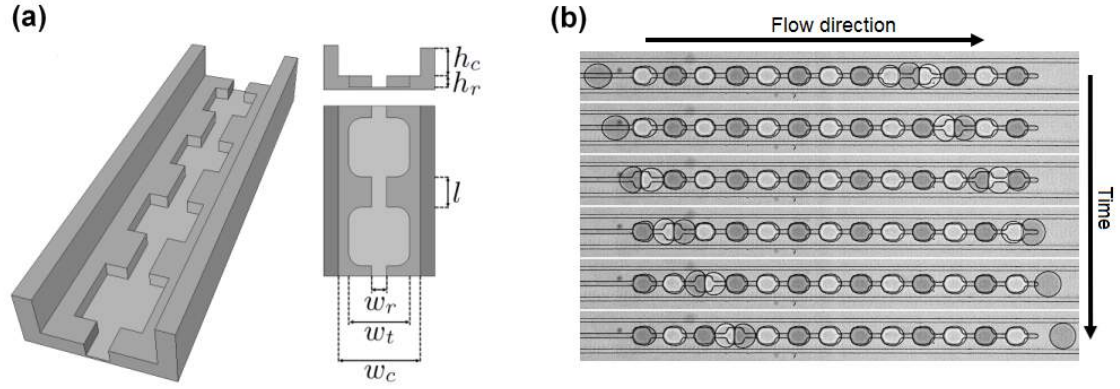

Figure 4.4: Schematic of the construction of minimal emulsion. (a) Three dimensional view (left) and top and side view of a typical surface energy landscape (right). (h_c=20 μm, h_r=15 μm, w_r=20 μm, w_t=80 μm, w_c=100 μm, l varies between 6 and 36 μm). (b) Working principle of the experimental zone. Droplets buffer each other from one towards the next local minimum in surface energy (sequence frame rate: 10 frames per second)

microfluidic channel and do not enter the experimental zone. When increasing the pressure to about 130 mbar, the behaviour is inverted such that all droplets are directed towards the experimental zone of the chip. Here they buffer each other from one towards the next local minimum in surface energy (see figure 4.4). Lowering the switch pressure to 50 mbar will lead to an immediate stop of the delivery of droplets towards the experimental zone. However, the remaining pressure difference between the inlets and outlets results in a flow, such that the droplets are still buffering each other from one local minium in surface energy to the next one. As a result, no droplets will be immobilized in between the local minima of surface energy. By coupling several microarrays with each other, trains of droplets were immobilized in 5 independent one-dimensional microarrays, each with varying distances between the droplets (1, 4, 10, 15 and 30 μm edge-edge distance). Each microarray consists of 13 to 15 droplets (figure 4.5).

4.4.5 | Fluorescence measurement and data processing

Images were taken every 5 minutes with a digital camera (Canon, EOS D600). A light emitting diode (CoolLED pE-2, 550 nm) was used for excitation of the fluorophores. The camera and the LED were synchronized and triggered with a home made LabVIEW program. The recorded intensity in the red channel was found to be proportional with the dye concentration in the relevant range (0.1 - 100 μM). Images were analysed with home made scripts using MATLAB.

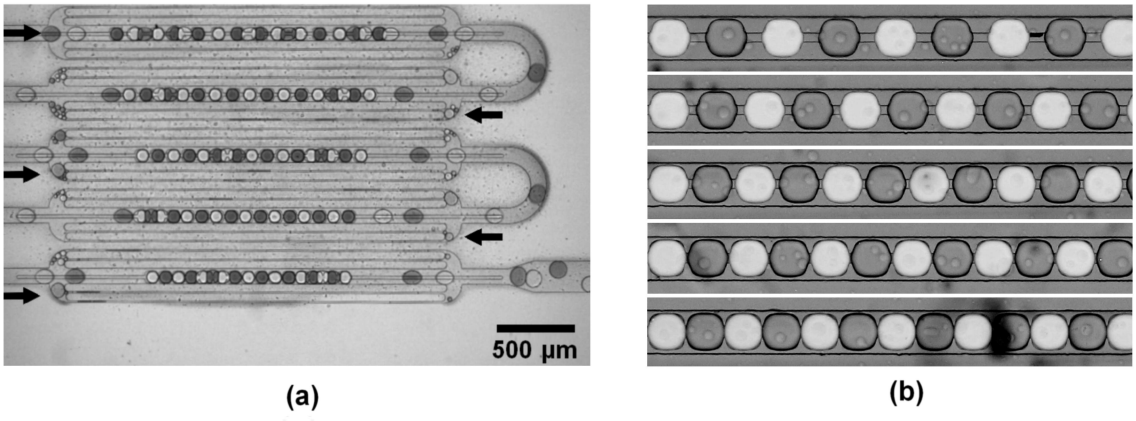

Figure 4.5: Multiple coupled one-dimensional droplet arrays. (a) White light picture of a train of droplets with alternating properties running through the experimental zone, composed of several coupled one-dimensional droplet arrays. The arrows indicate the fluid flows. (b) Combined white light and fluorescence picture of immobilized droplets in the 5 microarrays with varying droplet spacing distances.

4.4.6 | Partition coefficient measurement

The partition coefficient between the aqueous and the fluorinated phase was determined by the shake flask method. 500 μL of HFE-7500 with a distinct concentration of surfactant (0.5 - 5 wt%) and the same amount of millipore water containing 100 μM of resorufin sodium salt and additionally in some cases sodium chloride (0 - 25 mg/mL) dissolved in millipore water were put into contact in a glass vial. Careful pipetting ensures that no emulsification is obtained. The mixture of the two liquids is incubated for at least 72 hours. The partition coefficient is calculated by measuring the change in fluorescence intensity of the aqueous phase with a microplate reader (Spectra Max Paradigm, Molecular Devices).

4.5 | Experimental results and discussion

In all experiments the transport of fluorophores between two populations of droplets immobilized on a microfluidic chip is observed. While all droplets are equivalent in size, only one population is initially fluorescent (resorufin sodium salt, 100 μM). The droplets are arranged in an alternating order on one-dimensional microarrays resulting in an emulsion with simple identical microenvironments. The dynamics of fluorophore transport from initially "filled" towards initially "empty" drops are accessed by analysing a time sequence of fluorescence images (figure 4.6).

The intensity of the emitted fluorescent light was found to be proportional with

the fluorophore concentration in the relevant concentration range between 0.1 and 100 μM. Hence the concentration of the fluorophores in single droplets can be quantified in a straight-forward way by analysing the fluorescence intensity. Fluorescence images are taken every 5 minutes until the fluorophore concentrations between the two populations are equilibrated. As the sum of intensity over all droplets stays constant during the experiment, a significant effect of photobleaching or chemical modification of the fluorophores is excluded.

Considering the fact that mass transfer between droplets spaced by the oil phase is observed, it can be concluded that the mechanism of fluorophore transport includes the following steps: (I) Diffusion of fluorophores towards the water-oil interface. (II) Partitioning of fluorophores from the aqueous towards the oil phase. (III) Diffusion of fluorophores through the oil phase towards a neighbouring droplet. (IV) Partitioning of fluorophores from the oil towards the aqueous phase. The observed rate of transport is determined by the rate-limiting step. However, from observing mass transfer in a single microarray it can not be concluded which step is rate limiting the transport.

To decouple potentially rate limiting steps from each other, several microarrays with varying spacing distances between the droplets were observed simultaneously. The decoupling is based on the idea that the spacing distance between the droplets is affecting the timescale of transport through the continuous phase (step III) while the timescale of the transport across the droplet interface (step II & IV) remains unaffected.

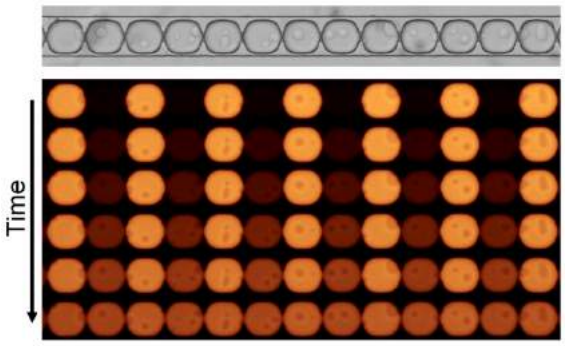

Figure 4.6: White light picture and time sequence of fluorescence pictures of a minimal emulsion. Top: white-light picture of an immobilized row of droplets spaced by 4 μm. Bottom: Time sequence of fluorescence images of an immobilized row of droplets (0, 1.5, 3, 6, 12 and 24 h after immobilization)

.

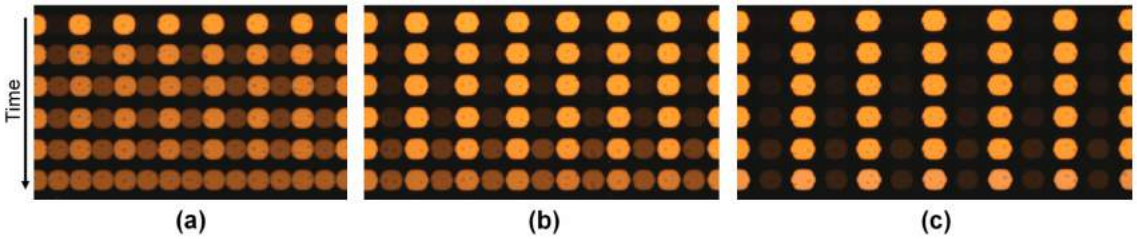

Figure 4.7: Time sequences of fluorescence pictures (0, 1.5, 3, 6, 12 and 24 h after immobilization) of minimal emulsions with varying droplet spacing distances. Edge-to-edge droplet spacing distance varies as (a) 1 μm, (b) 10 μm, (c) 30 μm.

With the minimal emulsion approach, it is experimentally unambiguously shown, that the timescale of the transport process is dependent on the spacing distance between the droplets (figure 4.7). The rate of transport increases with decreasing droplet spacing distance, which suggests that the transport through the continuous phase (step III) is rate limiting the transfer of fluorophores between the droplets.

For all investigated droplet spacing distances, including cases where the droplets are separated by a several μm thick oil layer and cases where the droplet interfaces are pushed into close contact, an exponential decaying behaviour is observed (figure 4.8). In chapter 3 it was shown that the spatial organization of droplets has a major influence on the exchange dynamics. In that study, the dynamics of equilibration in an emulsion with randomly distributed microenvironments did not follow a simple exponential decay but was slowed down to a power-law. In contrast, here an exponential decay over the whole relaxation dynamics is found, reflecting the fact that the emulsion is made of identical microenvironments.

To understand the influence of the droplet spacing distance on the timescale of transport an analytical model, where it is assumed that the transfer of fluorophores from one droplet to another is entirely rate limited by the diffusive transport through the continuous phase, was developed. For simplicity it is approximated that the immobilized droplets have the shape of cylinders. Due to the symmetrical structure of the emulsion, the relaxation dynamics of the whole droplet array is identical with a single self-contained microenvironment as shown in figure 4.1. Here, the molar flux of fluorophores J between the two aqueous reservoirs can be described with Fick's first law as the product of concentration gradient $\frac{\Delta c}{\Delta x}$ and the diffusion coefficient D.

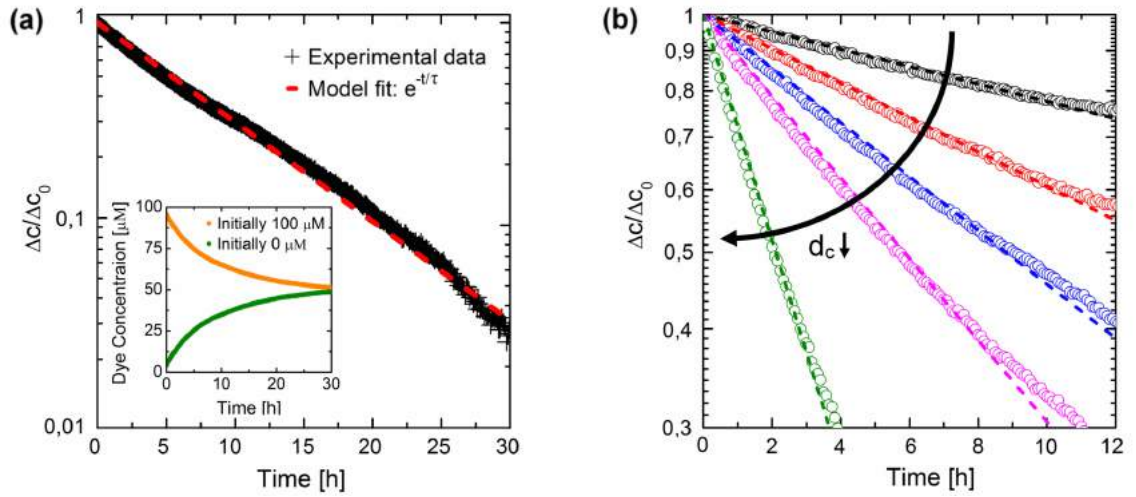

Figure 4.8: Characteristics of molecular transport in minimal emulsions. (a) The experimentally observed exponential decay of the normalized concentration difference $\Delta c/\Delta c_0$ between the two populations of droplets is recovered by an exponential fit with a timescale τ as a fitting parameter. The inset shows the equilibration of the fluorophore concentrations. One population of droplets initially contains 100 μM resorufin sodium salt (orange) while the other population consists of millipore water (green). (b) Relaxation dynamics of 5 one-dimensional droplet microarrays with varying droplet spacing distances d_c. The edge-to-edge distance between the droplets varies as 30 μm (black), 15 μm (red circles), 10 μm (blue circles), 4 μm (pink circles) and 1 μm (olive circles). The relaxation in every array can by recovered by an exponential fit with timescale τ as fitting parameter (dashed lines).

To give respect to the fluorophore concentration in the oil phase the partitioning coefficient K between the oil phase and the aqueous phase has to be taken into account.

$$J(t) = -K\,D\,\frac{\Delta c(t)}{\Delta x} \tag{4.1}$$

In this diffusion limited approach, chemical equilibria across the interfaces are present at all time. K is here defined as the quotient of the fluorophore concentrations in the oil $c_{eq,oil}$ and the aqueous phase $c_{eq,aq}$ in equilibrium:

$$K = \frac{c_{eq,oil}}{c_{eq,aq}} \tag{4.2}$$

The distance d_x between the interfaces of droplets, in the direction of the flux x, can be described as:

$$d_x(y) = d_c - 2\sqrt{r^2 - y^2} \tag{4.3}$$

With d_c as the centre-to-centre distance between the droplets and the droplet radius

r. With equation (4.1) and (4.3), the molar flux is expressed as the sum of all infinitesimal fluxes of the elements dy:

$$J(t) = -K\,D\,\Delta c(t)\,\frac{1}{2r}\int_{-r}^{r}\frac{1}{d_c - 2\sqrt{r^2-y^2}}\,dy \tag{4.4}$$

After integration the following expression is obtained:

$$J(t) = -K\,D\,\Delta c(t)\,\frac{d_c\left(\pi + 2\,\arctan\frac{2r}{\sqrt{d_c^2-4r^2}}\right) - \pi\sqrt{d_c^2-4r^2}}{4r\sqrt{d_c^2-4r^2}} \tag{4.5}$$

To propose a time-independent parameter that reflects the rate of fluorophore exchange, the permeability P as the quotient of $-J(t)$ and $\Delta c(t)$ is introduced (see section 2.3.3 'Solute transport'). The permeability is inversely proportional to the timescale of transport.

$$P = K\,D\,\frac{d_c\left(\pi + 2\,\arctan\frac{2r}{\sqrt{d_c^2-4r^2}}\right) - \pi\sqrt{d_c^2-4r^2}}{4r\sqrt{d_c^2-4r^2}} \tag{4.6}$$

The resulting expression describes the dependency of the permeability P on the centre-to-centre distance d_c between the droplets for the presented one-dimensional droplet array. The permeability as a function of d_c rescaled by the droplet diameter $2r$ is shown in figure 4.9. Experimentally the permeability is accessed by calculating the quotient of the molar flux of fluorophores $J(t)$ and the concentration difference $\Delta c(t)$ obtained by analysing the recorded time sequence of fluorescence images. The timescale of fluorophore transport respectively the permeability of the system is, besides the spacing distance between the droplets, also influenced by the partitioning coefficient K and the diffusion coefficient of the fluorophores in the oil phase D. To be able to fit the experimentally obtained data with the theoretical description, the partition coefficient between the oil and the aqueous phase was measured by the shake-flask method via Vis-spectroscopy. In a first approximation, a linear relationship of K with the surfactant concentration is found (figure 4.10), which confirms that surfactant molecules mediate solubility in the fluorinated oil. Being able to experimentally access the partition coefficient K, the experimental data are fitted with the theoretical prediction for the permeability (eq. 4.6) with the diffusion coefficient D as a fitting parameter.

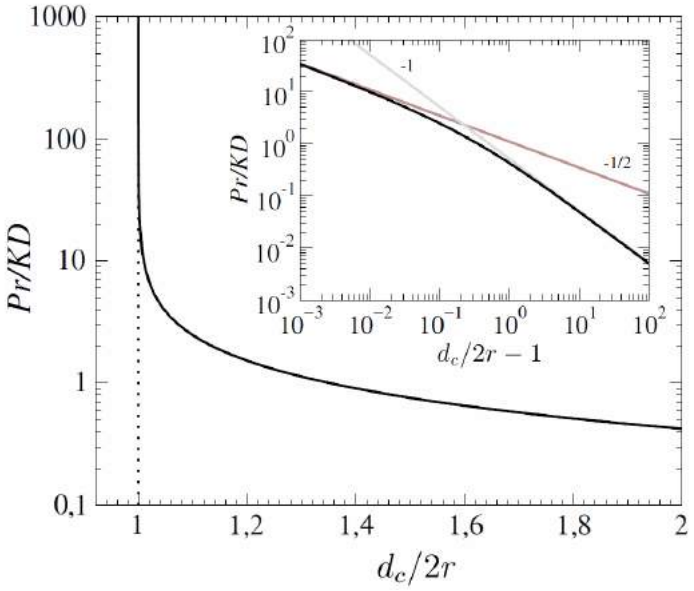

Figure 4.9: Permeability of the membrane separating two droplets in a diffusion limited model as a function of the droplet spacing distance. The permeability diverges for touching droplets ($d_c/2r = 1$). The asympotic scaling shows a -1/2 power law exponent for touching droplets and a -1 exponent for spaced droplets ($d_c/2r \to \infty$).

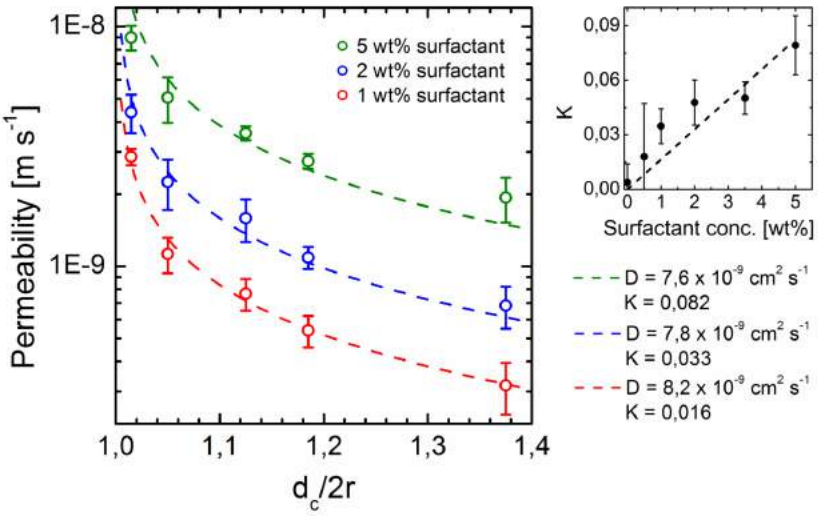

Figure 4.10: Correlation of experimentally obtained and theoretically predicted values for the permeability as a function of droplet spacing distance. Left: Theoretical description (dashed lines) and experimentally observed values (circles) for the permeability P as a function of the centre-to-centre distance between the droplets d_c normalized by the droplet diameter $2r$. Three data sets are shown corresponding to different surfactant concentrations. The error bars correspond to the standard deviation resulting from three independent experiments. Right: Partition coefficient of resorufin sodium salt between the fluorous phase and the aqueous phase measured via shake flask method as a function of surfactant concentration.

In all investigated cases, the obtained experimental data fit well with the analytical expression (equation 4.6) describing the transport as rate limited by the diffusive transport through the oil phase. Hence, the transport of fluorophores is rate limited by the diffusion of fluorophores through the oil phase rather than by the transport across the droplet interface. As a consequence and in agreement with Dunstan et al. [76], no significant energy barrier influencing the timescale of exchange for molecules crossing the droplet interface exists - at least in the here investigated case.

The permeability of the system, as a function of the droplet spacing distance, was measured for three different concentrations of surfactant (1 wt%, 2 wt% and 5 wt%). In agreement with the results presented in chapter 3, the permeability respectively the rate of transport is found to be proportional with the surfactant concentration.

Furthermore, the fitting yields in all cases a diffusion coefficient of about 10^{-8} m^2 s^{-1}. The translational diffusion coefficient D of a spherical particle with a radius R in liquids at low Reynolds numbers is estimated by the Stokes-Einstein equation:

$$D = \frac{k_B T}{6\pi\eta R} \tag{4.7}$$

with the Boltzmann constant $k_B = 1.38\times\ 10^{-23}$ J K^{-1}, the dynamic viscosity η of the medium of $\eta = 1.24$ cP (HFE7500, 3M) and the absolute temperature T, which was in all experiments about 294 K. Under these conditions the diffusion coefficient of a single fluorophore molecule with a diameter of about 1 nm is estimated to be D = 3,5 $\times$ 10^{-6} cm^{2}s^{-1}. In agreement with literature values for surfactants of the same type and in the same solvent [122, 138], the average diameter of surfactant assemblies, measured by dynamic light scattering is about 250 nm as shown in figure 4.11.

The corresponding average diffusion coefficient of surfactant assemblies with such dimensions is estimated to be 1,4 $\times$ 10^{-8} cm^2 s^{-1}. The measured diffusion coefficient in minimal emulsions of about 10^{-8} cm^2 s^{-1} correlates well with the expected value for surfactant assemblies. Hence, the obtained results suggest that the fluorophores are diffusing through the fluorous phase as part of surfactant assemblies.

In agreement with the results obtained in chapter 3, it is concluded that assemblies of surfactant molecules such as reverse micelles or vesicles are providing a nanoscopic environment for the solubilization of organic molecules in fluorinated

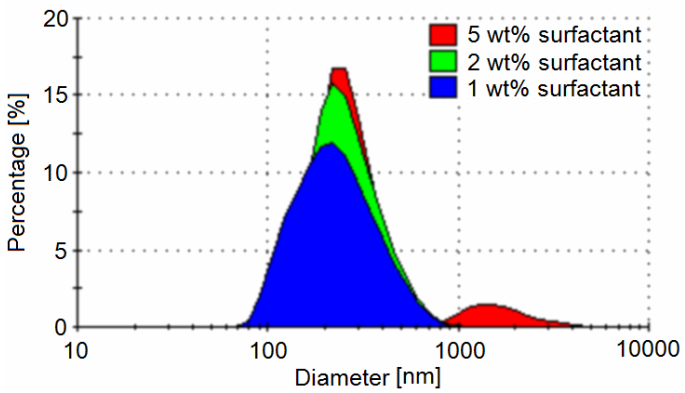

Figure 4.11: Size distribution of surfactant assemblies at surfactant concentrations of 1 wt%, 2 wt% and 5 wt% in HFE 7500 determined by dynamic light scattering.

oils, which ultimately results in cross-talk between droplets. Further it was demonstrated that the mass transfer of small organic molecules such as resorufin sodium salt in fluorinated emulsions is rate limited by the diffusion through the continuous phase rather than by the transfer across the droplet boundary. Therefore increasing the spacing distance between droplets is an efficient strategy to reduce cross-talk between droplet microreactors while strategies focusing on slowing down the transport of molecules across the droplet interface might be less effective.

Having the mechanism of mass transfer clarified, methods to control the transport of chemicals in emulsions are considered. The partition coefficient between the aqueous and the fluorinated phase is an important parameter affecting the rate of transport. This parameter is influenced by altering the surfactant concentration or alternatively by the addition of chemicals to droplets. For example Bovine serum albumin (BSA) can be added to slow down the rate of transport. The protein is acting on the partitioning behaviour of the dye such that droplets containing BSA will enrich with fluorophore molecules while droplets not containing the protein become impoverished (see chapter 3). The solubility of organic molecules in an aqueous medium can also be altered by the addition of inorganic salts [155]. The decrease of the aqueous solubility of organic molecules in the presence of inorganic salts such as sodium chloride is commonly known as the "salting out" effect. The addition of sodium chloride results in the formation of hydration shells around the inorganic ions, which effectively reduces the availability of water molecules dissolving other molecules. As a result the aqueous solubility of fluorophores decreases with increasing sodium chloride concentration. That principle was used to alter the partition coefficients of the solutes such that a scenario is created, where an almost complete

transfer of fluorophore molecules from a first towards a second population of droplets is obtained (figure 4.12).

As presented before, droplets are immobilized in an alternating order on an one-dimensional microarray. The two droplet populations are now initially not only different in the concentration of fluorophores but also in the concentration of sodium chloride. Droplets initially containing fluorophores are additionally containing sodium chloride (1 to 25 mg/mL). The other droplet population initially neither contains fluorophores nor sodium chloride.

Under such conditions, the fluorophore molecules enrich in droplets that do not contain sodium chloride. Hence, an almost complete transport of fluorophores from a first towards a second population of droplets is obtained. Hence, the value for the concentration difference Δc normalized by the initial concentration difference Δc_0 is changing from +1 to approximately -1 with time (figure 4.13a). As expected, in the presented 'minimal emulsions', the dynamics of the fluorophore transport are described by an exponential law. However, it is assumed that the equilibration of sodium chloride concentrations between the droplet populations results in equal solute concentrations in all droplets, occurring on a much longer timescale than here the investigated fluorophore transport. Furthermore the variety of solute concentrations among the droplets is expected to result in a net transport of water molecules between the populations. However, here no significant effect of an osmotically driven water transport was observed on the timescale of the experiment. The transport of

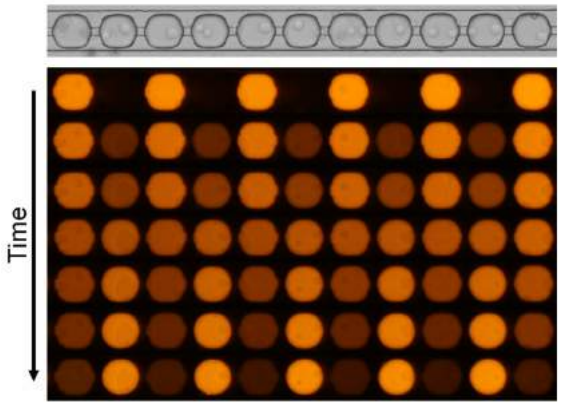

Figure 4.12: Fluorophore transport in minimal emulsions modified with additives. While one droplet population initially contains fluorophores (Resorufin sodium salt 100 μM) and sodium chloride (10 mg/mL), the other droplet population does not contain any solutes. Top: white-light picture of an immobilized row of droplets spaced by 15 μm. Bottom: Time sequence of fluorescence images (0, 0.5, 1, 1.5, 2, 2.5 and 3 h after immobilization).

water between droplets, driven by different solute concentrations, is investigated in chapter 5. Due to the dependence of the partition coefficient on the concentration of sodium chloride, the transport process is accelerated with increasing salt concentration. As predicted by equation 4.6 the measured permeability of the system is proportional to the partition coefficient (figure 4.13b).

In conclusion, additives such as sodium chloride or bovine serum albumin affect the rate of transport of organic molecules in emulsions by acting on the partition coefficient. Heterogeneously distributed among the emulsion droplets, the use of additives allows to influence the transport dynamics and the temporal distribution of organic molecules. Hence, controlling the concentrations of additives or combinations of additives opens new ways to temporally program the composition of droplet microreactors.

The use of additives is one approach to temporally control solute concentrations in emulsion droplets. Another way is to control the chemical consumption of the continuous phase. Driving the system out of equilibrium by abruptly changing the solute concentrations in the continuous phase will result in an uptake respectively release of solutes from the droplets as a consequence of the equilibration process.

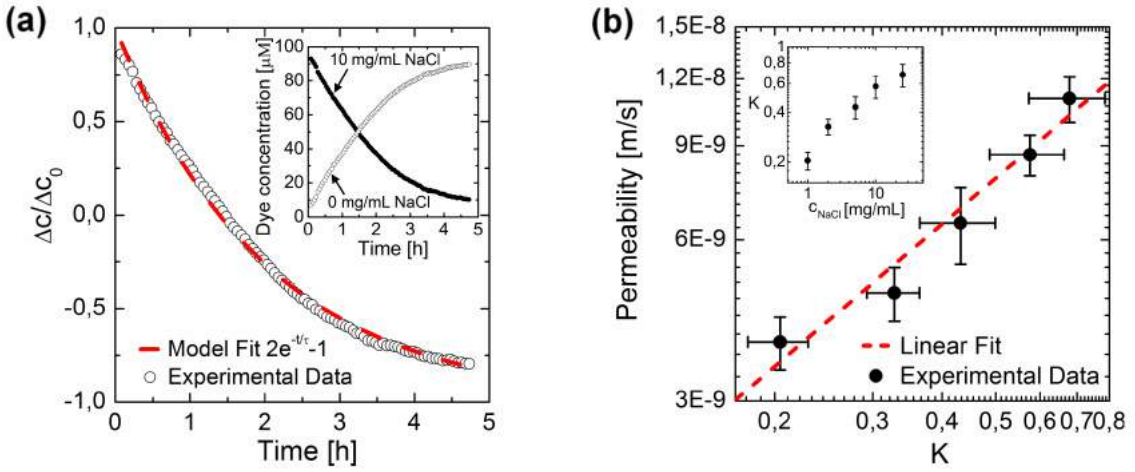

Figure 4.13: Influence of additives on the characteristics of fluorophore transport in minimal emulsions. (a) Dynamics of fluorophore transfer between the droplet populations described by an exponential law with the timescale τ as a fitting parameter. Inset: fluorophore concentrations in the two populations as a function of time. One population of droplets initially contains 100 μM resorufin sodium salt and 10 mg/mL sodium chloride (filled circles) while the other population consists of millipore water (empty circles). (b) Linear dependency of the permeability P on the partitioning coefficient K. The partitioning coefficient was altered by adding various amounts of sodium chloride to the aqueous solution.

Such an approach was demonstrated by controlling the fluorophore concentration in the environment of an immobilized droplet (figure 4.14).

Fluorophores were transferred into the fluorous phase by phase partitioning in the presence of surfactants before each experiment (shake flask method as described in section 4.4.6). The droplets were immobilized with the help of circular wells in the microchannel ('anchor', see section 2.2.2) having a diameter of 40 μm. Expos-

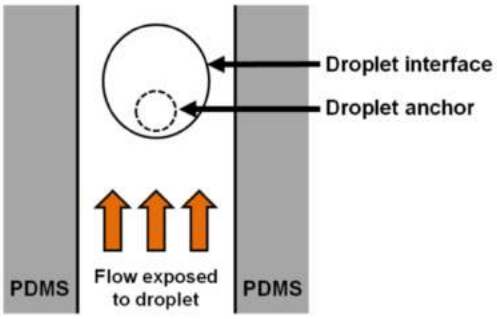

Figure 4.14: Schematic representation of the control of the chemical composition of a droplet by controlling the composition of the continuous phase that the droplet is exposed to. Droplets are immobilized with the help of a circular channel depressions ('droplet anchors') and exposed to a flow of the continuous phase with a specific chemical composition.

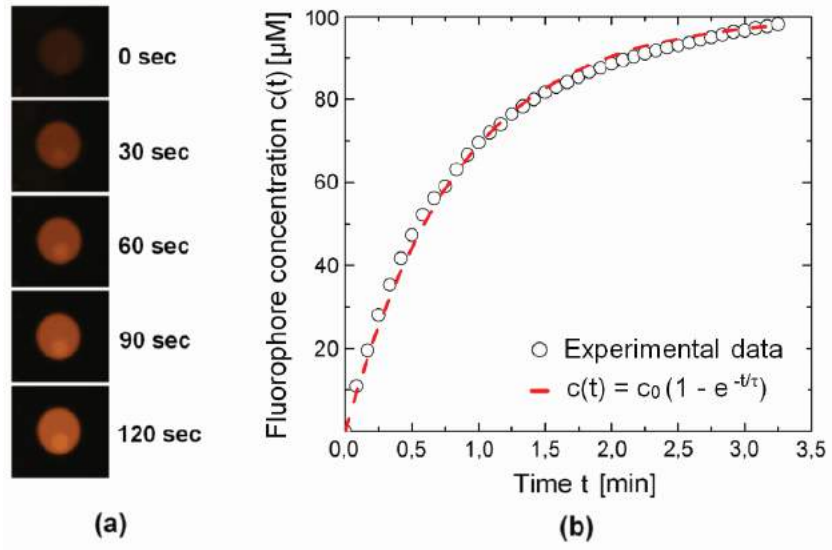

Figure 4.15: Uptake of resorufin sodium salt of an immobilized droplet exposed to a continuous flow (0.2 μL/min) of a fluorophore containing fluorous phase (1 wt% surfactant, exposed to 100 μM resorufin sodium salt). (a) Time sequence of fluorescence images demonstrating the temporal increase of the fluorophore concentration in the immobilized droplet. Droplet diameter corresponds to 100μm. (b) The fluorophore concentration c as a function of time t is shown. The experimentally obtained data fit with an exponential asymptotic function with τ as a fitting parameter and c_0 as the intial fluorophore concentration in the aqueous phase (here 100 μM). The fluorophore concentration in the droplet was determined by calibration of the fluorescent signal with the fluorescence intensity.

ing a droplet, initially not containing fluorophores, to a flow of the fluorous phase containing fluorophores results in the uptake of fluorophore molecules as illustrated by a temporal increase of the droplets fluorescent signal (figure 4.15).

The timescale for the fluorophore uptake under the given conditions ($\sim$ minutes) is significantly smaller than the timescale measured for the exchange between droplets ($\sim$ hours) reflecting the fact that the transport of fluorophores between droplets is rate limited by their diffusion in the continuous phase and not by the transport across the droplet interface. Hence, constantly renewing the environment of a droplet by exposing it to a constant flow, results in an accelerated fluorophore uptake. The transport may here be considered as an equilibration between two fluid reservoirs, where one (the continuous phase) posses a constant fluorophore concentration. Hence, the dynamics of transport are still recovered by an exponential fit. Addressing individual droplets is achieved by locally controlling the solute concentrations in the continuous phase. Figure 4.16 shows a proof of principle experiment.

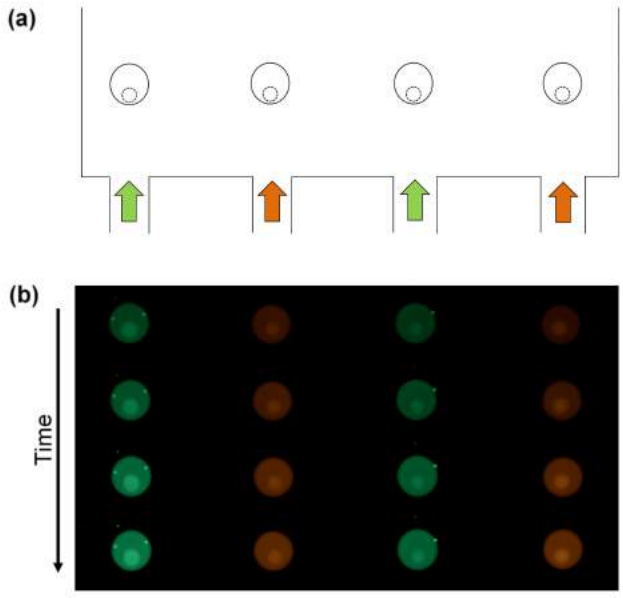

Figure 4.16: Proof of principle experiment demonstrating the ability to control the composition of individual droplets. (a) Schematic representation of the conducted experiment for targeted delivery. Droplets, initially not containing any fluorophores, are immobilized in wells of surface energy and each is exposed to an individual flow of the continuous phase containing either fluorescein sodium salt (green arrows) or resorufin sodium salt (orange arrows). (b) Time sequence of fluorescence images (0, 30, 60 and 90 seconds after the droplets were exposed to the fluorophore containing fluorous phase). The continuous phase was in each case comprised of HFE 7500 containing 1 wt% of the PFPE-Jeffa600-PFPE surfactant (see section 3.3). Each droplet was exposed to a flow rate of 0.2 μL/min of the fluorous phase containing either fluorescein sodium salt or resorufin sodium salt. The droplet diameters correspond to 100 μm.

Here, four droplets are immobilized next to each other in a microfluidic channel. In the laminar flow regime each droplet might be exposed to a different environment. Concretely, two droplets were exposed to a fluorous phase containing fluorescein sodium salt, the other droplets were exposed to a fluorous phase containing resorufin sodium salt. To illustrate that such a strategy is suited for the targeted delivery of molecules to droplets, these fluid flows were exposed in an alternating order. The selective uptake of fluorophores, corresponding to the presence of the respective fluorescent molecules in the fluorous phase, is obtained. Hence, the approach allows for a dynamic control of the concentration of compounds in individual droplets.

4.6 | Conclusion

In this chapter 'minimal emulsions' were introduced. With the help of microfluidic tools, calibrated droplets were produced, ordered and spaced in a controlled manner such that emulsions with a precisely defined microstructure are obtained. Investigating such systems allows to directly experimentally access fundamental information about molecular transport processes in emulsion on a microscopic level.

It was demonstrated that the transport of fluorophores in the investigated water-in-fluorinated-oil emulsion is rate limited by the diffusive transport through the continuous phase supporting the model of Dunstan *et al.* [76], where no significant energy barrier for solutes crossing a droplet interface exists. As a consequence and in contrast to the calculations of Chen *et al.* [77], the properties of continuous phase are expected to affect the rate of solute exchange between emulsion droplets. Hence, increasing the spacing distance between droplets is an efficient strategy to reduce cross-talk between droplet microreactors. For such purpose, one approach is the incubation of droplets in spatially separated wells of surface energy. Additionally, the methodology allowed to determine the diffusion coefficient of the fluorophores in the continuous phase, supporting a transport mechanism by assemblies of surfactant molecules.

Understanding the mechanistic details of molecular transport in emulsion allows to develop suited strategies to control the exchange of solutes between emulsion droplets and to temporally control the chemical composition of droplet microreactors. It was pointed out that the partitioning coefficient between the oil and the aqueous phase is a key parameter to control the timescale of transport. Hence, using additives, acting on the partitioning coefficient of solutes, is an effective strategy to

influence the timescale of exchange between droplets. Furthermore a heterogeneous distribution of additives allows to concentrate compounds in targeted droplets. Interestingly, such an approach also provides the tools to temporally program the composition of droplet microreactors by controlling the release and uptake of compounds. Additionally, these findings are important for typical applications of droplet-based microfluidics. Here the biological activity within droplets is coupled to a fluorescent signal by biochemical assays [156, 157]. However, it has to be taken into account that the measured fluorescent signal is not only dependent on the performance of the fluorometric assay but also on the individual solubility of the fluorophores in the droplets.

An alternative approach to manipulate droplet compositions is to control the consumption of the continuous phase. In such manner, compounds can be efficiently delivered to emulsion droplets without the need to manipulate them individually. This approach allows for example the constant delivery of nutrients to emulsion droplets containing cells. Additionally, addressing droplets individually is enabled by exploiting laminar flow in microfluidic environments.

In summary, these findings are not only relevant as a practical guideline to control mass transport in droplet-based microfluidics but pave the way for a dynamic control of droplet composition in emulsions.

5 | Transport of water and inorganic ions

Philipp Gruner and Jean-Christophe Baret

In chapter 3 and 4 the transport of organic solutes between emulsion droplets was investigated. In this chapter, the developed methods are applied to investigate the osmotically driven transport of water and the transport of magnesium ions between emulsion droplets.

Contents

5.1 | Abstract

The transport of water between two initially monodisperse droplet populations with different solute concentrations is investigated. The mass transfer of the dispersed phase results in significant changes of the droplet sizes and ultimately in a bidisperse emulsion. The timescale of the transport process is found to be independent on the surfactant concentration and dependent on the properties of the continuous phase, giving rise to a transport mechanism by direct partitioning. The equilibration of concentration differences among the droplets is found to take place by mass transfer of water and solutes simultaneously. To quantify the transport of inorganic ions, a fluorescent indicator, sensitive to the presence of magnesium ions, is used. The experimental findings suggest that, depending on the characteristics and the concentration of the used surfactant, substantial fractions ($> 90\%$) of the magnesium ions are transferred to the continuous phase.

5.2 | Introduction

Generally, the mass transport of water molecules in water-in-oil emulsions is observed as a result of heterogeneities in the distribution of droplet sizes (Ostwald ripening [53]) or heterogeneities in the chemical composition of the droplets (Osmotically driven transport [158]). The transport either occurs by phase partitioning and diffusion of water molecules through the continuous phase [54] or alternatively through bilayers of surfactants forming between the droplets [65].

Recently, the osmosis-driven transport of water between emulsion droplets was exploited to monitor biochemical processes occuring in droplets. For example the metabolic activity of single cells was studied using such approach [158, 159]. Here, the underlying principle is that bioactivity in droplets lowers the solute concentrations inducing a water flux towards droplets not containing cells. Hence, droplets containing cells can be efficiently sorted from droplets without any bioactivity, for example by deterministic lateral displacement [160]. Aside from being used to monitor bioactivity in droplets and sort them accordingly, osmotically driven size changes are also relevant for common droplet-based screening applications. Here, droplet volume variations result in the modification of fluorophore concentrations commonly used to couple geno- and phenotype of a droplet. Hence the screening accuracy might suffer from droplet size changes.

As the control of water transport processes between droplet microreactors becomes increasingly important, it is essential to understand the mechanism of water mass transfer in such emulsions. Interestingly, there is no common opinion about the mechanism in water-in-oil emulsions [54]. Some authors found that water transport occurs mainly through the solubilization of water molecules in reverse surfactant micelles [161, 162], others proposed that the mass transfer occurs through hydrated single surfactant molecules [163]. Furthermore, also mechanisms based on the diffusion of single water molecules without the involvement of surfactants have been proposed [164]. For water-in-fluorinated-oil emulsions it was hypothesized that water transport takes place by diffusion of single water molecules [160] or alternatively by solubilization in reverse surfactant micelles [165]. However, no experimental results have been presented, supporting one of the two mechanisms.

In this chapter, to clarify the role of surfactants in mediating water transfer in such emulsions, microfluidic tools, as introduced in chapter 3 and 4, are utilized. The osmotically driven water transport as a result of heterogeneous concentrations of inorganic ions among the droplets is investigated. However, it has to be considered that a simultaneous transport of water and the inorganic ions occurs as both processes result in the equilibration of the chemical potentials in the emulsion. To address the characteristics of the transport of inorganic ions, additionally the mass transfer of magnesium ions is investigated.

5.3 | Materials and methods

5.3.1 | Chemicals

All aqueous solutions were prepared with deionized water (Milli-Q, Millipore). For droplet encoding either a fluorescently labelled dextran (Dextran, Fluorescein, 3000 g/mol, Invitrogen) or fluorescently labelled microparticles (Fluoresbrite YG Microspheres 2.00 μm, Polysciences) were used. Sodium chloride was purchased from Sigma-Aldrich. The magnesium indicator was purchased from Invitrogen (Mag-Fluo-4, Tetrapotassium Salt). The continuous phase was comprised of a hydrofluoroether (HFE-7500, 3M) or alternatively a perfluorinated oil (FC40, 3M) containing a specific concentration of a non-ionic surfactant.

5.3.2 | Surfactant

In all experiments a home made non-ionic block-copolymer surfactant was used. The surfactant was prepared from the commercially available fluorous carboxylic acid Krytox 157-FSH (Dupont) and Jeffamine polyether diamines (ED 600, Huntsmann). Surfactants from two different batches (batch 1 and 2) were used. The synthesis scheme was based on the synthesis described in Holtze *et al.* [139].

5.3.3 | Laser-based measurements

All laser-based measurements were performed in microfluidic devices with a channel depth 60 μm, produced with standard soft-lithography techniques. The devices were made of PDMS that was bound to glass after oxygen plasma activation and hydrophobized using a commercial coating agent (Aquapel, PPG Industries). Droplets were incubated in a collection vial as introduced in chapter 3. After droplet reinjection, the fluorescence signal of each droplet was measured as it was flowing through the microfluidic channel using a laser-induced fluorescence setup (see chapter 3). The laser spot size was focused to be only a few microns in diameter and hence much smaller than both the droplets and the microfluidic channels, which have a width of 100 μm. For each droplet, the maximum fluorescence intensity (fluorescein signal) was recorded. The relative fluorescence unit RFU is here defined as the measured voltage U rescaled by the Gain G as: RFU $= U/G^{6.8}$.

5.3.4 | Measurements in 'minimal emulsions'

Microfluidic chips for 'minimal emulsions' were made of Norland Optical Adhesive 81 (NOA81) as described in chapter 4. To treat the internal channel surface fluorophilic, Aquapel (PPG Industries) is flown through the microchannel. Images were taken with a digital camera (Canon, EOS D600). A light emitting diode (CoolLED pE-2, 470 nm) was used for excitation of the fluorophores. The camera and the LED were synchronized and triggered with a home made LabVIEW program. The recorded intensity in the green channel was found to be proportional with the dye concentration in the relevant range (0.1 - 100 μM). Images were analysed with home made scripts using MATLAB.

5.4 | Experimental results and discussion

A similar technique as presented in chapter 3 is applied to access the dynamics of water transport in emulsion. Two populations of monodisperse droplets are produced on a microfluidic chip and incubated off chip in a macroscopic vial. The volume of the droplets is measured after re-injection of the droplets into the microfluidic chip. The water transport is driven by different concentrations of sodium chloride among the droplets. To accurately determine the volume of the droplets, fluorophores are added to the droplets. As the fluorophore concentration is inversely proportional with the volume of the droplet, measuring the fluorescence signals of the droplets as a function of time allows to access the dynamics of water transport in a straight-forward way. However, that approach is relying on the assumption that the fluorophore molecules are retained in the droplets and not released to the continuous phase respectively exchanged between the droplets throughout the experiment. In chapter 4 it has been shown that the presence of sodium chloride significantly lowers the solubility of organic molecules in an aqueous phase and hence the rate of exchange was found to be substantially enhanced. In fact, in the presence of high concentrations of sodium chloride (100 mg/mL), fluorescein sodium salt was found to be exchanged between the droplets on a relatively short timescale ($\sim$ minutes). For this reason a fluorescently labelled dextran (Dextran, fluorescein labelled, 3000 g/mol, Invitrogen) was chosen as fluorophore encoding the size of droplets. No mass transfer of these hydrophilic polysaccharides was obtained even in the presence of high sodium chloride concentrations.

Among the two droplet populations, one contains sodium chloride (100 mg/mL) and fluorescently labelled dextran (100 μM), while the other droplets consist of deionized water. For the shrinking droplet population (deionized water), the measurement of the fluorophore concentrations is not straight-forward. Below a critical volume, the droplets are not confined between the channel walls anymore. In such a case, the fluorescence signal is not accurately measured with the presented approach. Therefore, fluorophores were only added to the population, whose droplet volume is increasing with time (containing sodium chloride).

A decrease of the fluorescence signal of droplets containing sodium chloride is observed, indicating an increase of the droplet volumes (figure 5.1a). Images taken at different times after reinjection of the droplets confirm this finding (figure 5.1b).

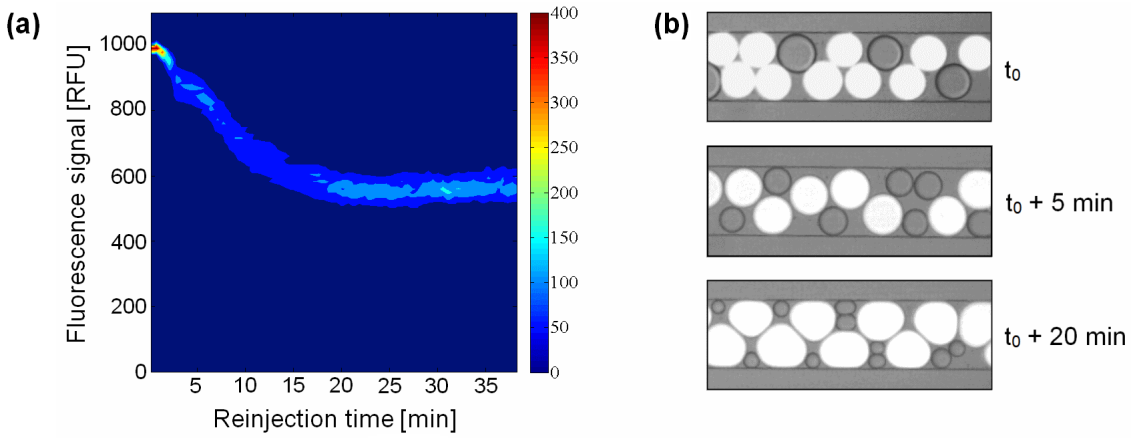

Figure 5.1: Measurement of osmotically driven water transport in emulsion. The transport of water between two initially monodisperse populations of droplets is investigated. While one populations initially contains sodium chloride (100 mg/mL) and fluorescently labelled dextran (100 μM) the other population consists of deionized water. (a) Full time histogram (colorplot) of the fluorescence signal recorded over $\sim$ 40 minutes in HFE-7500 with 1 wt% of surfactant of the droplets initially containing sodium chloride. No fluorescence signal was obtained for the other droplet population. (b) Combined fluorescence and white-light image after droplet production (time = t_0) and 5 minutes as well as 20 minutes after incubation. Droplets containing fluorophores appear bright. Initial droplet diameters correspond to 100 μm.

To investigate the role of the surfactant in the water transport process, the dynamics were recorded for different surfactant concentrations (0.2 wt%, 1 wt%, 5 wt%). The volume of the droplets is assumed to be inversely proportional to the measured fluorescence signal. The temporal increase of the droplet volume V normalized by the initial droplet volume V_0 is shown in figure 5.2a for different surfactant concentrations. The timescale of the water transport process is found to be independent on the surfactant concentration. Hence, the water solubility in the continuous phase mediated by the surfactant is negligible. Instead, the obtained results support a mechanism by direct partitioning as a result of a finite solubility of water in the fluorinated oil (45 ppm by weight, value obtained from supplier 3M). When instead of the fluorinated oil HFE7500 an alternative fluorous fluid (FC-40) is used, the water transport is significantly slowed down by a factor of $\sim$ 2.5. Interestingly, the viscosities of the two fluids differ approximately by the same factor. The supplier states a viscosity of $\eta = 1.24$ cP for HFE7500 and $\eta = 3.4$ cP for FC40. Rescaling by the viscosity results in a collapse of the experimental data as shown in figure 5.2b.

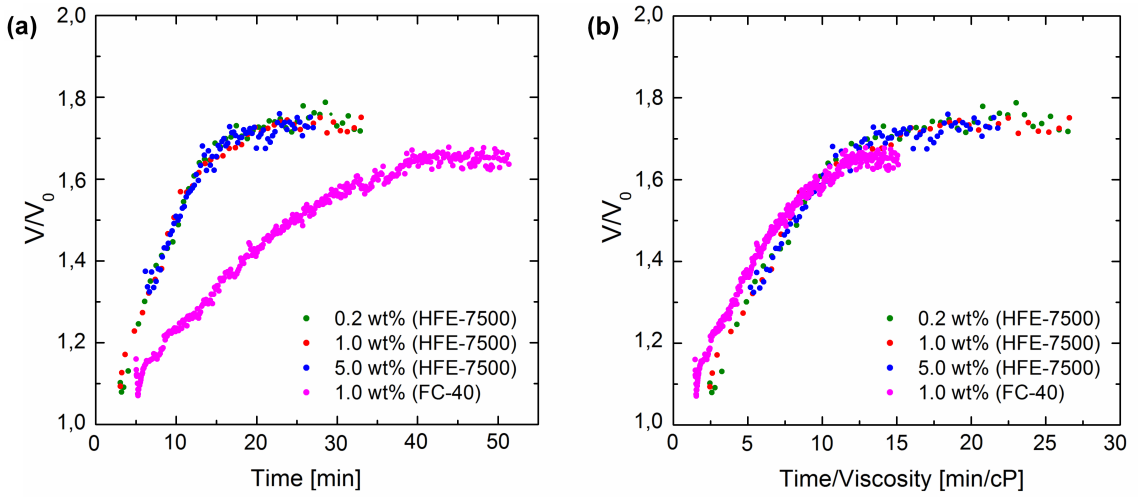

Figure 5.2: Volume increase of droplets containing sodium chloride by osmotically driven water transport for different surfactant concentrations and in different fluorinated oils. The data points correspond to the peaks of the Gaussian distributions. (a) Temporal increase of the droplet volume V, normalized by the initial droplet volume V_0 shown as a function of surfactant concentration (0.2 wt%, 1.0 wt%, 5.0 wt%) in the fluorinated oils HFE-7500 and FC-40. (b) Temporal increase of the normalized droplet volume V/V_0 rescaled by the viscosity η of the continuous phase (HFE7500: $\eta = 1.24$ cP, FC40: $\eta = 3.4$ cP).

The dependence on the viscosity of the fluorinated oil suggests that the rate limiting step of transport is the diffusion of water molecules through the continuous phase.

The osmotically driven water transport between droplets was also investigated by applying the 'minimal' emulsion concept, introduced in chapter 4. Here, the two droplet populations have been immobilized in an alternating order on a one-dimensional microarray. The encoding of the droplet type was relying on fluorescent microparticles present in the droplet type containing sodium chloride. The mass transfer of water between droplets, spatially separated by the continuous phase, was observed. Interestingly, when exclusively the transport of water molecules between the droplet populations is considered, the population consisting of deionized water is expected to dissolve completely as the absence of solutes as well as the decreasing droplet size would result in a chemical potential of the water molecules constantly being greater than in the droplets containing sodium chloride. However, stable droplet sizes are obtained after about 12 hours of immobilization with the minimal emulsion approach (figure 5.3) as well as for the quantitative measurement in macroscopic emulsion after $\sim$ 20 minutes of incubation indicated by the normalized droplet volume V/V_0 reaching a value of only $\sim$ 1,7 (figure 5.2). If one population completely dissolves into the other, the resulting droplet volume V after equilibra-

Figure 5.3: Combined white light and fluorescence image of a one dimensional droplet array. Droplets encoded with fluorescent microparticles (Fluoresbrite YG Microspheres 2.00 μm, Polysciences) contain 100 mg/mL sodium chloride. The other droplet population consist of deionized water. The continuous phase consists of the fluorinated oil HFE7500 containing a surfactant concentration of 1 wt%. Images are shown after 0, 3, 6, 9, 12, 15 and 18 hours after droplet immobilization. Initial droplet diameters correspond to approximately 80 μm.

tion of the chemical potentials is expected to be twice the initial droplet volume V_0, corresponding to a value of 2 for V/V_0.

The equilibration of the chemical potentials, without one population completely dissolving into the other, is explained when a simultaneous transport of sodium chloride is considered. To characterize the transport of inorganic ions, the transport of magnesium ions was investigated. To quantitatively determine its presence in the droplets, a fluorescent indicator (Mag-Fluo-4 Tetrapotassium Salt, Invitrogen) was used. The indicator is essentially non fluorescent in the absence of divalent cations and strongly increases its fluorescence upon binding of magnesium ions. It is sensitive to Mg^{2+}-concentrations ranging from 0.1 to 10 mM (figure 5.4). The indicator was chosen as it is, as a tricarboxylate, expected to be long-term retained within the droplets due to the highly hydrophilic character.

The transport of magnesium ions between emulsion droplets was investigated using the 'minimal emulsion' approach. Here, while one populations contains the Mg^{2+}-indicator (100 μM), the other population comprises magnesium sulphate (200

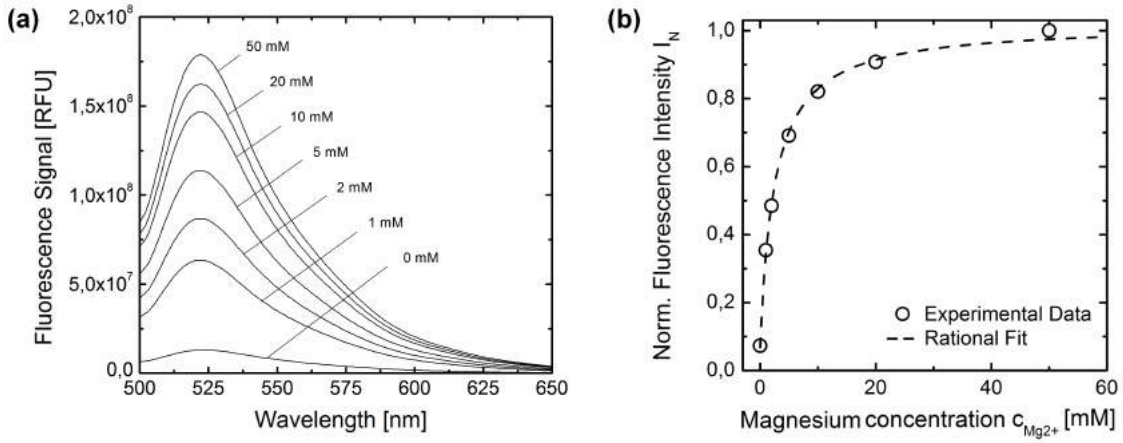

Figure 5.4: Characterization of the fluorescent magnesium indicator (mag-fluo-4, Invitrogen). (a) Fluorescence emission spectra of the indicator (100 μM) in the presence of various concentrations of magnesium sulphate (0 to 50 mM). (b) The normalized fluorescence intensity I_N as a function of the magnesium concentration $c_{\mathrm{Mg^{2+}}}$. I_N was obtained by dividing the measured fluorescence intensity with the intensity in saturation of magnesium (above 50 mM) at 524 nm. The experimental data fit with a rational function: $I_N = 1 + \frac{-2{,}38}{2{,}5 + c_{\mathrm{Mg^{2+}}}/c_S}$. c_{S} corresponds to 1 mM.

mM) in deionized water. This approach allows to investigate the transport of magnesium ions and the indicator simultaneously. While the transport of the inorganic ions between the droplets results in an increase of the fluorescence signal in the droplets containing the indicator, the transport of the indicator itself results in an increase of the fluorescence signal in the droplets containing the inorganic salt.

Experimentally, an increase of the fluorescence signal of the droplets containing the indicator is observed, while droplets containing the inorganic salt remain non-fluorescent throughout the timescale of the experiment (figure 5.5a). Hence, while the indicator is efficiently retained within the droplets, the magnesium ions are transported between the droplets. Surprisingly, the obtained increase of the fluorescence signal corresponds to an increase of the concentration of the magnesium ions of only ~ 0.8 mM (figure 5.5b). As one droplet population was provided with a significantly higher concentration of the inorganic salt (200 mM), it is assumed that a major part is partitioned to the continuous phase.

To qualitatively validate this assumption an additional experiment was conducted. Here, droplets initially containing indicator and magnesium sulphate were produced on a microfluidic chip and the change of the fluorescence signal after droplet production was examined. Droplets with different concentrations of magnesium sulphate (100 mM and 500 mM) were produced simultaneously in a microflu-

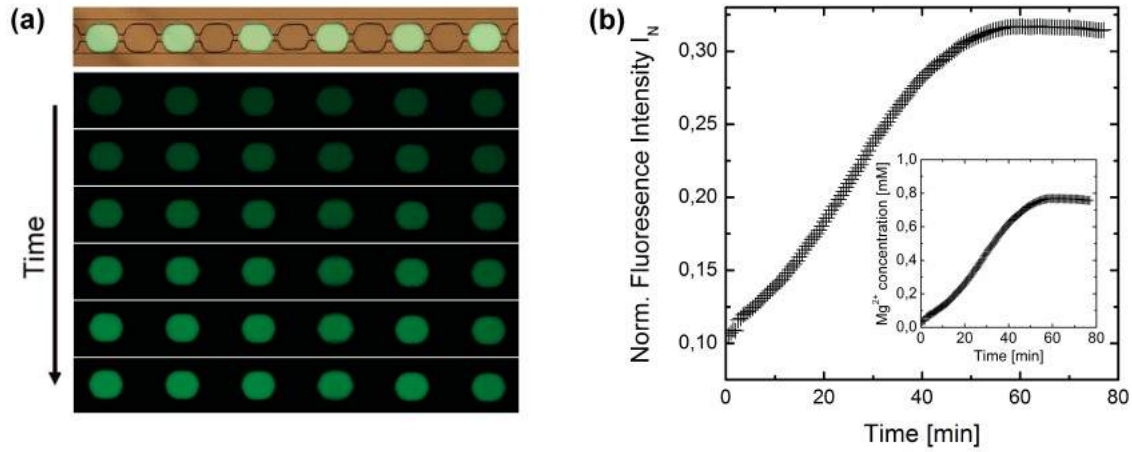

Figure 5.5: Transport of magnesium ions between two droplet populations in a minimal emulsion illustrated by a fluorescent indicator. (a) Combined white light and fluorescence image (top) and fluorescence images (bottom) after 0, 10, 20, 30, 40 and 50 minutes of immobilization. Throughout the experiment, no fluorescence signal is obtained in the droplet population initially containing 200 mM of magnesium sulphate indicating that the fluorescent indicator is retained in the other droplet population. The increase of the fluorescence signal of the droplets containing the indicator reflects the transport of magnesium ions between the droplets. (b) Normalized fluorescence intensity I_N of the droplet population containing the indicator as a function of time. The inset shows the corresponding temporal increase of the magnesium concentration calculated with the calibration shown in figure 5.4b.

idic junction. The concentration of the fluorescent indicator was identical in both populations (100 μM). A substantial decrease of the fluorescence signal after droplet production is obtained for droplets containing 100 mM of magnesium sulphate, while the fluorescence signal of droplets containing 500 mM of the inorganic salt remains almost unaffected in the presence of 2 wt% surfactant (figure 5.6a). When lowering the surfactant concentration to 0.2 wt%, this effect is significantly less pronounced (figure 5.6b). Interestingly, a substantial decrease of fluorescence after droplet production was only observed when specific batches of the surfactant were used. For other batches, even in relatively high concentrations (2 wt%), no significant decrease of the fluorescence signal was observed (figure 5.6c).

It becomes clear that the decrease of the fluorescence signal after droplet formation is related to the characteristics and the concentration of the used surfactant. It is standing to reason that the obtained decrease in fluorescence is a result of a surfactant mediated mass transfer of magnesium ions to the continuous phase. In fact, in other studies it was found that surfactants can facilitate the mass transfer of inorganic ions from an aqueous to an oil phase [166, 167]. Here, such a transport

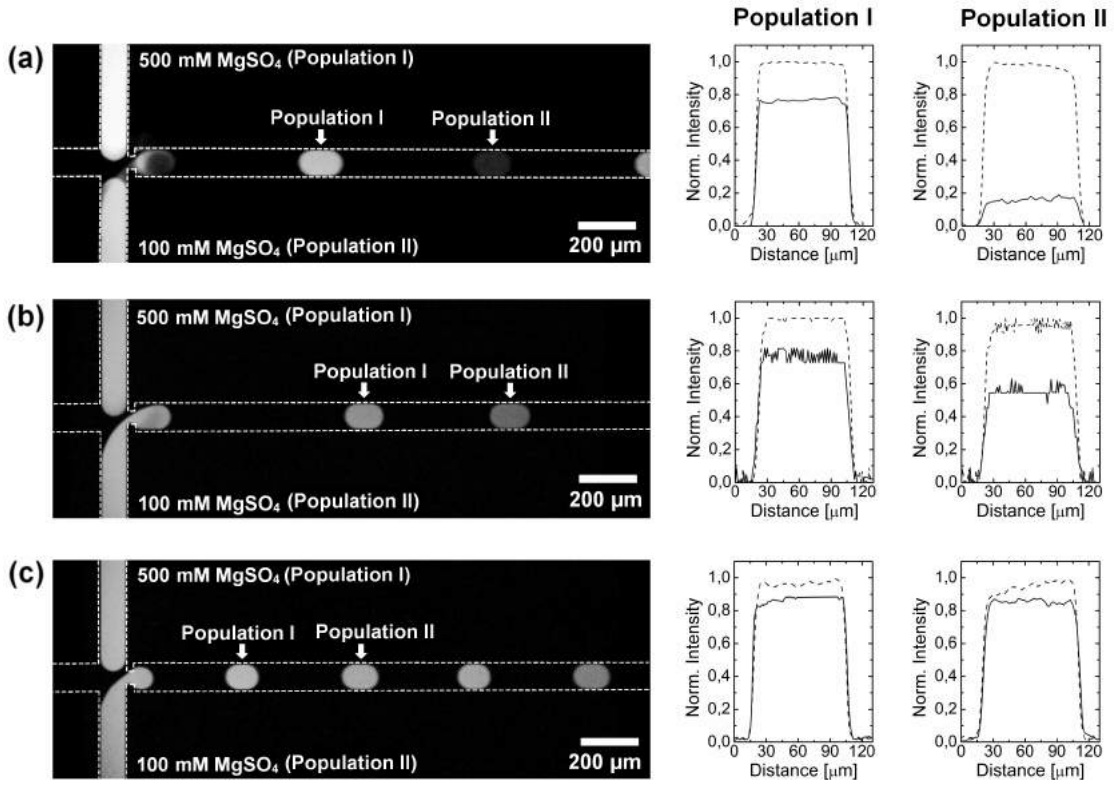

Figure 5.6: Qualitative study of the mass transfer of magnesium ions to the continuous phase during microfluidic droplet production. Fluorescence images are shown on the left and the corresponding measured intensities before (dashed line) and after droplet formation (full line) are shown on the right. Each aqueous phase contains 100 μM of the fluorescent indicator mag-fluo-4 and either 500 mM and 100 mM of magnesium sulphate as indicated in the images. (a) Droplet formation in the presence of 2 wt% of a KrytoxFSH-Jeffa600-KrytoxFSH (batch 1) surfactant. (b) Droplet formation in the presence of 0.2 wt% of a KrytoxFSH-Jeffa600-KrytoxFSH (batch 1) surfactant. (c) Droplet formation in the presence of 2 wt% of a KrytoxFSH-Jeffa600-KrytoxFSH (batch 2) surfactant.

results in a decrease of the concentration of magnesium ions and hence in a decrease of the fluorescence signal of the aqueous phase after droplet formation. The extent of the immediate loss of the fluorescence signal of up to 80%, observed for droplets initially containing a concentration of 100 mM of the inorganic salt suggests that a substantial fraction ($> 90\%$) is phase partitioned to the continuous phase. As a consequence, relatively low concentrations of magnesium ions are present in the aqueous droplets after equilibration of the chemical potentials confirming the results of the 'minimal emulsion' approach. An alternative explanation for the decrease in fluorescence signal after droplet formation is the quenching of the fluorophores by

molecules partitioned from the oil to the aqueous phase. However, in such case one would not expect the temporal increase of the fluorescence signal as shown in figure 5.5a.

Importantly, in this study it was shown that for different batches of surfactants with the same structural formula ('KrytoxFSH-Jeffa600-KrytoxFSH', see section 5.3 'Materials and Methods') a highly diverse performance is obtained. It is assumed that impurities remaining from the synthesis of these surfactants, specific for each batch, highly affect its properties. This topic is investigated and discussed in detail in the next chapter.

5.5 | Conclusion

In this chapter, the osmotically driven transport of water between emulsion droplets was investigated. As a consequence of the water transport, two initially monodisperse droplet populations with different solute concentrations, were undergoing significant changes in droplet volume ultimately leading to a bidisperse emulsion. The mass transfer of water was found to be independent on the surfactant concentration, but dependent on the properties of the fluorinated oil phase used, suggesting that the transport of water molecules takes place by direct partitioning and diffusion of water molecules through the oil phase. The droplet population consisting of deionized water was not dissolving completely as a result of an exchange of solutes between the droplets. The simultaneous transport of water and solutes allows to indirectly investigate the mass transfer of solutes by analysing the volume changes that the droplets undergo. To exclusively investigate the transport of water molecules between droplets, highly hydrophilic solutes with a high molecular weight such as polyethylenglycol or dextran might be chosen.

To investigate the mass transfer of inorganic ions, a fluorescent indicator, sensitive to the presence of magnesium ions was used. The experimental findings suggest that significant fractions ($> 90\%$) may be extracted from the aqueous phase in the presence of surfactants. However, the mass transfer was found to be sensitive to the specific batch of surfactant that was used. It is assumed that impurities resulting from the synthesis of the surfactant and specific for each batch, mediate solubility for the inorganic ions in the continuous phase. This topic is discussed in more detail in the next chapter. For the use of droplets as microreactors for biotechnological applications, the leakage of magnesium ions to the continuous phase is of great rel-

evance as key methods such as polymerase chain reaction in droplets are highly sensitive to the concentration of magnesium ions. Significant concentration changes after droplet formation will substantially affect the performance of for example DNA screening in droplets [16].

6 | Surfactant-mediated solubility in fluorous media

Philipp Gruner, Birte Riechers, Mira Prior, Jörg Enderlein and Jean-Christophe Baret

In the previous chapters, it was shown that surfactants play a major role for the transport of solutes between emulsion droplets. In this chapter, basic interactions by which surfactants mediate solubility in fluorinated oils are described and characterized.

Contents

6.1 | Abstract

The role of fluorosurfactants in mediating solubility for organic molecules in fluorous media is investigated. Surfactants comprising a carboxylic acid head group are found to be efficient in extracting the organic fluorophore rhodamine 6G from an aqueous into a fluorous phase. The extracted fraction of the fluorophores is found to be proportional with the surfactant concentration. An almost complete fluorophore transfer is obtained when the molar concentration of the surfactant exceeds the concentration of the fluorophore. The method of continuous variations is used to determine the receptor-fluorophore complex stoichiometry of 1:1 suggesting that the surfactant acts as a molecular receptor for the fluorophore. The diffusion coefficient of the intermolecular association is determined to be $D = 1.5 \times 10^{-6}\mathrm{cm}^2\mathrm{s}^{-1}$ by dual-focus fluorescence correlation spectroscopy . Interestingly, non-ionic block copolymer surfactants are found to be much less effective in extracting the fluorophore from an aqueous phase. Such biocompatible fluorosurfactants rely on the amidation of fluorous carboxylic acids. Hence, impurities of the base material remaining after synthesis significantly influence the retention of organic molecules within aqueous droplets.

6.2 | Introduction

Fluorinated oils are considered to be the most promising carrier fluids for aqueous droplet microreactors [26]. This has two major reasons. On the one hand, organic molecules are largely insoluble in perfluorinated oils [73, 74], effectively reducing the leakage of compounds from the droplets to the continuous phase. On the other hand, respiratory gases are highly soluble in these media, which is a key for cell survival [98–101]. Although water-in-fluorinated-oil emulsions represent a promising platform for various screening applications, the range of commercially available fluorosurfactants, required to stabilize the emulsion, is very limited. This is especially critical as the properties of the applied surfactant have a wide influence on the performance of the droplet-based system. Major requirements such as the emulsion stability against coalescence, the bio-compatibility of the interface and encapsulation efficiency of compounds over time are heavily dependent on the surfactant used [26].

It has been shown that surfactants with short fluorocarbon tails do not provide long-term stability for emulsified systems [168–170]. In contrast, surfactants with

long tails, such as perfluorinated polyethers (PFPE), are capable of providing excellent emulsion stability [139, 171, 172]. Furthermore, to ensure biocompatiblity, a non-ionic head group of the surfactant is required as ionic headgroups have been shown to interact with biomolecules, leading for example to the denaturation of proteins [173, 174].

Until now, only a few surfactants have been presented that were successfully applied for droplet-based biotechnological applications [139, 171, 172]. Interestingly, all of them are synthesized from a commercially available perfluorpolyether(PFPE)-based surfactant comprising a carboxylic acid headgroup, brand named "Krytox 157FSH" by DuPont (referred to herein as "Krytox"). To impart biocompatibility, the head group of the surfactant is usually modified by synthesis [139, 172] or alternatively shielded by primary amines added to the aqueous phase [171].

In this work, block copolymer surfactants were used that have been synthesized by coupling Krytox with polyetheramines. Interestingly, significant deviations concerning the retention of molecules in the droplets were observed between several batches of the synthesized surfactant. One of the major reasons for such variations are deviating amounts of impurities of the base material 'Krytox' remaining after synthesis of the non-ionic surfactant as shown in this work. This is raising the question about why carboxylic acid surfactants are much more efficient in mediating solubility than non-ionic block copolymer surfactants.

To gain insight into how the properties of the surfactants impacts the mediation of solubility in fluorous media, a general understanding of the interactions of fluorosurfactants with organic molecules is required. In this context, several experiments were performed investigating molecular associations between fluorous carboxylic acids and organic molecules.

6.3 | Materials and methods

6.3.1 | Chemicals

Rhodamine 6G was purchased from Sigma-Aldrich and dissolved in deionized water (milli-Q, Millipore). Krytox 157FSH was obtained from DuPont and dissolved in Novec 7500 Engineered Fluid (HFE-7500) purchased from 3M. For surfactant synthesis, the fluorous fluids HFE7100 and FC3283 were used as solvents (Iolitec). Oxalylchloride (98%), Triethylamine ($\geq$ 98%), anhydrous THF ($\geq$ 99.9%), Jeffa600

and Celite 545 were obtained from Sigma Aldrich.

6.3.2 | Microfluidic experiments

Microfluidic devices were produced by standard soft-lithography techniques using polydimethylsiloxane (PDMS, Sylgard 184 Silicone Elastomer Kit, Dow Corning). The PDMS stamp was bound to glass by oxygen plasma activation and subsequently hydrophobized using a commercial coating agent (Aquapel, PPG Industries). All flow rates were controlled by Nemesys syringe pumps (Cetoni GmbH). All images were taken with a digital camera (Canon, EOS D600). A light emitting diode (CoolLED pE-2, 470 nm) was used for excitation of the fluorophores.

6.3.3 | Partitioning experiments

Partitioning experiments were realized by pipetting 500 μL of HFE-7500 with a distinct concentration of surfactant (0.001 - 0.5 wt%) together with the same amount of milli-Q water containing 100 μM of rhodamine 6G in a glass vial. Careful pipetting ensures that no emulsification is obtained. The mixture of the two liquids is incubated for at least 72 hours when no further change in the absorbance was observed. The absorbance of the aqueous and the fluorous phase are measured with a microplate reader (Spectra Max Paradigm, Molecular Devices).

6.3.4 | Synthesis of the block copolymer surfactant

Krytox 157FSH (1 eq) is dissolved in HFE7100 under inert atmosphere (Argon). Oxaylchloride (10 eq) is injected to the solution and a drop of Dimethylformamid is added to catalyse the reaction. The mixture is stirred for several hours until no further gas development is observed. Subsequently, all solvents are evaporated and the product is redissolved in HFE7100. *O,O'*-Bis(2-aminopropyl)polypropylene gylcol-*block*-polyethylene glycol-*block*-polypropylene glycol 500, trivial named 'Jeffa 600' (0.5 eq) is dissolved in anhydrous Tetrahydrofurane and Triethylamine (5 eq) is added to the solution. The HFE7100 solution is then injected into the THF solution while stirring. The solution is stirred over night and afterwards the product is stable to be handled under atmospheric conditions. Subsequently, all solvents are evaporated and the product is dissolved in FC3283, filtrated and washed (3×25 mL) over Celite 545 using a glass frit (porosity 2) before being dried under vaccum.

A milky semisolid product is obtained with a yield of about 80%. Synthesis was conducted by Birte Reichers. A simplified synthesis scheme is shown in figure 6.1.

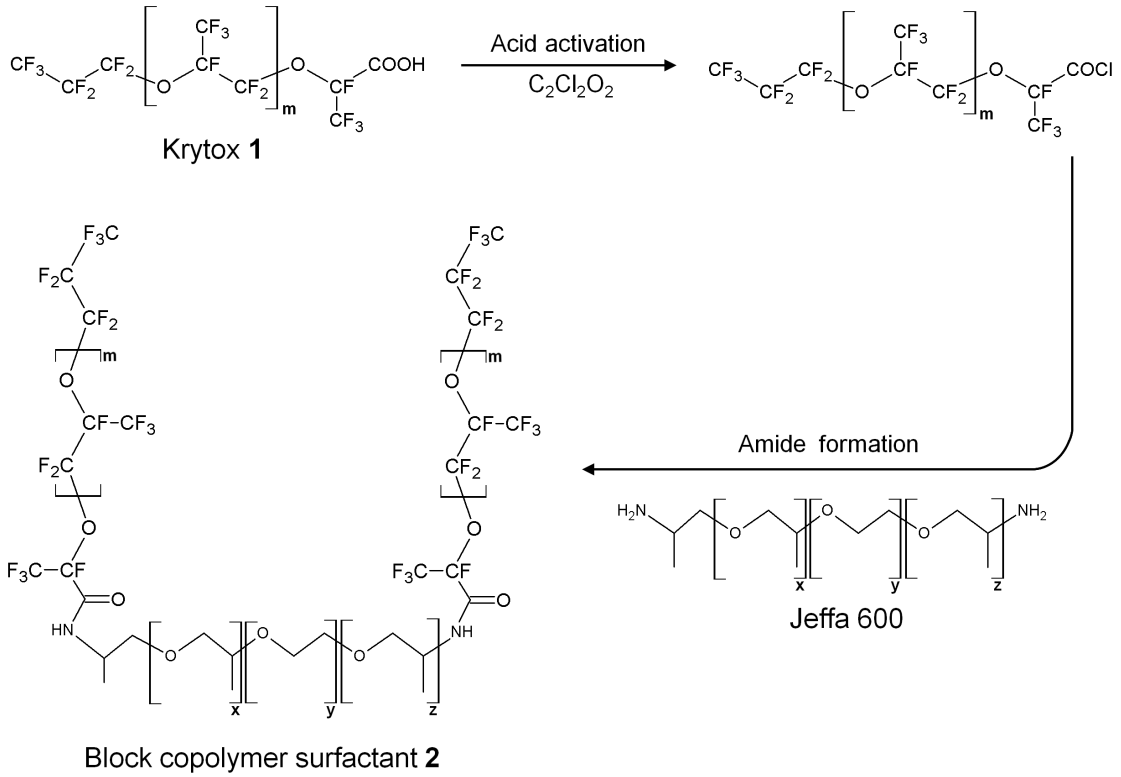

Figure 6.1: Simplified synthesis scheme of a non-ionic block copolymer surfactant performed in a two step process: first the PFPE-carboxylic acid is converted to the corresponding acid chloride. This then reacts with a polyether diamine (Jeffa600) yielding a peptide bond. The repeating unit m of Krytox was reported to be $\sim$ 33 [112] and $\sim$ 29 [103]. The repeating units of the Jeffa 600 correspond to: $x + z \sim 3.6$, $y \sim 9$ according to the supplier.

6.3.5 | NMR measurements

Krytox 157FSH was dissolved in a perfluorinated compound (FC-40, 3M). 1H-NMR measurements were conducted with an internal tubule containing deuterated dichlormethan as reference. 1H-NMR measurements were performed with Agilent DD2 400MR (400 MHz).

6.3.6 | Dual-focus fluorescence correlation spectroscopy

Samples of rhodamine 6G in the fluorinated compound (HFE7500, 3M) were prepared by phase partitioning of the fluorophores from an aqueous solution with a concentration of 1 nM of rhodamine 6G to the fluorous phase comprising 1 μM of

KrytoxFSH as described in section 'Partitioning experiments'. Dual-focus fluorescence correlation spectroscopy (2fFCS) measurements were performed at an excitation wavelength of 531 nm. The non-polarized light of a super-continuum laser (repetition rate 20 MHz, SC400-2-PP, Fianium Ltd.) was divided by a polarizing beam splitter into two linearly polarized beams. The beams were spectrally filtered using an acousto-optical tunable filter (AOTFnC-400.650, AA sa) for each beam. The light of the first branch was delayed by 25 ns (i.e. half of the laser repetition rate) using a polarization-preserving optical fiber of appropriate length (PMC-400Si, Schäfter und Kirchoff GmbH). For combining both beams before coupling them into a polarization-preserving single-mode fiber (PMC-400Si, Schäfter und Kirchoff GmbH), a second polarizing beam splitter was used. At the fiber output, the light formed a train of pulses (FWHM < 10 ps) with alternating polarization and a temporal spacing of 25 ns. An average power of 50 μW for each polarization was chosen. At the fiber output, the light was collimated (1/e2 diameter ca. 4 mm) and reflected by a dichroic mirror (FF545/650-Di01, Semrock Inc.) towards the microscopes water-immersion objective (UPLSAPO 60x W, 1.2 N.A., Olympus Europe). Before entering the back aperture of the objective, the light was passed through a Nomarski prism (U-DICTHC, Olympus Europe). In this way, two laterally shifted but overlapping excitation foci with about 477 nm center distance were created. The centers of the two foci were positioned about 30 μm above the glass slide surface. Fluorescence was collected by the same objective (epi-fluorescence mode), passed through the dichroic mirror, and focused through a single circular aperture (diameter 150 μm). After the pinhole, the light was re-collimated, split by a polarizing beam splitter cube, and refocused onto two SPADs (τ-SPAD-50, PicoQuant GmbH). Emission longpass filters HQ545LP (Chroma Technology Corp., Rockingham) were positioned directly in front of each detector. TCSPC electronics (HydraHarp 400, PicoQuant GmbH) recorded the detected photons of both detectors independently with an absolute temporal resolution of 2 ps on a common time frame, allowing association of the detected photons with their corresponding excitation pulse and focus. With this information the autocorrelation function for each focus separately and the cross-correlation function between the foci were calculated. Fluorescence correlation spectroscopy experiments and data analysis were performed by Mira Prior.

6.4 | Experimental results

To illustrate the efficiency of fluorous carboxylic acid surfactants in extracting organic compounds from aqueous droplets, emulsions were formed with 0.5 wt% of **2** (synthesized block copolymer) comprising low (< 1 %) and high (30 %) mass fractions of **1** (unreacted carboxylic acid surfactant). To visualize the leakage of compounds from droplets, the organic fluorophore rhodamine 6G was added to the aqueous phase. The fluorophore was chosen for two major reasons: (i) It is fluorescent in both: the aqueous and the fluorous phase. (ii) It is readily water soluble, but sufficiently hydrophobic to be quickly partitioned into the fluorous phase in the presence of **1**. When low concentrations of **1** are present, no significant leakage of compounds into the fluorous phase is obtained (figure 6.2a). In contrast, in the presence of high concentrations of **1**, the fluorophores are almost completely extracted into the fluorous phase within less than one second (figure 6.2b).

To quantitatively analyze the extraction of the fluorophores into the fluorous phase, macroscopic partitioning experiments were conducted. Aqueous solutions of rhodamine 6G (100 μM) are exposed to a fluorous phase (HFE7500) containing

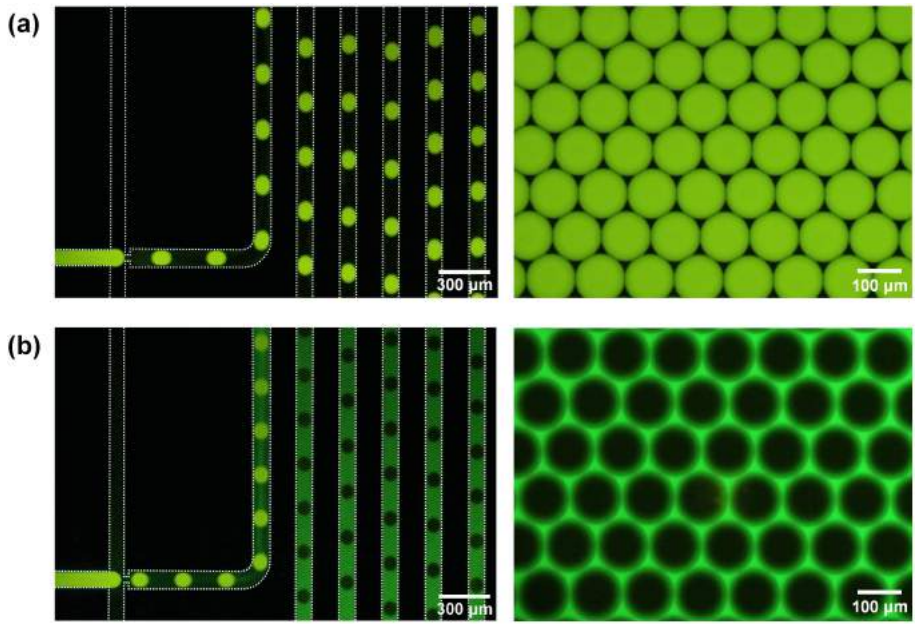

Figure 6.2: Microfluidic production of emulsions containing low (< 1%) and high (30%) mass fractions of **1**. (a) Fluorescence images of droplet production in a flow focussing geometry (left) and the resulting emulsion after production (right) in the presence of low concentrations of **1** compared to the presence of high concentrations of **1** (b). Flow rates were set to 1 μl min^{-1} for the aqueous stream and 4 μl min^{-1} for the fluorous phase.

various concentrations of surfactant. In the absence of surfactant, no significant extraction of molecules is observed. With increasing concentration of **1** the amount of organic molecules being extracted into the fluorous phase is increasing up to a level where an almost complete extraction (> 95 %) of molecules takes place (figure 6.3). The measured absorbance in the fluorous phase was found to be proportional with the concentration of **1** up to about 100 μM. After exceeding a 1:1 molar ratio of the fluorophore and **1** no further increase in absorbance, but a bathochromic shift is observed. These observations are attributed to **1** acting as a molecular receptor for rhodamine 6G resulting in the efficient extraction of the organic solutes into the fluorous phase.

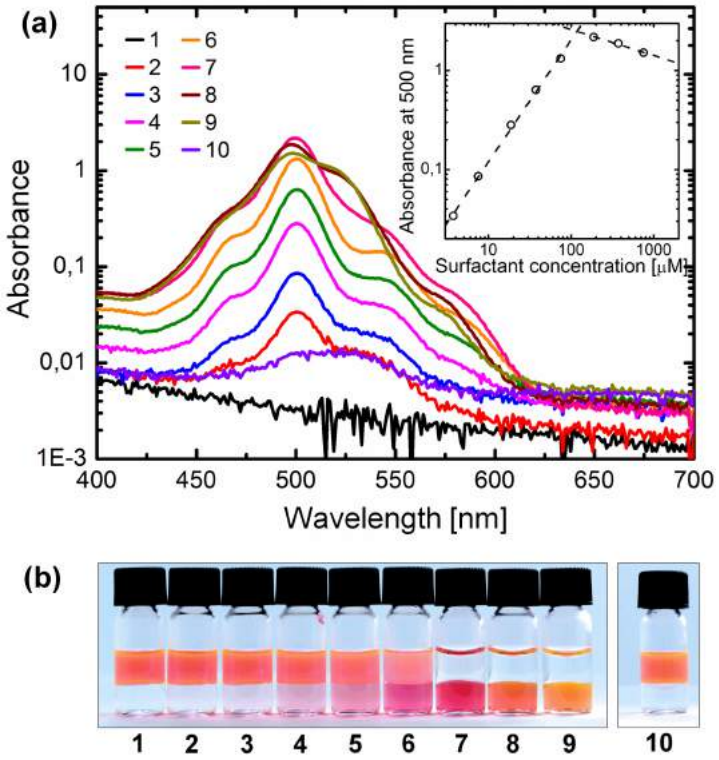

Figure 6.3: Partitioning behaviour of rhodamine 6G between an aqueous phase and a fluorous phase as a function of the applied surfactant and its concentration. (a) Absorption spectra of the fluorous phase after partitioning of rhodamine 6G from the aqueous phase towards the fluorous phase as a function of the surfactant concentration. The inset shows the absorption at 500 nm. (b) Images of the partitioning experiments in equilibrium. Aqueous solutions of rhodamine 6G (100 μM) were exposed to a fluorous phase (Hydrofluorether, HFE7500) comprising various concentrations of surfactant. The concentration of surfactant **1** increases from 1 to 9 as: 0 μM, 3.75 (0.001 wt%), 7.51 μM (0.002 wt%), 18.8 μM (0.005 wt%), 37.5 μM (0.01 wt%), 93.8 μM (0.02 wt%), 188 μM (0.05 wt%), 375 μM (0.1 wt%), 751 μM (0.2 wt%). Solution 10 contains surfactant **2** in a concentration of 877 μM (0.5 wt%).

To validate the stoichiometry of **1** and rhodamine 6G, a continuous variations experiment is conducted (figure 6.4). Here, the total molar concentration of **1** and the fluorophore is constant, but their mole fractions are varied. The maximum of absorption in the fluorous phase is found at a 1:1 molar ratio indicating that a complex with the corresponding stoichiometry is formed. Furthermore, dual-focus fluorescence correlation spectroscopy (2fFCS) experiments were conducted to determine the diffusion coefficient of the intermolecular association in the fluorous phase. This method is an extension of conventional fluorescence correlation spectroscopy and allows for determining absolute values of diffusion coefficients with high precision [176, 177]. A value of about 1.5×10^{-6} cm^2 s^{-1} is obtained. This value is lower than the diffusion coefficient of the freely diffusing fluorophore measured in water of about 4×10^{-6} cm^2 s^{-1}. Even when corrected for the slightly different solvent viscosities of the fluorous phase (1.24 cP at 25 °C) and water (0.89 cP at 25 °C),

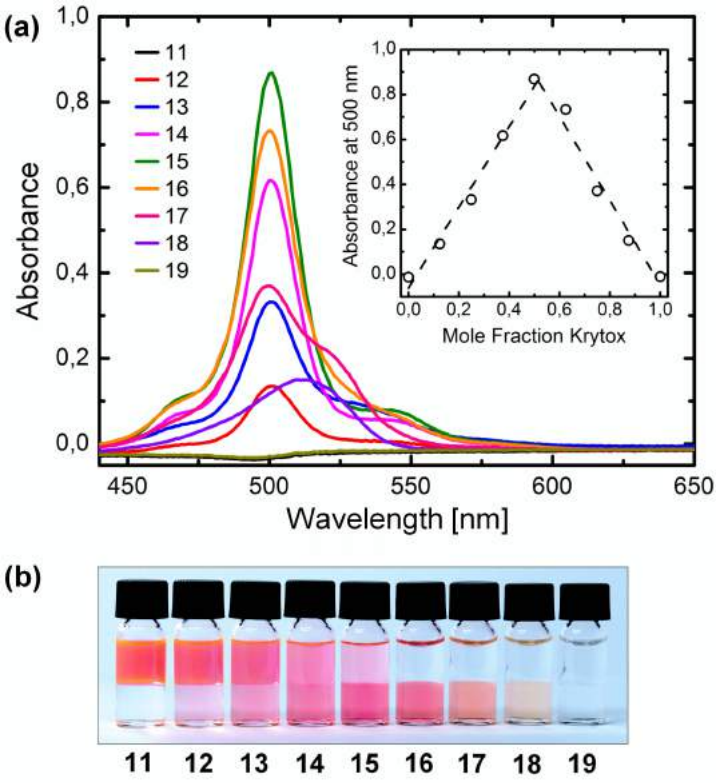

Figure 6.4: Determination of binding stoichiometry by the continuous variation method (Job plot). (a) Absorption spectra of rhodamine 6G in the presence of **1** for various mole fractions. Inset: Absorbance at 500 nm is shown as a function of the mole fraction of **1** (Job plot). (b) Images of the partitioning experiments in equilibrium. Samples 11 - 19 contain a constant total molar concentration of Rhodamine 6G and **1** (100 μM), but their mole fractions are varied. The fraction of **1** is increasing from 11 to 19 as: 0, 0.125, 0.25, 0.375, 0.5, 0.625, 0.75, 0.875, 1.0.

a significant reduction in diffusivity of about 50% in the presence of **1** remains. A decrease on this order is consistent with an interaction of fluorophores with single surfactant molecules. On the other hand, the solubilization of the fluorophores in surfactant assemblies such as reverse micelles or vesicles, where a significant reduction of diffusivity of at least one order of magnitude is expected, is excluded.

In literature it is reported that fluorosurfactants comprising a carboxylic acid head group are capable of forming strong hydrogen bonds with organic molecules [103, 112]. The efficiency of such surfactants in acting as a molecular receptor was reported to be based on their ability to act as a strong hydrogen bond donor in a fluorous phase [90]. Hence, interactions with molecules that can act as a H-bond acceptor such as tertiary amines are highly favourable. In our experiment, it is anticipated that the fluorophores act as a hydrogen bond acceptor via their imine group. Confirming these considerations, no significant extraction of the fluorophores in the presence of surfactant **2** is found. Here, no highly favourable hydrogen bonds can be formed between the surfactant and the fluorophores resulting in the retention of organic molecules in the aqueous phase.

With respect to applications of droplet-based microfluidics it becomes clear that impurities of **1** can have a tremendous effect on the performance of the compartmentalization system. Hence, characterizing the amount of **1** remaining after synthesis is crucial. Various methods such as NMR- and IR- measurements may be applied. However, these methods may not be sufficiently sensitive to trace impurities in a concentration range relevant for typical assays applied for biotechnological purposes (< 100 μM). With standard 1H-NMR the acidic proton of **1** is found at a chemical shift in a range of 7.0 - 13.0 ppm. Here, signal broadening occurs due to the dimerization of **1** [113]. Due to this fact, the presence of **1** in a fully fluorinated fluorocarbon compound (FC-40, 3M) could only traced down to a concentration of about 0.2 wt% (750 μM) with standard 1H-NMR. However, phase partitioning of a fluorescent indicator, such as rhodamine 6G, from a more protic solvent may be applied as a sensitive method for the determination of the concentration of **1**.

6.5 | Conclusions

In this chapter, it was shown that fluorosurfactants comprising a carboxylic acid head group are efficient in extracting organic molecules, such as the fluorophore rhodamine 6G, from an aqueous into a fluorous phase. The efficient extraction

from a more protic solvent is based on the surfactants ability to act as a molecular receptor. The interactions between solute and surfactant are found to be particularly strong, which is a result of the non-competitive nature of the solvent.

In general, it is expected that the hydrogen bond donor and acceptor ability as well as the compatibility of these properties for a given fluorosurfactant and a solute are important characteristics, allowing to predict their interactions and hence the partitioning behavior of solutes. Fluorosurfactants for droplet-based biotechnological applications have in the past mainly been designed according to their influence on surface tension and bio-compatibility. Since it now becomes clear that the retention of molecules within droplet microreactors depends also on the molecular structure of the applied surfactant, for example on the ability to form hydrogen bonds with organic solutes, future fluorosurfactants may be designed accordingly.

Non-ionic fluorosurfactants, currently used in typical droplet-based microfluidic applications, were found to be much less effective in extracting the organic fluorophore reflecting the absence of strong hydrogen-bond acceptor functions. However, their synthesis is based on commercially available surfactants comprising a carboxylic acid head group. Hence, the performance of these non-ionic surfactants is sensitive to impurities of the base material (Krytox 157FSH). To minimize the amount of Krytox remaining after synthesis, we consider that the hydrolysis of the acid chloride has to be strictly avoided and that the amine should be added in over-stoichiometric ratio.

In summary, in this chapter it has been shown how a specific fluorosurfactant mediates solubility for the organic fluorophore rhodamine 6G. These insights are valuable for a general prediction of the interactions between fluorosurfactants and organic molecules in fluorous media. On a short timescale the performance of commonly applied fluorosurfactants may be improved by adjusting the protocol for the synthesis. On a longer timescale, new fluorosurfactants and strategies for their synthesis may be designed based on the insights gained in this work.

7 | Conclusions and Outlook

In this work, information about the mechanism of molecular transport between emulsion droplets were experimentally accessed by applying microfluidic tools. The ability to produce, manipulate and analyze calibrated droplets in a microfluidic environment was shown to be a key to gain quantitative insights. Such insights are inherently difficult to gain with a bulk approach as controlling the properties and microenvironments of individual droplets is enormously challenging without applying methods of fluidic micromanipulation.

Concretely, we have investigated molecular transport between aqueous droplets dispersed in fluorinated oils, being the most promising platforms for biotechnological applications of emulsions. The collective dynamics of solute transport in a whole macroscopic emulsion were accessed following our microfluidic approach allowing measurements on the single droplet level. We found that the timescale of transport is inversely proportional to the surfactant concentration in the continuous phase and relates to a classical description of a porous membrane, where mass transfer occurs through the partitioning of molecules between the dispersed and continuous phase. Furthermore, it was shown how the relaxation dynamics are influenced by the packing of the emulsion droplets. In addition, our studies have clarified the role of additives such as bovine serum albumin in modulating the timescale of solute transport between droplets. In contrast to reports in literature [19], here this effect was found to be relying on an increased solubility of solutes in the aqueous droplets rather than on creating a barrier at the droplet interface. Accordingly, the concept of using such additives may has to be revisited [175].

Furthermore, a microfluidic strategy allowing to create emulsions with a minimized degree of complexity was introduced. Investigating such 'minimal emulsions' allows to experimentally access fundamental information about mass transport in emulsion. Following this strategy, we were able to experimentally identify the rate limiting step of mass transfer between emulsion droplets, which was controversially debated in literature [75–77]. Our findings are in agreement with the suggestion of

Dunstan *et al.* [76] stating that no significant energy barrier for solutes crossing the droplet interface exists, unless charged species are concerned.

Consistent between all our studies, we found that solubility for organic molecules in fluorous media was generally mediated by surfactants. Our studies support two different mechanisms for the mediation of solubility. Depending on the type of surfactant used, solubility is either mediated by the surfactants acting as a molecular receptor for the solute or alternatively by forming assemblies creating a nanoscopic environments for solubilization.

The developed microfluidic methods were also applied to investigate the osmotically driven transport of water and inorganic ions between emulsion droplets. Interestingly, we found that the timescale for the transport of water molecules is independent on the surfactant concentration, reflecting the fact that the presence of surfactant does not significantly enhance their solubility in the fluourous phase. In addition, we found that significant fractions of inorganic ions may be extracted from aqueous droplets in the presence of surfactants. Such an extensive leakage of inorganic ions from emulsion droplets has, to the best of our knowledge, not been reported yet. As key methods of molecular biology, such as polymerase chain reaction, are highly sensitive to specific ion concentrations, such mass transfer is expected to significantly affect droplet-based biotechnological applications, such as DNA screening.

Understanding the mechanistic details of molecular transport in emulsion allows to develop suited strategies to control the exchange of solutes between droplets. For example, demonstrating that solute transfer between droplets is rate limited by the diffusive transport through the continuous phase reveals that increasing the spacing distance between droplets is an effective strategy to reduce cross-talk whereas strategies focusing on the droplet interface may be less effective.

On the one hand, we consider our results as a practical guideline for droplet-based microfluidics, for example for the design of biochemical assays and droplet incubation strategies. On the other hand, we believe that our findings pave the way for a dynamic control of droplet composition. New strategies based on selective transport are obtained by controlling the concentration of additives in the droplets resulting in the enrichment or extraction of compounds of interest. Such an approach also provides the tools to dynamically program the composition of droplet microreactors by temporally controlling the release and uptake of compounds. We

consider such systems as a versatile platform for the control of solute concentrations in emulsion droplets. Furthermore, we have also introduced an alternative concept to dynamically manipulate droplet compositions. Here, mass transfer to aqueous droplet microreactors relies on controlling the consumption of the continuous phase. In such manner, compounds are efficiently delivered to or extracted from emulsion droplets without the need of individual manipulation.

In summary, this work has three major aspects:

(i) It is demonstrated how microfluidic tools are applied to access fundamental information on mass transfer between emulsion droplets, which are inaccessible with classical methods of bulk emulsification.

(ii) Our studies were focused on aqueous droplets dispersed in fluorinated oils, the major platform for biotechnological applications of emulsions. Hence, our results directly impact the development of efficient strategies to reduce cross-talk between droplet microreactors, which is of great importance for the establishment of droplet-based screening applications.

(iii) Based on the gained insights into the mechanistic details of mass transport in emulsion, concepts for a dynamic control of droplet composition were introduced. We consider that such strategies will allow to realize droplet-based investigations as well as applications that have not been feasible so far in screening, diagnostics, single cell manipulation and as tools for synthetic biology.

A | Additional contributions

A.1 | Micro-optical lens array for fluorescence detection in droplet-based microfluidics

Jiseok Lim, Philipp Gruner, Manfred Konrad and Jean-Christophe Baret

A strategy for the enhanced detection of fluorescent signals in droplet-based microfluidic devices is introduced. It is shown that the integration of microlenses and mirror surfaces results in a significant increase in the fluorescence signal and in improved spatial resolution. Furthermore, besides providing increased sensitivity and resolution through the focusing of light by a single element, increased throughput is achieved by integration of the lenses in an array. As a consequence, massively parallel detection of droplets containing fluorescent dyes is achieved, leading to a significantly increased detection throughput.

This work is published in reference [178].

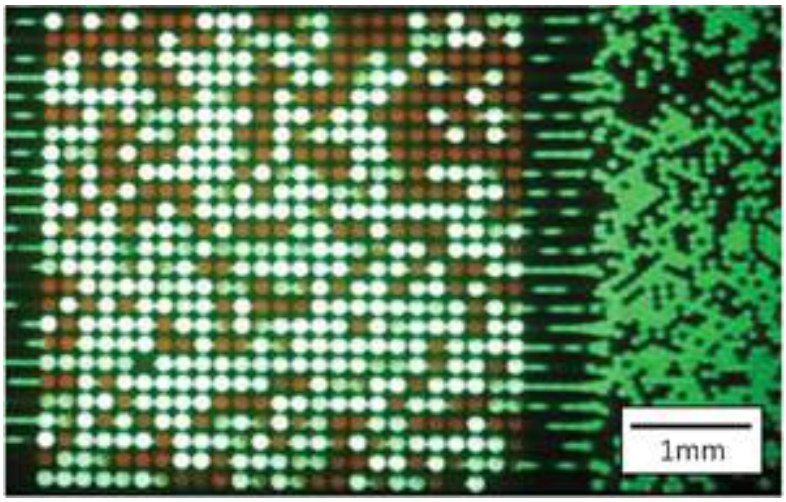

Figure A.1: Droplets containing fluorophores (100 μM resorufin or 100 μM fluorescein) flowing through a microlens array. Droplets flow from right to left. A significant increase of the fluorescent signal is obtained when the droplets enter the microoptical lens array. Image is taken from reference [178].

A.2 | Ultra-high throughout detection of single cell β-galactosidase activity in droplets using micro-optical lens array

Jiseok Lim, Jeremy Vrignon, Philipp Gruner, Christos Karamitros, Manfred Konrad and Jean-Christophe Baret

In this work a micro-optical lens array is applied for the screening of enzymatic activity of single cells in 100 pL droplets. The screening relies on the measurement of a fluorescence-based assay in individual droplets. The measurement is parallelized over 100 microlenses, recorded using a high-speed camera and analysed by image processing. The emulsion is produced following the concept introduced in chapter 3. A throughput of 100 000 droplets per second is achieved by storing an emulsion off chip and reinjecting as presented in chapter 3.

This work is published in reference [179].

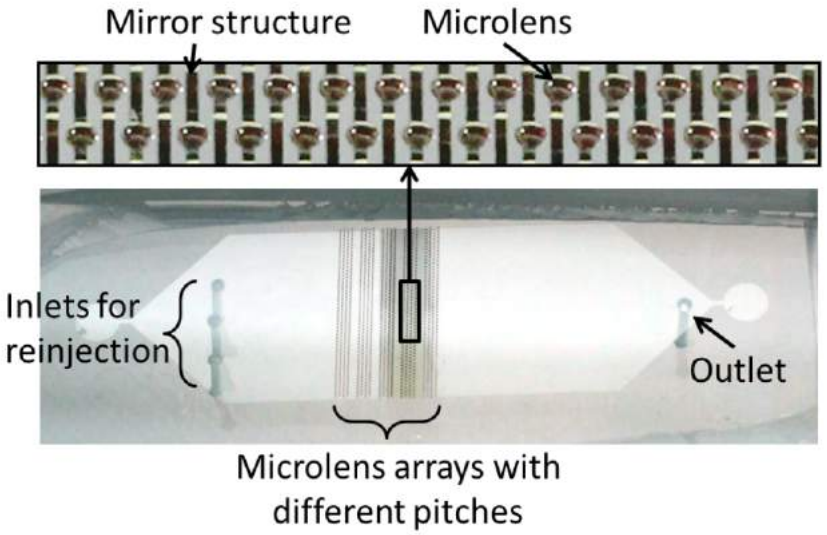

Figure A.2: Image showing a microfluidic chip with 100 parallel channels equipped with micro-optical elements used for the determination of enzymatic activity of single cells. Image is taken from reference [179].

A.3 | Quantitative analysis of L-asparaginase at the single cell level using droplet-based microfluidics

Jiseok Lim, Christos Karamitros, Philipp Gruner, Manfred Konrad and Jean-Christophe Baret

In this study, enzymatic activity of the therapeutic enzyme L-asparaginase is measured in picoliter-sized droplets. Purified enzyme as well as single cells displaying L-asparaginase in the inner membrane are investigated. Enzymatic activities are obtained by using a three-step coupled-enzyme assay. Dynamic measurements became accessible by using the methods and tools introduced in chapter 3. Here, the emulsion is produced and stored off chip in a first step and subsequently reinjected into the microfluidic chip such that the dynamics of the process become accessible. Following the strategies introduced in chapter 3, two populations of droplets are produced in order to implement a negative control. We consider the results of this study to be of general interest for quantitative measurements of single cells in droplets and to pave the way for the directed evolution of the therapeutic enzyme L-asparaginase using droplet-based microfluidics.

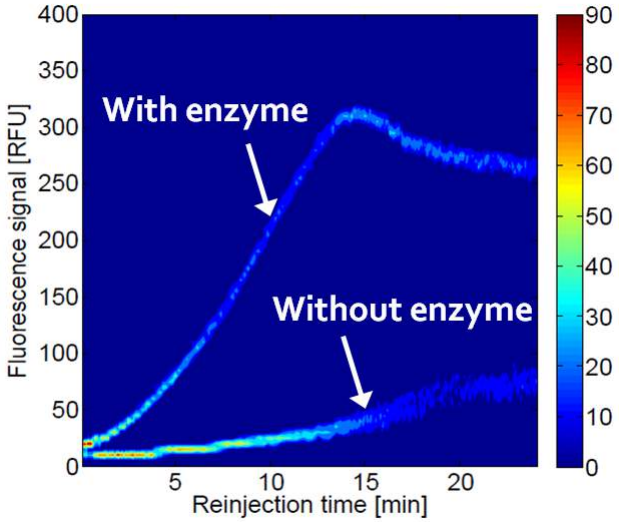

Figure A.3: Direct kinetic measurement of L-Asparaginase in droplets. The fluorescent signal is observed as a result of the presence of resorufin as the final product of the assay. The data correspond to a measurement of droplets with and without the purified enzyme.

B | List of Abbreviations

a	Activity
A	Interfacial Area
AC	Alternating current
b	Quotient of d and h
BSA	Bovine Serum Albumin
c	Molar concentration
CP	Control pump
d	Distance
dFCS	Dual-focus Fluorescence Correlation Spectroscopy
D	Diffusion coefficient
DNA	Deoxyribonucleic acid
DLS	Dynamic Light Scattering
E_γ	Surface energy
F_d	Hydrodynamic drag force
F_γ	Anchoring force
FCS	Fluorescence Correlation Spectroscopy
FPGA	Field Programmable Gate Array
h	height of microchannel
J	Molar flux
k_B	Boltzmann constant
K	Partitioning coefficient
L	Membrane Thickness
NMR	Nuclear Magnetic Resonance
p	Pressure
P	Permeability
PBS	Phosphate Buffer Saline
PCR	Polymerase Chain Reaction
PDMS	Polydimethylsiloxane

PMT	Photomultiplier tube
r	Droplet radius
R	Ideal gas constant
RFU	Relative fluorescence unit
t	Time
T	Absolute Temperature
U	Flow velocity
V	Droplet volume
$\bar{V_i}$	Partial molal volume
V_m	Molar volume
w	diameter of a circular well
x_i	Mole fraction
γ	Interfacial tension
Γ	Activity coefficient
η	Absolute viscosity
μ	Chemical potential
μ_∞	Chemical potential in bulk
Π	Osmotic pressure
τ	Timescale

Bibliography

[1] Chappat M (1994) Some applications of emulsions. *Colloids and Surfaces A* 91:57-77.

[2] Tawfik DS, Griffiths AD (1998) Man-made cell-like compartments for molecular evolution. *Nature* 16:652-656.

[3] Taly V, Kelly BT, Griffiths AD (2007) Droplets as Microreactors for High-Throughput Biology. *ChemBioChem* 8:263-272.

[4] Lederberg J (1954) A simple method for isolating individual microbes. *Journal of Bacteriology* 68:258-259.

[5] Thorsen T, Roberts RW, Arnold FH, Quake SR (2001) Dynamic Pattern Formation in a Vesicle-Generating Microfluidic Device. *Physical Review Letters* 86:4163-4166.

[6] Baret JC, Miller OJ, Taly V, Ryckelynck M, El-Harrak A, Frenz L, Rick C, Samuels ML, Hutchison JB, Agresti JJ, Link DR, Weitz DA, Griffiths AD (2009) Fluorescence-activated droplet sorting (FADS): efficient microfluidic cell sorting based on enzymatic activity. *Lab Chip* 9:1850-1858.

[7] Abate A, Hung T, Mary P, Agresti JJ, Weitz DA (2010) High-throughput injection with microfluidics using picoinjectors. *Proceedings of the National Academy of Sciences* 107:19163-19166.

[8] Priest C, Herminghaus S, Seemann R (2006) Controlled electrocoalescence in microfluidics: Targeting a single lamella. *Applied Physics Letters* 89:134101.

[9] Kelly BT, Baret JC, Taly V, Grffiths AD (2007) Miniaturizing chemistry and biology in microdroplets. *Chemical Communications* 103:1773-1788.

[10] Teh SY, Lin R, Lung-Hsin H, Lee AP (2008) Droplet microfluidics. *LabChip* 8:198-220.

[11] Theberge AB, Courtois F, Schaerli Y, Fischlechner M, Abell C, Hollfelder F, Huck WTS (2010) Microdroplets in Microfluidics: An Evolving Platform for Discoveries in Chemistry and Biology. *Angewandte Chemie* 49:5846-5868.

[12] Guo MT, Rotem A, Heyman JA, Weitz DA (2012) Droplet microfluidics for high-throughput biological assays. *LabChip* 12:2146-2155.

[13] Seemann R, Brinkmann M, Pfohl T, Herminghaus S (2012) Droplet based microfluidics. *Reports on Progress in Physics* 75:016601.

[14] Joensson HN, Andersson Svahn H (2012) Droplet Microfluidics - A Tool for Single-Cell Analysis.*Angewandte Chemie* 51:12176-12192.

[15] Agresti JJ, Antipov E, Abate A, Ahn K, Rowata AC, Baret JC, Marquez M, Klibanov AM, Griffith AD, Weitz AD (2009) Ultrahigh-throughput screening in drop-based microfluidics for directed evolution. *Proceedings of the National Academy of Sciences* 107:4004-4009.

[16] Pekin D, Skhiri Y, Baret JC, Le Corre D, Mazutis L, Salem CB, Millot F, El Harrak A, Hutchison JB, Larson JW, Link DR, Laurent-Puig P, Griffiths AD, Taly V (2011) Quantitative and sensitive detection of rare mutations using droplet-based microfluidics. *Lab Chip* 11:2156-2166.

[17] Miller OJ, El Harrak A, Mangeat T, Baret JC, Frenz L, El Debsa B, Mayot E, Samuels ML, Rooney EK, Dieue P, Galvan M, Link DR, Griffith AD (2012) High-resolution dose-response screening using droplet-based microfluidics. *Proceedings of the National Academy of Sciences* 10:378-383.

[18] Mazutis L, Baret JC, Treacy P, Skhiri Y, Araghi AF, Ryckelynck M, Taly V, Griffiths AD. (2009) Multi-step microfluidic droplet processing: kinetic analysis of an in vitro translated enzyme. *Lab Chip* 9:2902-2908.

[19] Courtois F, Olguin LF, Whyte G, Theberge AB, Huck WTS, Hollfelder F and Abell C (2009) Controlling the Retention of Small Molecules in Emulsion Microdroplets for Use in Cell-Based Assays. *Anal. Chem.* 81:3008-3016.

[20] Bai Y, He X, Liu D, Patil SN, Bratton D, Huebner A, Hollfelder F, Abell C, Huck WTS (2009) A double droplet trap system for studying mass transport across a droplet-droplet interface. *Lab Chip* 10:1281-1285.

[21] Wu N, Courtois F, Zhu Y, Oakeshott J, Easton C, Abell C (2010) Management of the diffusion of 4-methylumbelliferone across phases in microdroplet-based systems for in vitro protein evolution. *Electrophoresis* 31:3121-3128.

[22] Woronoff G, El Harrak A, Mayot E, Schicke O, Miller OJ, Soumillion P, Griffiths AD, Ryckelynck M (2011) New Generation of Amino Coumarin Methyl Sulfonate-Based Fluorogenic Substrates for Amidase Assays in Droplet-Based Microfluidic Applications. *Analytical Chemistry* 83:2852-2857.

[23] Colin A, Squires TM, Bocquet L (2012) Soft matter principles of microfluidics. *Soft Matter* 8:10527-10529.

[24] Mazutis L, Gilbert J, Ung WL, Weitz DA, Griffiths AD, Heyman JA (2013) Single-cell analysis and sorting using droplet-based microfluidics. *Nature Protocols* 8:870-891.

[25] Bremond N, Bibette J (2012) Exploring emulsion science with microfluidcs. *Soft Matter* 8:10549-10559.

[26] Baret JC (2012) Surfactants in droplet-based microfluidics. *LabChip* 12:422-433.

[27] Taylor GI (1934) The Formation of Emulsions in Definable Fields of Flow. *Proceedings of the Royal Society A* 146:501-523.

[28] Rosen MJ (2004) Surfactants and Interfacial phenomena. *John Wiley & Sons, Inc.* pp. i-xiii.

[29] Dai B, Leal L (2008) The mechanism of surfactant effects on drop coalescence. *Physics of Fluids* 20:040802.

[30] Whitesides GM (2006) The origins and the future of microfluidics. *Nature* 442:368-373.

[31] Qin D, Xia Y, Whitesides GM (1996) Rapid Prototyping of Complex Structures with Feature Sizes Larger Than 20 μm. *Advanced Materials* 8:917-919.

[32] Ballagadde FK, You L, Hansen CL, Arnold FH, Quake SR (2005) Long-term monitoring of bacteria undergoing programmed population control in a microchemostat. *Science* 309:137-140

[33] Weibel DB, Kruithof M, Potenta S, Sia SK, Lee A, Whitesides GM (2005) Torque-actuated valves for microfluidics. *Analytical Chemistry* 77:4726-4733.

[34] Anna SL, Bontou X, Stone HA (2003) Formation of dispersions using 'flow focusing' in microchannels. *Applied Physics Letters* 82:364-366.

[35] Nisisako T, Torii T (2008) Microfluidic large-scale integration on a chip for mass production of monodisperse droplets and particles. *Lab Chip* 8:287-293.

[36] Shim J, Ranasinghe RT, Smith CA, Ibrahim SM, Hollfelder F, Huck WTS, Klenerman D, Abell C (2013) Ultrarapid generation of femtoliter microfluidic droplets for Single-Molecule-Counting Immunoassays. *ACS Nano* 7:5955-5964.

[37] Dangla R, Fradet E, Lopez Y, Baroud CN (2013) The physical mechanisms of step emulsification. *Journal of Physics D: Applied Physics* 46:114003

[38] Franke T, Abate AR, Weitz DA, Wixforth A (2009) Surface acoustic wave (SAW) directed droplet flow in microfluidics for PDMS devices. *LabChip* 9:2625-2627

[39] Abate AR, Agresti JJ, Weitz DA (2010) Microfluidic sorting with high-speed single-layer membrane valves. *Applied Physics Letters* 96:203509.

[40] Baroud CN, De Saint Vincent MR, Delville JP (2007) An optical toolbox for total control of droplet microfluidics. *LabChip* 7:1029-1033.

[41] Ruiter R, Pit AM, de Oliveira VM, Duits MH, van den Ende D, Mugele F (2013) Electrostatic potential wells for on-demand drop manipulation in microchannels. *LabChip* 14:883-891.

[42] Priest C, Gruner P, Szili EJ, Al-Bataineh SA, Bradley JW, Ralston J, Steele DA, Short RD (2011) Microplasma patterning of bonded microchannels using high-precision injected electrodes. *LabChip* 11:541-544.

[43] Siegel AC, Shevkoplyas SS, Weibel DB, Bruzewicz DA, Martinez AW, Whitesides GM (2006) Cofabrication of Electromagnets and Microfluidic Systems in Poly(dimethylsiloxane). *Angewandte Chemie* 45:6877-6882.

[44] Ahn K, Kerbage C, Hunt TP, Westervelt RM, Link DR, Weitz DA (2006) Dielectrophoretic manipulation of drops for high-speed microfluidic sorting devices. *Applied Physics Letters* 88:024104.

[45] Shim J, Cristobal G, Link DR, Thorsen T, Jia Y, Piattelli K, Fraden S (2007) Control and Measurement of the Phase Behaviour of Aqueous Solutions Using Microfluidics. *Journal of the American Chemical Society* 129:8825-8835.

[46] Cordero ML, Burnham DR, Baroud CN, McGloin D (2008) Thermocapillary manipulation of droplets using holographic beam shaping: Microfluidic pin ball. *Applied Physics Letters* 93:034107.

[47] Shi W, Qin J, Ye N, Lin B (2008) Droplet-based microfluidic system for individual Caenorhabditis elegans assay. *Lab Chip* 8:1432-1435.

[48] Huebner A, Bratton D, Whyte G, Yang M, Demello AJ, Abell C, Hollfelder F (2009) Static microdroplet arrays: a microfluidic device for droplet trapping, incubation and release for enzymatic and cell-based assays. *Lab Chip* 9:692-698.

[49] Schmitz C, Rowat A, Köster S, Weitz D (2009) Dropspots: a picoliter array in a microfluidic device. *Lab Chip* 9:44-49.

[50] Abbyad P, Dangla R, Alexandrou A, Baroud CN (2011) Rails and anchors: guiding and trapping droplet microreactors in two dimensions. *Lab Chip* 11:813-821.

[51] Fradet E, McDougall C, Abbyad P, Dangla R, McGloin D, Baroud CN (2011) Combining rails and anchors with laser forcing for selective manipulation within 2D droplet arrays. *LabChip* 11:4228-4234

[52] Dangla R, Lee S, Baroud CN (2011) Trapping Microfluidic Drops in Wells of Surface Energy. *Physical Review Letters* 107:124501-124504

[53] Taylor P (1998) Ostwald ripening in emulsions. *Advances in Colloid and Interface Science* 75:107-163.

[54] Koroleva MY, Yurtov EV (2006) Water mass transfer in W/O emulsions. *Journal of Colloid and Interface Science* 297:778-784.

[55] Thomson W (1871) Hydrokinetic Solutions and Observations. *Proceedings of the Royal Society* 7:63.

[56] Skinner LM, Sambles JR (1972) The Kelvin equation - a review. *Journal of Aerosol Science* 3:199-210.

[57] Pfeffer W (1877) Osmotische Untersuchungen. Studien zur Zellmechanik. *Leipzig: Wilhelm Engelmann*

[58] Van't Hoff JH (1887) The role of osmotic pressure in the analogy between solutions and gases. *Zeitschrift für Physikalische Chemie* 1:481-508.

[59] Borg F (2003) What is osmosis? Explanation and understanding of a physical phenomenon. *arXiv:physics/0305011 [physics.gen-ph].*

[60] Raghunathan A, Aluru N (2006) Molecular Understanding of Osmosis in Semipermeable Membranes. *Physical Review Letters* 97:1-4

[61] Ben-Sasson SA, Grover NB (2003) Osmosis: a macroscopic phenomen, a microscopic view. *AJP: Advances in Physiology Education* 27:15-19

[62] Chinard FP, Enns T (1956) Osmotic pressure. *Science* 124:472-474.

[63] Trotta M, Gasco MR, Morel S (1989) Release of drugs from oil-water microemulsions. *Journal of Controlled Release* 10:237-243.

[64] Koizumi T, Higuchi WI Analysis of Data on Drug Release from Emulsions II. *Journal of Pharmaceutical Sciences* 57:87-92.

[65] Thiam AR, Bremond N, Bibette J (2012) From Stability to Permeability of Adhesive Emulsion Bilayers. *Langmuir* 28:6291-6298.

[66] Caldero G, Garcia-Celma MJ, Solans C, Plaza M, Pons R(1997) Influence of Composition Variables on the Molecular Diffusion from Highly Concentrated Water-in-Oil Emulsions (Gel-Emulsions). *Langmuir* 13:385-390.

[67] Calderoo G, Garcia-Celma MJ, Solans C, Stebe MJ, Ravey JC, Rocca S, Pons R (1998) Diffusion from Hydrogenated and Fluorinated GelâĹŠEmulsion Mixtures. *Langmuir* 14:6840-6845.

[68] Caldero G, Garcia-Celma MJ, Solans C, Pons R (2000) Effect of pH on Mandelic Acid Diffusion in Water in Oil Highly Concentrated Emulsion. *Langmuir* 16:1668-1674

[69] Sandoz, Chung AJ, Westbrook MW, Di Carlo D (2014) Sugar Additives Improve Signal Fidelity for Implementing Two-Phase Resorufin-Based Enzyme Immunassays. *Langmuir* 30:6637-6643.

[70] BabakV, Stebe MJ, Fa N (2003) Physico-chemical model for molecular diffusion from highly concentrated emulsions. *Mendeleev Communications* 13:254-256.

[71] Fa N, Babak VG, Stebe MJ (2004) The release of caffeine from hydrogenated and fluorinated gel emulsions and cubic phases. *Colloids and Surfaces A* 243:117-125.

[72] Rocca S, Garcia-Celma MJ, Caldero G, Pons R, Solans C, Stebe MJ (1998) Hydrophilic Model Drug Delivery from Concentrated Reverse Emulsions. *Langmuir* 14:6840-6845.

[73] Scott RL (1948) The solubility of fluorocarbons. *Journal of the American Chemical Society* 70:4090-4093 .

[74] Simons JH, Linevsky MJ (1952) The solubility of organic solids in fluorocarbon derivatives. *Journal of the American Chemical Society* 74: 4750-4751.

[75] Llinas M, Caldero G, Garcia-Celma MJ, Patti A, Solans C (2013) *Journal of Colloid and Interface Science* 394:337-345.

[76] Dunstan TS, Fletcher PDI (2011) Compartmentalization and Separation of Aqueous Reagents in the Water Droplets of Water-in-Oil High Internal Phase Emulsions. *Langmuir* 27:3409-3415.

[77] Chen Y, Gani AW, Tang SKY (2012) Characterization of sensitivity and specificity in leaky droplet-based assays. *Soft Matter* 12:5093-5103.

[78] Caldero G, Llinas M, Garcia-Celma MJ, Solans C (2010) Studies on Controlled Release of hydrophilic drugs from W/O Internal Phase Ratio Emulsions. *Journal of Pharmaceutical Sciences* 99:701-711

[79] Overton E. (1899) Über die allgemeinen osmotischen Eigenschaften der Zelle. *Vierteljahrsschrift der Naturforschenden Gesellschaft in Zürich* 44:88-135

[80] Al-Awqati Q (1999) One hundred years of membrance permeability: does Overton still rule? *Nature Cell Biology* 1:E201-E202.

[81] Poulin P, Bibette J (1998) Adhesion of Water Droplets in Organic Solvents. *Langmuir* 14:6341-6343.

[82] Funakoshi K, Suzuki H, Takeuchi S (2006) Lipid Bilayer Formation by Contacting Monolayers in a Microfluidic Device for Membrane Protein Analysis. *Analytical Chemistry* 78:8169-8174.

[83] Thutupalli S, Herminghaus S, Seemann R (2011) Bilayer membranes in microfluidics: from gel emulsions to soft functional devices. *Soft Matter* 7:1312-1320.

[84] Finkelstein A (1987) Water Movement Through Lipid Bilayers, Pores, and Plasma Membranes: Theroy and Reality. *Wiley Interscience, New York*

[85] Nagle JF, Scott HL (1978) Lateral compressibility of lipid mono- and bilayers. Theory of membrane permeability. *Biochimica et Biophysica Acta* 513:236-243.

[86] Paula S, Volkov AG, Van Hoek AN, Haines TH, Deamer DW (1996) Permeation of Protons, Potassium Ions, and Small Polar Molecules Through Phospholipid Bilayers as a Function of Membrane Thickness. *Biophysical Journal* 70:339-348.

[87] Lemal DM (2004) Perspective on fluorocarbon chemistry. *Journal of Organic Chemistry* 69:1-11.

[88] O'Hagan (2007) Understanding organofluorine chemistry. An introduction to the C-F bond. *Chemical Society Reviews* 37:308-319.

[89] Brady JE, Carr PW (1982) Perfluorinated Solvents as Nonpolar Test Systems for Generalized Models of Solvatochromic Measures of Solvent Strength. *Analytical Chemistry* 54:1751-1757.

[90] Vincent JM (2008) Noncovalent associations in fluorous fluids. *Journal of Fluorine Chemistry* 129:903-909.

[91] Gladysz JA, Curran DP, HorvÃąth IT (2005) Handbook of Fluorous Chemistry. *Wiley & Sons, New York.*

[92] Abbyad P, Tharaux PL, Martin JL, Baroud CN, Alexandrou A (2010) Sickling of red blood cells through rapid oxygen exchange in microfluidic drops. *Lab Chip* 10:2505-2512.

[93] Clausell-Tormos J, Lieber D, Baret JC, El-Harrak A, Miller OJ, Frenz L, Blouwolff J, Humphry KJ, Köster S, Duan H, Holtze C, Weitz DA, Griffiths

AD, Merten CA (2008) Droplet-Based Microfluidic Platforms for the Encapsulation and Screening of Mammalian Cells and Multicellular Organisms. *Chemistry & Biology* 15:427-437.

[94] Hamza MA, Serratrice G, Stebe MJ, Delpuech JJ (1981) Solute-Solvent Interactions in Perfluorocarbon Solutions of Oxygen. An NMR Study. *Journal of the American Chemical Society* 103:3733-3738.

[95] Gollan F, Clark LC (1966) Organ perfusion with fluorocarbon fluid. *Physiologist* 9:191.

[96] Andjus RK, Suhara K, Sloviter NA (1967) An isolated, perfused rat brain preparation, its spontaneous and stimulated activity. *Journal of Applied Physiology* 22:1033-1039.

[97] Geyer RP (1973) Fluorocarbon-Polyol Artificial Blood Substitutes. *The New England Journal of Medicine* 289:1077-1082.

[98] Riess JG, Dalfors JL, Hanna GK, Klein DH, Krafft MP, Pelura TJ, Schutt EG (1992) Development of highly fluid, concentrated and stable fluorocarbon emulsions for diagnosis and therapy. *Biomaterials, artificial cells, and immobilization biotechnology* 20:839-842.

[99] Krafft MP, et al. (1992) Drop size stability assessment of fluorocarbon emulsions. *Biomaterials, artificial cells, and immobilization biotechnology* 20:865-868.

[100] Riess JG, Krafft MP (1997) Advanced fluorocarbon-based systems for oxygen and drug delivery, and diagnosis. *Biomaterials, artificial cells, and immobilization biotechnology* 25:43-52.

[101] Riess JG, Krafft MP (1998) Fluorinated materials for in vivo oxygen transport (blood substitutes), diagnosis and drug delivery. *Biomaterials* 19:1529-1539.

[102] Lee JN, Park C, Whitesides GM (2003) Solvent Compatibility of Poly(dimethylsiloxane)-Based Microfluidic Devices. *Analytical Chemistry* 75:6544-6554.

[103] O'Neal KL, Weber SG (2009) Molecular and Ionic Hydrogen Bond Formation in Fluorous Solvents. *Journal of Physical Chemistry B* 113:149-158.

[104] Vincent JM, Rabion A, Yachandra VK, Fish RH (1997) Fluorous Biphasic Catalysis: Complexation of $1,4,7-[C_8F_{17}(CH_2)_3]_3$-1,4,7-Triazacyclononane with $[M(C_8F_{17}(CH_2)_2C0_2)_2]$ (M = Mn, Co) To Provide Perfluoroheptane-Soluble Catalysts for Alkane and Alkene Functionalization in the Presence of t-BuOOH and 0_2. *Angewandte Chemie* 36:2346-2349.

[105] Pozzi G, Cavazzini M, Quincy S, Fontana S (1997) Metal Complexes of a Tetraazacyclotetradecane Bearing Highly Fluorinated Tails: New Catalysts for the Oxidation of Hydrocarbons under Fluorous Biphasic Conditions. *Tetrahedron Letters* 38:7605-7608.

[106] Chen LX, Jäger WJH, Gosztola DJ, Niemczyk MP, Wasielewski MR (2000) Ionochromic Effects and Structures of Metalated Poly(*p*-phenylenevinylene) Polymers Incorporating 2,2'-Bipyridines *Journal of Physical Chemistry B* 104:1950-1960.

[107] Pozzi G, Cinato F, Montanari F, Quici S (1998) Efficient aerobic epoxidation of alkenes in perfluorinated solvents catalysed by chiral (salen) Mn complexes. *Chemical Communications* 877-878.

[108] Klement I, Lütjens H, Knochel P (1997) Transition Metal Catalyzed Oxidations in Perfluorinated Solvents. *Angewandte Chemie International Edition* 36:1454-1456.

[109] De Campo F, Lastecoueres D, Vincent JM, Verlhac JB (1999) Copper(I) Complexes Mediated Cyclization Reaction of Unsaturated Ester under Fluoro Biphasic Procedure. *Journal of Organic Chemistry* 64:4969-4971.

[110] Richter B, Spek AL, van Koten G, Deelman BJ (2000) Fluorous Versions of Wilkinsons Catalyst. Activity in Fluorous Hydrogenation of 1-Alkenes and Recycling by Fluorous Biphasic Separation. *Journal of the American Chemical Society* 122:3945-3951.

[111] Palomo C, Aizpurua JM, Loinaz MJ, Fernandez-Berridi MJ, Irusta L (2001) Scavenging of Fluorinated N,N'-Dialkylureas by Hydrogen Binding: A Novel Separation Method for Fluorous Synthesis. *Organic Letters* 3:2361-2364.

[112] O'Neal KL, Geib S, Weber SG (2007) Extraction of Pyridines into Fluorous Solvents Based on Hydrogen Bond Complex Formation with Carboyxlic Acid Receptors. *Analytical Chemistry* 79:3117-3125.

[113] Doan V, Köppe R, Kasai PH (1997) Dimerization of Carboxylic Acids and Salts: An IR Study in Perfluoropolyether Media. *Journal of the American Chemical Society* 119:9810-9815.

[114] Remko M (1979) A Theoretical (PCILO) Study of hydrogen bonding in carboxylic acids and their adducts with pyridine. *Advances in Molecular Relaxation and Interaction Processes* 15:193-206.

[115] Vishweshwar P, Nangia A, Lynch VM (2002) Recurrence of Carboxylic AcidâĹŠPyridine Supramolecular Synthon in the Crystal Structures of Some Pyrazinecarboxylic Acids. *Journal of Organic Chemistry* 67:556-565.

[116] Burns JR, Ramshaw C (2001) The intensification of rapid reactions in mulitphase systems using slug flow in capillaries. *LabChip* 1:10-15.

[117] Mary P, Studer V, Tabeling P (2008) Microfluidic Droplet-Based Liquid-Liquid Extraction. *Analytical Chemistry* 80:2680-2687.

[118] Xu JH, Tan J, Li SW, Luo GS (2008) Enhancement of mass trnasfer performance of liquid-liquid system by droplet flow in microchannels. *Chemical Engineering Journal* 141:242-249.

[119] Kralj JG, Schmidt MA, Jensen KF (2005) Surfactant-enhanced liquidâĂŞliquid extraction in microfluidic channels with inline electric-field enhanced coalescence. *LabChip* 5:531-535.

[120] Kumemura M, Korenaga T (2006) Quantitative extraction using flowing nanoliter droplet in microfluidic system. *Analytica Chimica Acta* 558:75-79.

[121] Gupta C, Chauhan A, Mutharasan R, Srinivas SP (2010) Measurement and modeling of diffusion kinetics of a lipophilic molecule across rabbit cornea. *Pharmaceutical Research* 27:699-711.

[122] Skhiri Y, Gruner P, Semin B, Brosseau Q, Pekin D, Mazutis L, Goust V, Kleinschmidt F, El Harrak A, Hutchison JB, Mayot E, Bartolo JF, Griffiths AD,

Taly V and Baret JC (2012) Dynamics of molecular transport by surfactants in emulsion. *SoftMatter* 8:10618-10627.

[123] Baret JC, Beck Y, Billas-Massobrio I, Moras D, Griffith AD (2010) Quantitative Cell-Based Reporter Gene Assays Using Droplet-Based Microfluidics. *Chemistry & Biology* 10:528-536.

[124] Brouzes E, Medkova M, Savenelli N, Marran D, Twardowski M, Hutchison JB, Rothberg JM, Link DR, Perrimon N, Samuels ML (2009) Droplet microfluidic technology for single-cell high-throughput screening. *Proceedings of the National Academy of Sciences* 106:14195-14200

[125] Sela Y, Magdassi S, Garti N (1995) Release of markers from the inner water phase of W/O/W emulsions by silicone based polymeric surfactants. *Journal of Controlled Release* 33:1-12.

[126] Garti N, Aserin A, Cohen Y (1994) Mechanistic considerations on the release of electrolytes from multiple emulsions stabilized by BSA and nonionic surfactants. *Journal of Controlled Release* 29:41-51.

[127] Bonnet M, Cansell M, Berkaoui A, Ropers MH, Anton M, Leal-Calderon F (2009) Release rate profiles of magnesium from multiple W/O/W emulsions. *Food Hydrocolloids* 23:92-101.

[128] Jager-Lezer N (1997) Influence of lipophilic surfactant on the release kinetics of water-soluble molecules entrapped in a W/O/W multiple emulsion. *Journal of Controlled Release* 45:1-13.

[129] Hai M, Magdassi S (2004) Investigation on the release of fluorescent markers from w/o/w emulsions by fluorescence-activated cell sorter. *Journal of Controlled Release* 96:393-402.

[130] Fletcher P, Howe A, Robinson B (1987) The kinetics of solubilisate exchange between water droplets of a water-in-oil microemulsion. *Journal of the Chemical Society, Faraday Transactions 1* 83:985-1006.

[131] Chidambaram N, Burgess DJ (2000) Effect of cationic surfactant on transport of surface-active and non-surface-active model drugs and emulsion stability in triphasic systems. *AAPS PharmSciTech* 2:E28.

[132] Chidambaram N, Burgess DJ (2000) Effect of nonionic surfactant on transport of surface-active and non-surface-active model drugs and emulsion stability in triphasic systems. *AAPS PharmSciTech* 2:E30.

[133] Thiam AR, Bremond N, Bibette J (2009) Breaking of an Emulsion under an ac Electric Field. *Physical Review Letters* 102:188304

[134] Thiam AR, Bremond N, Bibette J (2011) Adhesive Emulsion Bilayers under an Electric Field: From Unzipping to Fusion. *Physical Review Letters* 107:068301

[135] Bremond N, Thiam AR, Bibette J (2009) Decompressing Emulsion Droplets Favors Coalescence. *Physical Review Letters* 100:024501.

[136] Bremond N, Domejean H, Bibette J (2011) Propagation of Drop Coalescence in a Two-Dimensional Emulsion: A Route towards Phase Inversion. *Physical Review Letters* 106:214502.

[137] Baret JC, Kleinschmidt F, Harrak AE, Griffiths AD (2009) Kinetic Aspects of Emulsion Stabilization by Surfactants: A Microfluidic Analysis. *Langmuir* 25:6088-6093.

[138] Brousseau Q, Vrignon J, Baret JC (2014) Microfluidic Dynamic Interfacial Tensiometry (muDIT). *SoftMatter* 10:3066-3076.

[139] Holtze C, Rowat AC, Agresti JJ, Hutchison JB, Angile FE, Schmitz CH, Köster S, Duan H, Humphry KJ, Scanga RA, Johnson JS, Pisignano D, Weitz DA (2008) Biocompatible surfactants for water-in-fluorocarbon emulsions. *LabChip* 8:1632-1639.

[140] Xia YN, Whitesides GM (1998) Soft Lithography. *Annual Review of Materials Research* 28:153-184.

[141] Wang BL, Ghaderi A, Zhou H, Agresti J, Weitz DA, Fink GR, Stephanopoulos G (2014) Microfluidic high-throughput culturing of single sells for selection based on extracellular metabolite production or consumption. *Nature Biotechnology* 32:473-480.

[142] Karamitros C, Lim J, Konrad M (2014) An Amplex Red-based fluorometric and spectrophotometric assay for L-asparaginase using its natural substrate. *Analytical Biochemistry* 445:20-22.

[143] Leo A, Hansch C, Elkins D (1971) Partition coefficients and their uses. *Chemical Reviews* 71:525-616.

[144] Lee D, Ashcraft N, Verploegen E, Pashkovski E, Weitz DA (2009) Permeability of Model Stratum Corneum Lipid Membrane Measured Using Quartz Crystal Microbalance. *Langmuir* 25:5762-5766.

[145] Zwolinski BJ, Eyring H, Reese CE (1949) Diffusion and membrane permeability. *The Journal of Physical Chemistry* 53:1426-1453.

[146] Saparov SM, Antonenko YN, Koeppe RE, Pohl P (2000) Desformylgramicidin: A Model Channel with an Extremely High Water Permeability. *Biophysical Journal* 79:2526-2534.

[147] Yampolskaya G, Platikanov D (2006) Proteins at fluid interfaces: Adsorption layers and thin liquid films. *Advances in Colloid and Interface Science* 128-130:159-183.

[148] Peters T (1995) All about Albumin: Biochemistry, Genetics and Medical Applications. *Academic Press*

[149] Surenjav E, Herminghaus S, Priest C, Seemann R (2009) Discrete microfluidics: Reorganizing droplet arrays at a bend. *Applied Physical Letters* 95:154104

[150] Toiya M, Vanag K, Epstein IR (2008) Diffusively Coupled Chemical Oscillators in a Microfluidic Assembly. *Angewandte Chemie International Edition* 47:7753-7755.

[151] Thutupali S, Seemann R, Herminghaus S (2011) Swarming behavior of simple model squirmers. *New Journal of Physics* 13:073021.

[152] Zheng B, Tice JD, Ismagilov RF (2004) Formation of droplets of alternating composition in microfluidic channels and applications to indexing of concentrations in droplet-based assays. *Analytical Chemistry* 76:4977-4982.

[153] Hung LH, Choi KM, Tseng WY, Yung-Chieh T, Sheab KJ, Lee AP (2006) Alternating droplet generation and controlled dynamic droplet fusion in microfluidic device for CdS nanoparticle synthesis. *Lab Chip* 6:174-178.

[154] Tang SKY, Li T, Abate AR, Agresti JJ, Weitz DA, Psaltis D, Whitesides GM (2009) A multi-color fast-switching microfluidic droplet dye laser. *Lab Chip* 9:2767-2771

[155] Poulsen SR, Harrington RR, Drever JI (1999) The solubility of toluene in aqueous salt solutions. *Talanta* 48:633-641

[156] Fallah-Araghi A, Baret JC, Ryckelynck M, Griffiths AD (2012) A completely in vitro ultrahigh-throughput droplet-based microfluidic screening system for protein engineering and directed evolution. *LabChip* 12:882-891.

[157] Sjostrom SL, Bai Y, Huang M, Liu Z, Nielsen J, Joensson HN, Andersson Svahn H (2014) High-throughput screening for industrial enzyme production hosts by droplet microfluidics. *LabChip* 14:806-813.

[158] Hofmann TW, Hänselmann S, Janiesch JW, Rademacher A, Böhm CHJ (2012) Applying microdroplets as sensors for label-free detection of chemical reactions. *Lab Chip* 12:916-922.

[159] Boitard L, Cottinet D, Kleinschmitt C, Bremond N, Baudry J, Yvert G, Bibette J (2012) Monitoring single-cell bioenergetics via the coarsening of emulsion droplets. *Proceedings of the National Academy of Sciences* 109:7181-7186.

[160] Joensson HN, Uhlen M, Svahn HA (2011) Droplet size based separation by deterministic lateral displacement - separating droplets by cell-induced shrinking. *Lab Chip* 11:1305-1310.

[161] Liu DJ, Ma JM, Cheng HM, Zhao ZG (1998) Solubilization behavior of mixed reverse micelles: effect of surfactant component, electrolyte concentration and solvent. *Colloids and Surfaces A* 143:59-68.

[162] Kundu K, Paul BK (2013) Physicochemical investigtion of mixed surfactant reverse micelles: Water solubilization and conductometric studies. *Colloids and Surfaces A* 433:154-165.

[163] Colinart P, Delepine S, Trouve G, Renon H (1984) Water transfer in emulsified liquid membrane processes. *Journal of Membrane Science* 20:167-187.

[164] Matsumotot S, Inoue T, Kohda M, Ikura K (1980) Water permeability of oil layers in W/O/W emulsions under osmotic pressure gradients. *Journal of Colloid and Interface Science* 77:555-563.

[165] Hofmann T (2012) Applying microdroplets as label-free sensors for reactions inside the droplets. Dissertation, Ruperto-Carola-University of Heidelberg.

[166] Cheng J, Chen JF, Zhao M, Luo Q, Wen LX, Papadopoulos DK (2007) Transport of ions through the oil phase of $W_1/O/W_2$ double emulsions. *Journal of Colloid and Interface Science* 305:175-182.

[167] Uddin MS, Kathiresan M (1999) Extraction of metal ions by emulsion liquid membrane using bi-functional surfactant: equilibrium and kinetic studies. *Separation and Purification Technology* 19:3-9.

[168] Sadtler VM, Krafft MP, Riess JG (1996) Achieving Stable, Reverse Water-in-Fluorocarbon Emulsions. *Angewandte Chemie* 35:1976-1978

[169] Riess JG (2002) Fluorous micro- and nanophases with a biomedical perspective. *Tetrahedron* 58:4113-4131.

[170] Krafft MP, Chittofrati A, Riess JG (2003) Emulsions and microemulsions with a fluorocarbon phase. *Current Opinion in Colloid & Interface Science* 8:251-258

[171] DeJournette CJ, Kim J, Medlen H, Li X, Vincent LJ, Easley CJ (2013) Creating Biocompatible Oil-Water Interfaces without Synthesis: Direct Interactions between Primary Amines and Carboxylated Perfluorocarbon Surfactants.*Analytical Chemistry* 85:10556-10564

[172] Chiu YL, Chan HF, Phua KKL, Zhang Y, Juul S, Knudsen BR, Ho YP, Leong KW (2014) Synthesis of Fluorosurfactants for Emulsion-Based Biological Applications. *ACS Nano* 8:3913-3920

[173] Roach LS, Song H, Ismagilov RF (2005) Controlling non-specific protein adsorption in a plug-based microfluidic system by controlling interfacial chemistry using fluorous-phase surfactants. *Analytical Chemistry* 77:785-796.

[174] Lee A, Tang SKY, Mace C, Whitesides G (2011) Denaturation of proteins by SDS and tetraalkylammonium dodecyl sulfates. *Langmuir* 27:11560-11574.

[175] Tabeling P (2014) Recent progress in the physics of microfluidics and related biotechnological applications. *Current Opinion in Biotechnology* 25:129-134.

[176] Dertinger T, Pacheco V, Hocht I, Hartmann R, Gregor I, Enderlein J (2007) Two-Focus Fluorescence Correlation Spectroscopy: A New Tool for Accurate and Absolute Diffusion Measurements. *ChemPhysChem* 8:433-443.

[177] Dertinger T, Loman A, Ewers B, Müller CB, Kämer B, Enderlein J (2008) The optics and performance of dual-focus fluorescence correlation spectroscopy. *Optics Express* 16:14353-14368.

[178] Lim J, Gruner P, Konrad M, Baret JC (2013) Micro-optical lens array for fluorescence detection in droplet-based microfluidics. *LabChip* 13:1472-1475.

[179] Lim J, Vrignon J, Gruner P, Karamitros C, Konrad M, Baret JC (2013) Ultra-high throughout detection of single cell β-galactosidase activity in droplets using micro-optical lens array. *Applied Physics Letters* 103:203704.

Curriculum Vitae

Personal information

Name:	Philipp Gruner
Date of birth:	22. May 1986
Place of birth:	Frankenberg
Nationality:	German

Education

07/2011 - 07/2014	PhD student
	MPI for Dynamics and Self-Organization, Göttingen, Germany
06/2010 - 06/2011	Diploma Project
	University of Kassel, Germany
07/2009 - 05/2010	Research Internship
	Mawson Institute, Adelaide, Australia
10/2005 - 08/2009	Studies of Nanostructure and Molecular Sciences
	University of Kassel, Germany

Publications in refereed journals

[1] J. Lim, J. Vrignon, P. Gruner, C. Karamitros, M. Konrad, and J.-C. Baret
"Ultra-high throughout detection of single cell beta-galactosidase activity in droplets using micro-optical lens array"
Applied Physics Letters (2013), 103, 203704
[2] J. Lim , P. Gruner , M. Konrad, J.-C. Baret
"Micro-optical lens array for fluorescence detection in droplet-based microfluidics"
Lab Chip (2013), 13, 1472-1475
[3] P. Gruner, M. Arlt, T. Fuhrmann-Lieker
"Surface Wrinkling Induced by Photofluidization of Low Molecular Azo Glasses"
ChemPhysChem (2013), 14, 424-430

[4] Y. Skhiri*, P. Gruner*, B. Semin, Q. Brosseau, D. Pekin, L. Mazutis, V. Goust, F. Kleinschmidt, A. El Harrak, J.B. Hutchison, E. Mayot, J.-F. Bartolo, A.D. Griffiths, V. Taly, J.-C. Baret, *equal contribution
"Dynamics of molecular transport by surfactants in emulsions"
Soft Matter (2012), 8, 10618-10627
[5] S. A. Al-Bataineh, E. J. Szili, P. Gruner, C. Priest, H. J. Griesser, N. H. Voelcker, R. D. Short, D. A. Steele
"Fabrication and Operation of a Microcavity Plasma Array Device for Microscale Surface Modification"
Plasma Processes and Polymers (2012), 9, 638-646
[6] C. Priest, P. Gruner, E. J. Szili, S. A. Al-Bataineh, J. W. Bradley, J. Ralston, D. A. Steele, R.D. Short
"Microplasma patterning of bonded microchannels using high-precision injected electrodes"
Lab Chip (2011), 13, 1472-1475

Publications in refereed proceedings

[1] P. Gruner, B. Semin, J. Lim, J.-C. Baret
"Mass Transport in emulsion studied using a one-dimensional microarray"
Miniaturized Systems for Chemistry and Life Sciences (MicroTAS), 77-79 (2013)
[2] P. Gruner, Y. Skhiri, B. Semin, Q. Brosseau, A. D. Griffiths, V. Taly, J.-C. Baret
"Microfluidic Approaches for the Study of Emulsions: Transport of Solutes"
Material Research Society (MRS), Volume 1530 (2013)
[3] E. J. Szili, S. A. Al-Bataineh, C. Priest, P. J. Gruner, P. Ruschitzka, J. W. Bradley, J. Ralston, D. A. Steele, R. D. Short
"Integration of microplasma and microfluidic technologies for localised microchannel surface modification"
Proceedings of the Society of Photo-Optical Instrumentation Engineers, SPIEermann (2012)
[4] S. A. Al-Bataineh, E. J. Szili, G. Desmet, P. Ruschitzka, P. Gruner, C. Priest, N. H. Voelcker, D. A. Steele, R. D. Short, H. J. Griesser
"Chemical and biomolecule patterning on 2D surfaces using atmospheric pressure microcavity plasma array devices"
Proceedings of the Society of Photo-Optical Instrumentation Engineers, SPIE (2012)

Acknowledgements

At the end, I would like to thank all the people who have contributed to this work. First and foremost, I would like to thank Jean-Christophe Baret. I have learned so much from you during the last three years! Thank you for all the time and effort you put into introducing me to the world of droplets and microfluidics. You have inspired me so much with your your ideas and enthusiasm that I intend to never leave it! You have been an awesome supervisor! Merci beaucoup!

Furthermore, I would like to acknowledge Sarah Köster and Stephan Herminghaus for participating in my thesis committee and for their helpful input. I thank Jörg Enderlein most sincerely for stepping in as a reviewer of my thesis and keeping my future plannings on track. Moreover, I would like to acknowledge Thomas Burg and Manfred Konrad for participating in the examination board.

I thank Benoît Semin for his great support, especially during the time when I started this work. While writing this thesis, I often looked back on the numerous discussions we had. This has really contributed to my understanding of emulsion science! Many thanks also to Jiseok Lim. Not only for all the fun times and helping me out on a daily basis in the lab but also for your support as a friend. I also want to thank Dr. Polenz for innumerable funny moments but also for insightful discussions about science and its related phenomena. Furthermore, I would like to thank Abigail Johnston. The experiments you have performed at your time at the MPI have turned out to be very valuable for the understanding of important aspects of this work! Also, I am grateful to Kathleen Short for helping with the fabrication of an uncountable number of microfluidic chips and her contribution to several experiments. I also would like to acknowledge Craig Priest at this point. My knowledge about micro-fabrication goes mainly back to the things you have taught me during my time in Australia - this has helped very much in creating the microfluidic chips that were required for this work! Also thank you for the helpful discussions we had about this work! Many thanks to Mira Prior for performing numerous FCS-measurements. Similarly, I would like to acknowledge Jürgen Bienert

for performing NMR-measurements. Furthermore, I would like to thank Estelle Mayot and Birte Riechers for providing great surfactants and helpful insights on the synthesis of those. Quentin Brosseau is acknowledged for providing surface tension and DLS-measurements. Moreover, I would like to thank Andreas Renner for taking good care of the clean room. Because you have managed to keep everything working, I was able to leave it mostly with the desired product! Also, Wolf Keiderling is acknowledged for providing some specific devices and tools that were required for this work. I would like to thank Thomas Eggers and Kristian Hantke for the IT support. A special thanks also goes to Monika Teuteberg, especially for helping me with all the things that I will never understand concerning the MPI. I would like to thank GGNB, especially Antje Erdmann and Frauke Bergmann, for the great organization of the International Max Planck Research School "Physics of Biological and Complex Systems". Additionally, I am grateful for the financial support of the SFB 755 and for helpful discussions with the members.

Working at the Max-Planck-Institute for Dynamics and Self-Organization was always a pleasure for me. I would like to thank all my colleagues for a great working atmosphere. Especially the members of our working group, I have not mentioned so far: Deniz, Florine, Renaud, Ouriel, Jeremy, Say Hwa Tan, Arthur & Arthur, Erfan, Xiaopeng, Elena and Zakaria are acknowledged for providing an always helpful and most pleasant environment. Moreover, I would like to acknowledge the table soccer team: Marcin, Marco, Ingmar, Paolo, Arnaud, Julien, Jiseok, Tanya and Laura for a huge amount of fun.

It was a long way from learning addition and subtraction to this point. However, I very well realize that my education in Saxony and later in Kassel are the basement for this work. Hence, I would like to thank all the people that have been teaching me during the last 28 years of my life and therefore also contributed to this work.

Finally, I would like to thank my family for their constant support during all the years. Especially, my parents Cathrin and Jürgen Gruner are acknowledged for their endless support and encouragement. It is to them that I dedicate this work.

Thank you!